X-ray Diffraction Study of a Three-Component Lamellar Phase.

by

Reiko Oda

B.S., University of Tokyo(1988)

Submitted to the Department of Physics
in partial fulfillment of the requirements for the degree of

Doctor of Philosophy

at the

MASSACHUSETTS INSTITUTE OF TECHNOLOGY

Oct 1994 [Feb 1995]

Author .....
Department of Physics
Oct 26, 1994

Certified by .....
J. David Litster
Professor of Physics
Thesis Supervisor

Accepted by .....
George F. Koster
Chairman, Departmental Committee

X-ray Diffraction Study of a Three-Component Lamellar Phase.

by

Reiko Oda

Submitted to the Department of Physics
on Oct 26, 1994, in partial fulfillment of the
requirements for the degree of
Doctor of Philosophy

Abstract

Three-component lamellar phase has been investigated which consists of $C_{12}E_5$, octane and water . This is a layered phase, the lyotropic equivalent of a thermotropic smectic-A phase. X-ray scattering techniques were used on powder and aligned samples, as well as the optical microscopy investigations to understand the structure and the interactions that govern this lyotropic system, and also the temperature dependence of such important parameters as layer-periodicity, the layer thickness and the exponent η which characterizes quasi-long range order. Experiments were done with various surfactant concentrations and oil/water volume ratios.

The system was chosen for two reasons. First of all, a lamellar phase continuously exists from an oil-rich through an equal oil-water to a water rich region in the accessible temperature range ($\sim 33^{oC}$). Also the lamellar phase continue to exist with the wide range of the surfactant concentrations, which allowed us to study the dilution of the lamellar phases. Secondly, since it is a nonionic surfactant, there are no electrostatic interactions present in this system, i.e. it is a purely sterically stabilized lamellar phase. Our investigations pointed out the following: (1) The structure factor that describes the broad lamellar peaks that we found from the powder scattering should not be confined in the vicinity of peak-position (q_o), also the contributions from higher harmonic terms has to be taken into considerations. (2) The form factor had to be incorporated because of the finite size of the lamellar layers. A model has been proposed to describe the electronic density distribution within the layer and in the direction perpendicular to the layers. The form factor based on this model has successfully described the scattering intensity profiles with the variation of layer thickness. (3) Excess scattering was measured as $q \rightarrow 0$. This has been theoretically predicted to be due to concentration fluctuations (4) The x-ray scattering from aligned samples provided information on the temperature dependence of the layer periodicity within the lamellar phase with the constant surfactant concentration. This dependence can be described by the fluctuations of membranes.

Thesis Supervisor: J. David Litster

Title: Professor of Physics

Acknowledgement

It is with the help of so many people that I could finish this thesis.

First of all, I would like to thank Prof. J. D. Litster for having given me the oppotunity to work in his laboratory, and having supported me for all the years.

I would also like to thank Prof. S.J.G. Mochrie for having introduced me to the x-ray scattering technique, as well as having allowed me to use Rigaku Ru2000 in his laboratory.

George Nounesis gave me a tremendous amount of help and support until the end. What I have learned from him are invaluable, starting from the way to plot figures correctly, to where to look and find the essential points in data, more importantly, how to be a serious researcher without losing the integrity of a humanbeing. I would like to thank him for everything, and his patience for having dealt with me.

The MRS meeting on 1991 brought Pascale Fabre to Boston, since then she has been an incredible support for me. As she is an expert of the lamellar phases, she always gave me the light for the interpretations of my observations. The numerous e-mails, faxes and telephone calls between here and Paris are the precious records. Also I would like to thank her for her friendship as being one of my best friends.

Most of the analysis benefitted from the discussions with Frederic Nallet, not only from my several visits to Bordeaux, but the flood of my e-mails and faxes filled with questions, he always patiently passed me on his adequate ideas and analysis. Without his help, these analysis could not have been possible.

I would like to thank Raymond Ober at Collège de France for his generousity to let me use his x-ray source. Although I was an outsider, during my 6 weeks stay, he not only tried his best to accomodate the busy schedule of the usage of the machine he also helped me for the experiments and the data analysis, because of my poor French, our discussions always took more than it should, but he always was very patient.

I benefitted a lot from the several short but intense discussions with Prof. Didier Roux. With his acute sense of experiment, he gave me many eye-opening insights and directions.

Also the discussions with Prof. R.Strey were extremely useful, who pointed out some of the big mistakes I have been making for a long time.

In Building 13, I would like to thank almost everybody on the floor for their help as I was always running around, asking for helps. In my group. I specially benefitted from the interaction with Brian McClain who passed on his experimental knowledge based on the numerous experiences. Gerry Swislow, with his red bicycle, arrived always when I was lost.

I would also like to thank Michael Yoo, especially with programming, when I get into the complete mess which was quite often, he somehow always managed to find the problems and straighten them out. I also enjoyed our long discussions about various subjects during the late night experiments.

Claudio Cesar has been one of the most important friends all the time . I would like to thank him and his wife Raquel for their friendship as well as their help in the numerous occasions.

George and Charlotte Clark, I would never be able to thank them enough for their kindness as my second parents, without their warmness and love, my life in Boston would have been much more difficult.

I would like to thank Ivan Huc for his encouragement across the sea during the last few months which were specially difficult. His support gave me the strength and determination to go through the end.

And finally, my parents, Minoru and Tomoe Oda. It was with their support, love, and trust, that it was possible for me to continue. And I thank them as well as my brother and his wife, Katsuro and Naoko Oda, for their encouragement through all those years.

Contents

List of Figures

List of Tables

Chapter 1

Physical Properties of Lamellar Phases

1.1 Introduction

Surfactants in mixtures with solvents can self-assemble reversibly into spatially organized structures which are physically and not chemically associated. These structures have been of interest to physicists, chemists and biologists.

Water and oil do not mix due to the large surface tension($50mN/m$). Addition of surfactant *amphiphilic molecules* can decrease this surface tension drastically($\sim 10^{-3}mN/m$), and the mixture can form a stable emulsion of solvents with opposite polarity. This property of surfactants can be understood from their chemical composition. Their molecules have hydrophilic and hydrophobic ends and they can place themselves at the interfaces of oil and water, to form thermodynamically stable macro-molecular structures. Among these are the micellar, the bicontinuous/sponge, the hexagonal, and the lamellar phases.

The surfactant molecules concentrate at the interfaces between different solvents. Depending on whether the solvents have one or two polarities, they can form monolayer or bilayer structures. Monolayers separate oil and water regions, while bilayers create a separation inside a monopolar solvent. The bilayers are essentially the same structure as the lipid bilayer membranes which are found in living cells.

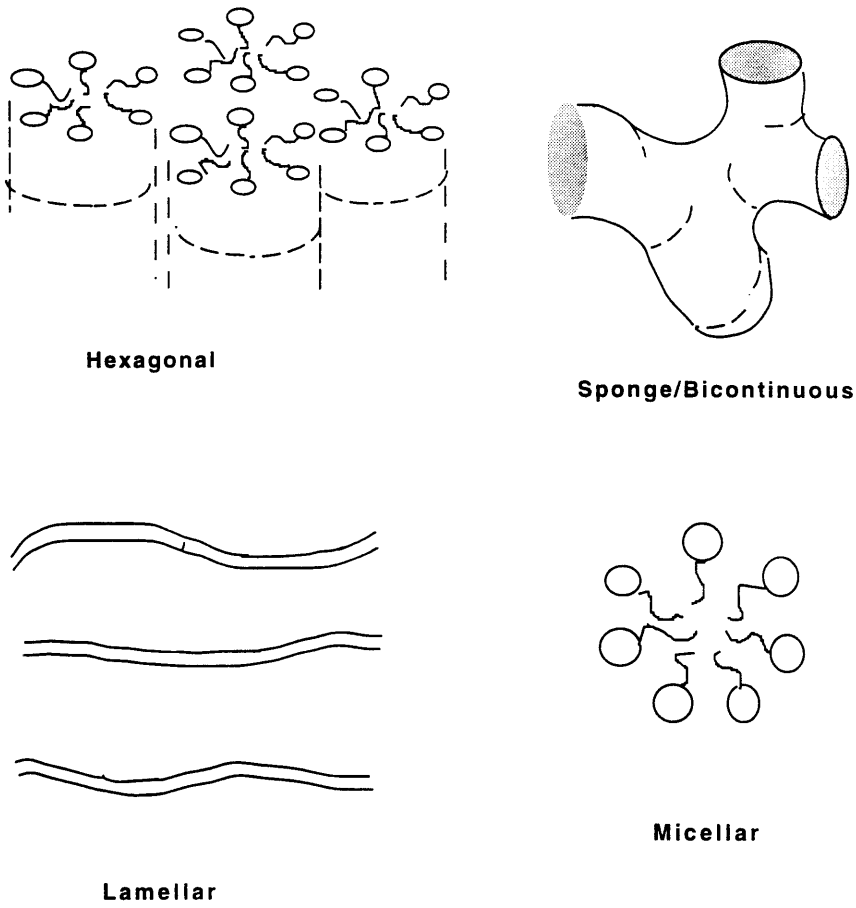

Figure 1-1: Some of the Phases encountered by mixing surfactants with solvents

Lamellar Phase

Lamellar phases are layered phases similar to the smectic-A phase of thermotropic liquid crystals. The order can be described as a one dimensional mass density modulation in the direction perpendicular to the layers. Within the layers the order is liquid-like, as there exist no long-range translational correlations. The layers are parallel to each other. The system is strongly birefringent as it can be observed with optical microscopy.

Theoretical and experimental investigations of lamellar phases have been carried out intensively in the last two decades [1, 2] The smectic layers have separations that

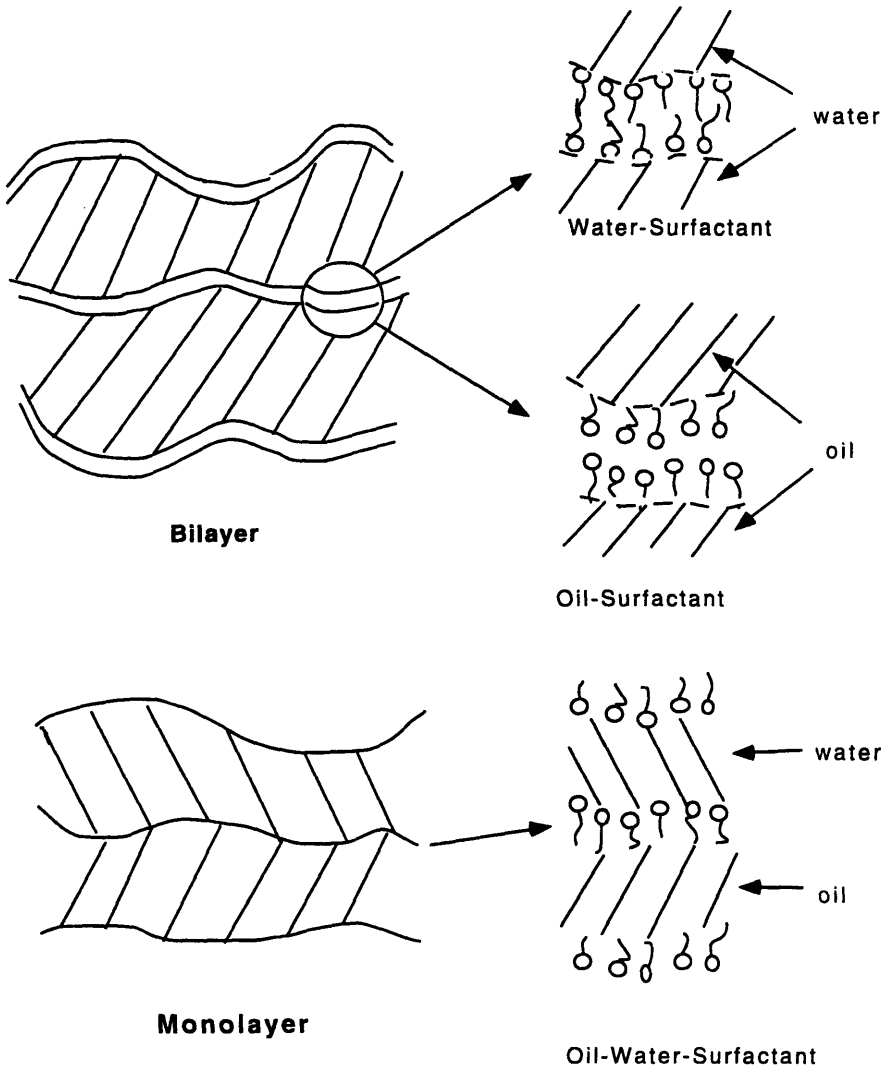

Figure 1-2: Lamellar phases: The geometry can vary depending on the concentration of the solvents

can range from a few Angstroms to a few thousand Angstroms. They are stabilized by interlayer interactions, such as the Van der Waals, the electrostatic, and the steric entropic interaction.

The distance between layers can be varied continuously by changing the concentration of the surfactant. This procedure is called swelling, and to date, layer separations of $\simeq 6000\mathring{A}$ have been observed[3].

To date, all the experiments as well as the theories have been carried out for almost-bilayer systems with one polar system. While water-surfactant binary lamel-

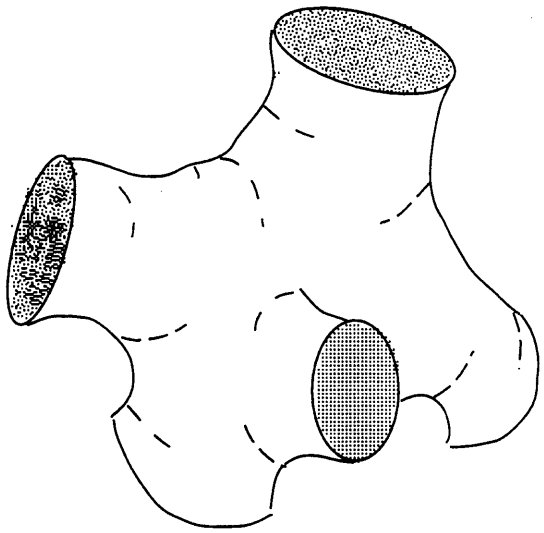

Figure 1-3: Sponge/Bicontinuous phase: when the interfaces consist of bilayer for the sponge, and monolayer for the bicontinuous phase

lae exist, the binary lamellar consisting of surfactant and oil has not been observed.

Bicontinuous/Sponge Phase

The bicontinuous phases are formed by self-avoiding, yet connected surfactant interfaces with a spatial distribution that is uniform only at large distances. The interfaces are curved everywhere with the two principal curvatures having opposite signs(*saddle like local shape*). There is no long-range orientational or positional ordering, and the phase is optically isotropic but shows shear birefringence. The term *bicontinuous* is used whenever the membranes are monolayers and *sponge* is used for the bilayer case. In spite of the absence of long-range order, the scattering pattern shows a clearly defined maximum, corresponding to the mean separation of the interfaces of the surfactant. The structure model for this system was proposed only recently by Cates et.al.[4] and also Porte et.al.[5].

1.2 Thermal Fluctuations

Without thermal fluctuations, a lamellar phase would just be a stack of flat surfactant layers. Thermal fluctuations cause each layer to fluctuate with energy of kT per mode, where T is the temperature, and k is Boltzman's constant. ($1.38 \times 10^{-23} JK^{-1}$) The relation between the amplitude and the wave length of the fluctuation undulation of a membrane is determined by the bending rigidity, as well as the interactions between successive layers.

1.2.1 Bending Elasticity of a Single Membrane

The bending elasticity of a single two dimensional sheet, isotropic within its plane, shows some interesting features when compared to the elasticity of a one-dimensional flexible thread.

For a thin thread, the elastic bending energy can be written as,

$$F_{bend} = \int \frac{1}{2}\kappa(\frac{1}{R})^2 dl \tag{1.1}$$

Here, κ is the bending rigidity of the thread, R is the local curvature imposed on the length element dl. This leads to the definition of the persistence length [6],

$$< l >= \frac{\kappa}{kT} \tag{1.2}$$

that distinguishes between short scales where the thread is stiff, and long scales where the thread loses the orientational correlation.

In the case of the two dimensional sheet, the elastic bending energy around its equilibrium position, within the harmonic approximation (the bending curvature is not large) has been derived by Helfrich[7].

$$F_{bend} = \int (\frac{\kappa}{2}(\frac{1}{R_1} + \frac{1}{R_2} - \frac{1}{R_0})^2 + \overline{\kappa}\frac{1}{R_1 R_2})dS \tag{1.3}$$

. Here, κ is the bending modulous which is related to the energy spent for a locally

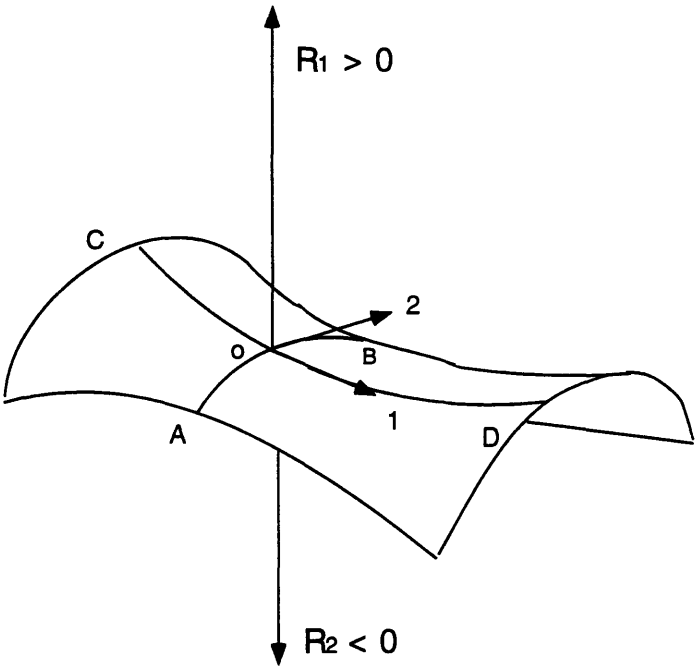

Figure 1-4: Principal radii of curvature associated with point o on the surface:1 is a tangential direction of C-D at o, 2 is the tangential direction of A-B at o, where A-B is perpendicular to C-D

cylindrical deformation of the surface caused by the thermal fluctuation. This is analogous to the rigidity of the one dimensional thread, and is always positive. $\overline{\kappa}$ is the gaussian bending modulous which has no analogue in the one dimension. R_1 and R_2 are the two principal radii of curvature of the surface in the local area element dS. R_0 is the spontaneous curvature of the film, which depends on the chemical composition as well as the temperature. In the case of a bilayer system, because of symmetry considerations one can assume $R_0 \rightarrow \infty$.

In the sponge phase, the two principal curvatures have the same magnitude but opposite signs(*saddle-like curvature*). In the lamellar phase, both curvatures are small. Consequently, in both phases, the mean-curvature contribution to the elastic energy is comparable. The main difference between the two phases is brought in by the second term which is responsible for the topology of the system.

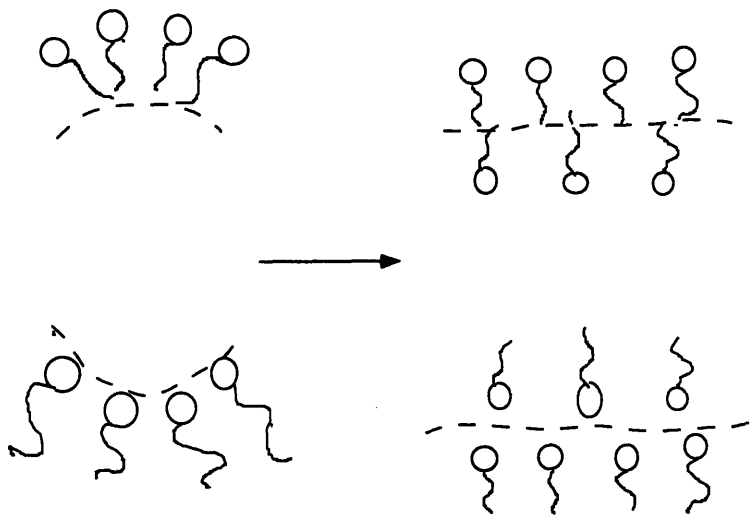

Figure 1-5: The spontaneous curvature of a monolayer film. It is zero for the bilayer membrane because of the geometrical symmetry

According to the Gauss-Bonnet theorem:

$$\int_S \frac{1}{R_1 R_2} dS = 4\pi(1 - N) \tag{1.4}$$

Here N is the number of disjoint components(*handles*). This relation states that the integral of the gaussian curvature over a given closed surface(no edges) is a topological invariant. Consequently the gaussian curvature $\overline{\kappa}$ is related to the degree of connectivity of the structure, and is therefore a function only of the topology. As the energy is constant for a given surface, this term is not important for surface deformations around the equilibrium position. So finally, the elastic energies of lamellar and sponge phases differ by $-4\pi\overline{\kappa}n$ where n is the density of disjoint components, i.e. N per unit area. It can be expected that negative values of $\overline{\kappa}$ stabilize the lamellar phases (L_α), while positive values favour the formation of the multi-connected area

and create sponge phases (L_3). Thus while $\overline{\kappa}$ is very important for a L_α to L_3 topological transformation, it has no effect on the thermal fluctuations, as is the case with κ.

As it is clear from the equation 1.3, the rigidities κ and $\overline{\kappa}$ are both expressed in units of energy. To acquire a better understanding of the effects of thermal fluctuations, we can define two regimes related to the thermodynamics of the films as follows:.

1) When $\kappa \gg kT$, the deformation of the films caused by the thermal energy is small. The films can be considered as *rigid* as is often the case with the lipid membranes.

2) When $\kappa \approx kT$, the films are *flexible* and fluctuate around their equilibrium positions: This is called an *undulation.*

Helfrich[8], Peliti et.al[9] and David et.al[10] have demonstrated that the main effect of small wavelength curvature fluctuations is to renormalize the elastic constants κ and $\overline{\kappa}$. Using perturbation theory, they have demonstrated that,

$$\kappa = \kappa_0 - \frac{3}{4\pi} kT ln(\frac{q_{max}}{q_{min}}), \tag{1.5}$$

$$\overline{\kappa} = \overline{\kappa_0} + \frac{5}{6\pi} kT ln(\frac{q_{max}}{q_{min}}), \tag{1.6}$$

Where κ_0 and $\overline{\kappa_0}$ are the mean and Gaussian bending rigidities without thermal fluctuations respectively, $q_{min} = 2\pi/\xi$ and $q_{max} = 2\pi/a$ are the cut-off wave length where a is the intermolecular distance (the smallest allowed length scale of fluctuations), and ξ is the in-plane correlation length of the fluctuations. In the case of a free membrane, ξ corresponds to the transverse size of the membrane. The logarithmic term in this renormalization relation is a well known characteristic of fluctuations in 2-D systems[6]. Positional correlations break down when the dimension of the system is smaller or equal to 2 because of the logarithmic divergence of the fluctuation amplitude with the increase of the size of the system.

The fact that κ is a decreaseing function of the in-plane correlation function

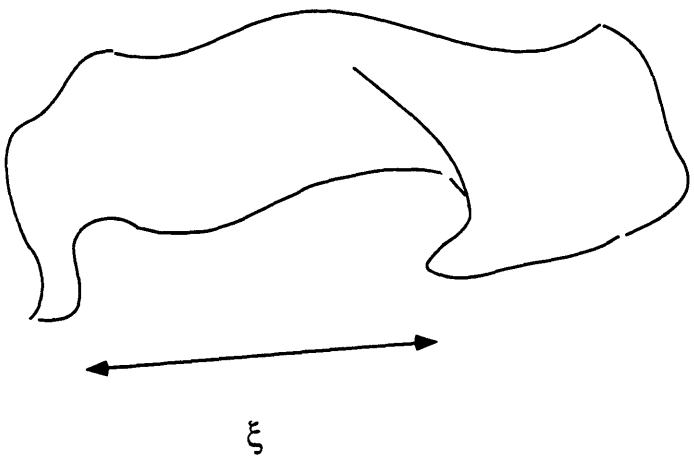

Figure 1-6: The persistence length is defined as the length where the in-plane correlations goes to zero.

indicates that the films lose their memory of in-plane correlations beyond certain distance. From Eq. 1.5, we can derive the *persistence length* ξ [11] in the case of a two dimensional film Fig. 1-6, as the distance at which κ goes to zero:

$$\xi_p = aexp(\frac{4\pi\kappa_0}{3kT}) \tag{1.7}$$

By incorporating both the renormalization of the rigidity and the topological analysis, several regimes can be identified[12].

1) $\overline{\kappa} < -2\kappa$, the surface forms a spherical configuration.

2) $-2\kappa < \overline{\kappa} < 0$, a locally bent conformation with R_1, R_2 having the same sign is favored (*flat configuration*). At very high dilution, L_α will transform into a dispersion of spherical vesicles. Sponge/bicontinuous phases are unstable at any dilution.

3) $\overline{\kappa} \approx -\kappa$, in the case $R_0 \rightarrow \infty$, the elasticity of the membrane becomes,

$$F_{bend} \approx \int (\frac{\kappa}{2}[(\frac{1}{R_1})^2 + (\frac{1}{R_2})^2])dS \tag{1.8}$$

The local conformation only depends on the magnitude of R_1 and R_2, and not on their relative signs. A transition from L_3 to L_α at high dilution should occur in this regime.

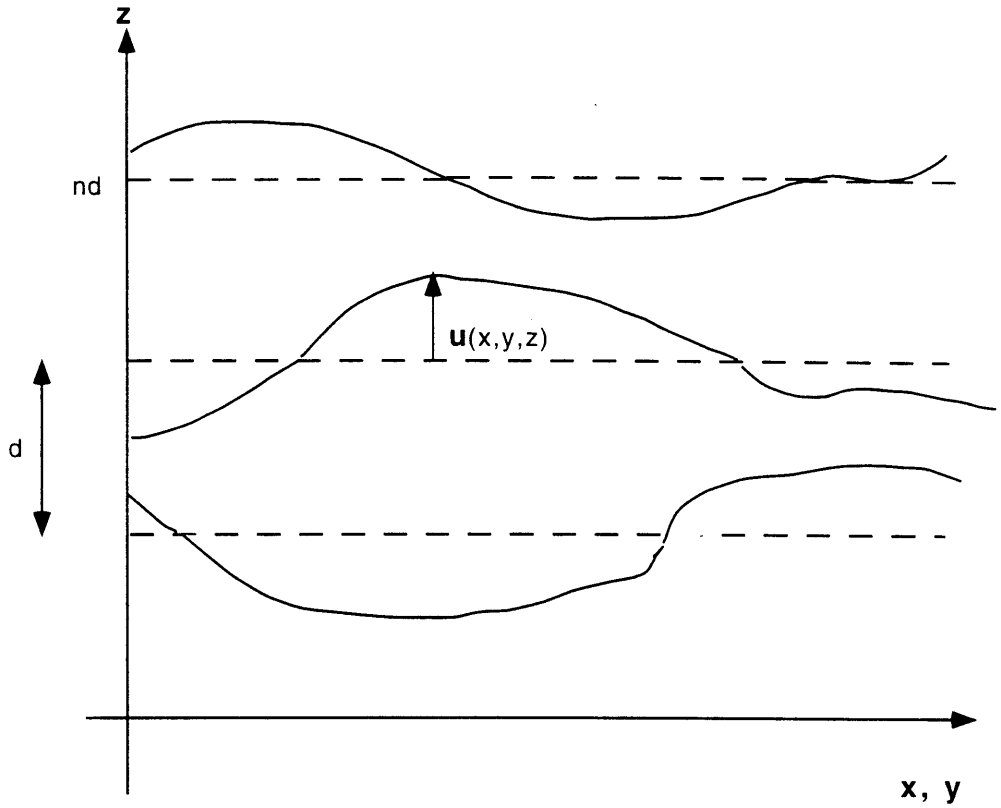

Figure 1-7: The schematic of a Lamellar phase

4) $\overline{\kappa} \gg -\kappa$ (presumably positive), the saddle-like configuration is favored at all dilution levels.

1.3 Thermotropic and Lyotropic Smectic Phases

1.3.1 The Free Energy for Smectic Order

The layer displacement in a smectic-A phase is defined as $u = \mathbf{u}(x, y, z)$, In Fig. 1-7 the schematics of the system are shown. Here the direction of z axis is defined parallel the layer normal. In terms of the periodicity d, the equilibrium position of the nth layer can be defined as $z = nd$. Thus, $u_n(x, y, z)$ is the displacement of the nth layer from the equilibrium position.

The free-energy density of this system can be written as a summation of two elastic energies, as was introduced by de Gennes[13].

$$f = f_o + \frac{1}{2}K_1(\frac{\partial^2 u}{\partial x^2} + \frac{\partial^2 u}{\partial y^2})^2 + \frac{1}{2}B(\frac{\partial u}{\partial z})^2 \tag{1.9}$$

Here the first term is the *splay* term with K_1 as the elastic constant. The second term is the compression energy with B as the compressibility constant.

The Absence of True Long Range Order in Lamellae

It was shown by Landau and Peierls[14], [15] that the long-range positional crystalline order in less-than-three dimensions, at finite temperatures, is destroyed by long wavelength thermal fluctuations. The smectic phase has long-range order in one dimension. It is shown below that in three dimensions, the thermal fluctuations of the layers diverge logarithmically with the size of the sample[16].

The free energy of the fluctuating membranes was introduced in Eq. 1.9. Using the Fourier transform and the equipartition theorem for Eq. 1.9 we get for the mean square displacement due to the qth mode of fluctuation with the expression:

$$< |u_{\mathbf{q}}|^2 > = \frac{kT}{Bq_z^2 + K_1 q_\perp^4} \tag{1.10}$$

The mean square of the displacement of the bilayer can be calculated by summing over all the wave vectors in the phase space, $-\infty < q_z < \infty$ and $q_{min} < q_\perp < q_{max}$. Here $q_{min} = 2\pi/L$ where L is the size of the sample, $q_{max} \approx 2\pi/a$, where a is the minimum conceivable curvature, typically the in-plane distance between consecutive molecules. Thus, the total mean square displacement is,

$$< u(\mathbf{r})^2 > = \frac{kT}{(2\pi)^3} \int \frac{d\mathbf{q}}{Bq_z^2 + K_1 q_\perp^4}$$

$$= \frac{kT}{(2\pi)^3} \int_{-\infty}^{\infty} dq_z \int_{q_{min}}^{q_{max}} \frac{2\pi q_\perp dq_\perp}{Bq_z^2 + Kq_\perp^4}$$

$$= \frac{kT}{4\pi\sqrt{BK_1}} \int_{q_{min}}^{q_{max}} \frac{dq_\perp}{q_\perp}$$

$$= \frac{kT}{4\pi\sqrt{BK_1}} ln(\frac{L}{a})$$

Here we see the divergence of the displacement fluctuations $< u(\vec{r})^2 >$ with the sample size L.This is the Landau-Peierls instability that states the one-dimensionally ordered system cannot have the true long-range order due to the long-wavelength fluctuations. However, since the divergence is logarithmic, there still exists a quasi-long range smectic order. This ordering may be defined in general by the density correlations, which as will be shown later, goes as the exponential power of the displacement. In the case of the one-dimensional system, the ordering shows the algebraic decay with the critical exponent η where we define η to be,

$$\eta = q_0^2 \frac{kT}{8\pi\sqrt{\bar{B}K}} \tag{1.11}$$

While the calculations described above concern only the thermotropic systems which consist of a single component for which the phase is determined only by the temperature, for lyotropic systems, phase transitions depend on both concentration and temperature. Therefore, for a lyotropic system, we not only have to consider the layer displacements, but also changes in the local concentration $\delta c(\vec{r})$[1]. This occurs only when the system consists of more than one component and the local concentration fluctuates. There are two origins for these fluctuations. The first is the change of the thickness of the bilayer. The second is the layer displacements at constant membrane thickness which can also cause the local concentration to fluctuate.

Because of the concentration fluctuations, the expression for free energy density

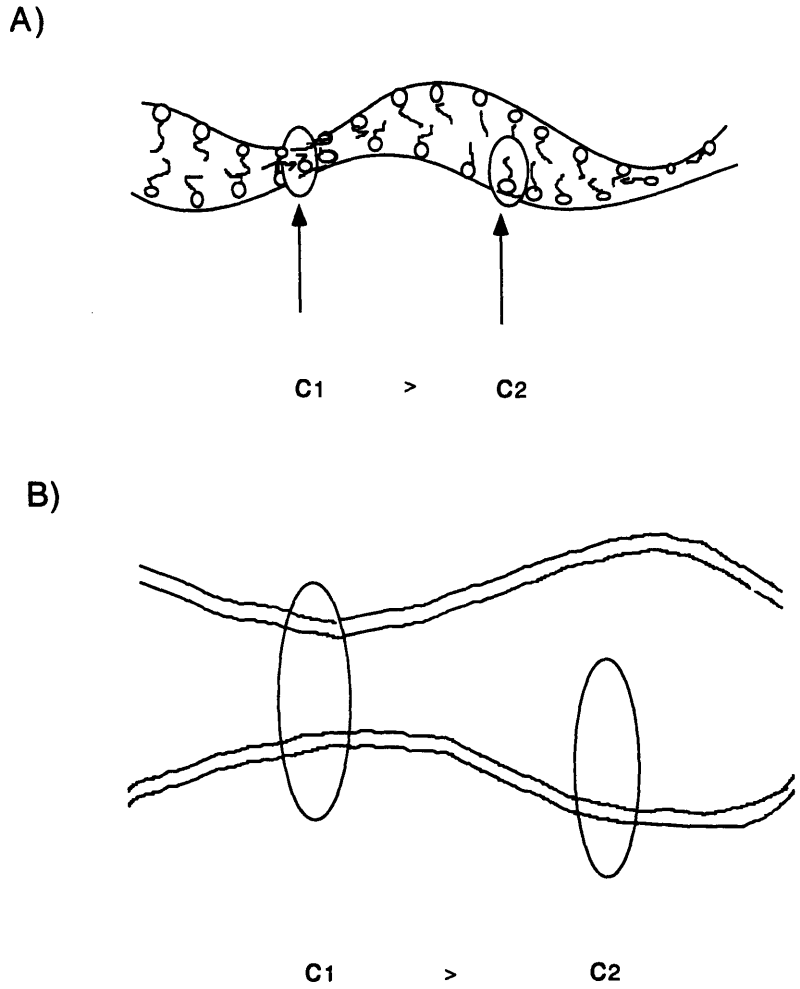

Figure 1-8: The two contributions for the concentration fluctuation:A) The fluctuation of the thickness of membranes. B) The fluctuation coming from the displacement of the membranes. c_1 and c_2 are the two local surfactant concentrations

Eq. 1.9 must be modified. Introducing the new parameter $\delta c(\vec{r})$, it becomes:

$$f = f_o + \frac{B}{2}(\frac{\partial u}{\partial z})^2 + \frac{1}{2}K(\frac{\partial^2 u}{\partial x^2} + \frac{\partial^2 u}{\partial y^2})^2 + \frac{1}{2\chi}\delta c^2 + C_c \delta c \frac{\partial u}{\partial z} \qquad (1.12)$$

Here K is the splay constant which was introduced as K_1 before in Eq. 1.9, and B is the compressibility modulus at fixed concentration. Note that in the case of lyotropic lamellae, the second term which describes the energy necessary for the configuration of the *bending* corresponds to the *splay* mode for thermotropic liquid crystals, and the terms *bending constant* or *bending/bulk modulus* are commonly used for K. χ is the osmotic compressibility, where only the compression of the bilayer at fixed periodicity is considered. C_c is the coupling constant between the layer displacements and the

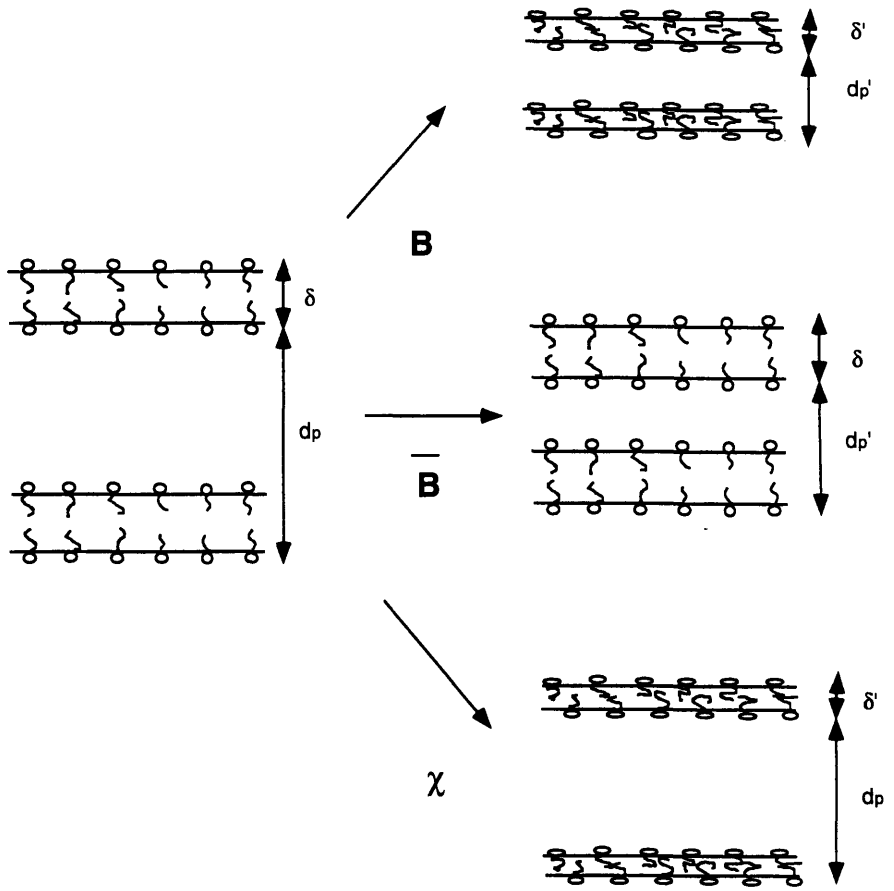

Figure 1-9: Schematic representations of the compression of a lyotropic smectic-A. The elastic stresses are controlled by the three elastic constants B, $\overline{B}$, χ respectively.

concentration fluctuations.

In the Appendix, it is shown that $\overline{B}$ which is defined by $\overline{B} = B - \chi C_c^2$, is the compressibility at fixed chemical potential, thus, the compressibility at constant surfactant-membrane thickness.

Macroscopic and Microscopic Parameters

The elastic constants B, $\overline{B}$ and χ depend on several microscopic parameters that characterize the system[17].

Here we define δ as the bilayer thickness, d_p as the layer periodicity, d as the intermembrane distance so that $d_p = d + \delta$, ρ as the total mass density, c as the

surfactant mass fraction of the total, m as the surfactant mass and v as the surfactant volume. The molecular number density of the surfactant is given by the equation:

$$n = \frac{\rho c}{m_s} = \frac{\delta}{d_p v} \tag{1.13}$$

For a membrane that is part of a layered structure, its thickness is affected by the presence of the neighboring membranes, so that it is more compressed than a free membrane. So, in the free energy for the bilayer structure, there exist two terms: the compression of the membrane, and the intermembrane interaction. So, if we determine δ_0 to be the membrane thickness without compression interaction, then d_{p0} is the periodicity calculated from Eq. 1.13 using δ_0 and the free energy density can be written as:

$$f = \frac{1}{2}\epsilon\frac{\rho c}{m}(\frac{\delta - \delta_0}{\delta_0})^2 + \frac{V(d_p)}{d_p} \tag{1.14}$$

Here $V(d_p)$ is the intermembrane interaction, and ϵ is the surfactant characteristic energy, evaluated by Golubovic et.al.[18] and typically of the order of kT .

Using Eq. 1.13, we can write Eq. 1.14 in the form:

$$f = \frac{1}{2}\epsilon\frac{\rho c}{m}(\frac{d_p - d_0}{d_0})^2 + \frac{V(d_p)}{d_p} \tag{1.15}$$

The equiliburium periodicity for this system is the periodicity which minimizes the free energy,

$$\frac{\partial f}{\partial d_p} = \epsilon\frac{\rho c}{m}(\frac{d_p - d_0}{d_0}) + \frac{\partial}{\partial d_p}(\frac{V(d_p)}{d_p}) = 0 \tag{1.16}$$

using a Taylor expansion, the free energy density can be written as:

$$f = f_0 + \frac{1}{2}[\frac{\partial^2 f}{\partial d_p^2}(d_p - d_{peq})^2 + \frac{\partial^2 f}{\partial d_p \partial c}(d_p - d_{peq})\delta c + \frac{\partial^2 f}{\partial c^2}\delta c^2]$$

Here d_{peq} is the equilibrium periodicity of the membranes. Using $\partial u/\partial z = (d_p -$

$d_{peq})/d_{peq}$, and comparing with Eq. 1.12:

$$B = U\frac{d_{peq}}{d_0} + \frac{\partial^2}{\partial d_p^2}(\frac{V(d_p)}{d_p})d_{peq} \tag{1.17}$$

$$C_c = \frac{U}{c}(\frac{3d_{peq}}{d_0} - 2) \tag{1.18}$$

$$\chi^{-1} = \frac{U}{c^2}(\frac{3d_{peq}}{d_0} - 2) \tag{1.19}$$

Where,

$$U = \epsilon\frac{\rho c}{m}\frac{d_{peq}}{d_0}$$

Using the definition $\overline{B} = B - \chi C_c^2$ and Eq. 1.16,

$$\overline{B} = d_{peq}(\frac{\partial^2 V(d_p)}{\partial d_{peq}^2}) \tag{1.20}$$

Using the definition of η 1.11,

$$\eta = q_0^2\frac{kT}{8\pi\sqrt{\overline{B}K}} \tag{1.21}$$

The bending modulus of the lyotropic smectic layers K can be expressed as a function of the rigidity of the individual membrane:

$$K = \frac{\kappa}{d_{peq}} \tag{1.22}$$

In order to proceed with the calculation, we have to know the intermembrane interaction $V(d)$. In the next section, we will discuss the different types of interactions and their persistent lengths.

1.4 Interlayer Interactions

The interactions between membranes have a variety of origins. The most important ones are described here.

1.4.1 Steric interaction

The idea of repulsive interactions between the layers, as the result of the decrease of the entropy due to layer stacking was introduced by Helfrich in 1980 [19]. For a freely undulating membrane of rigidity κ, the local bending energy can be described using u, the displacement of the membrane from the equilibrium position, The free energy is written as

$$F = F_o + \int \frac{\kappa}{2}(\nabla_\perp^2 u)^2 dS \tag{1.23}$$

Here, dS is the area element perpendicular to the layer normal. And

$$\nabla_\perp^2 u^2 = \frac{\partial^2 u}{\partial x^2} + \frac{\partial^2 u}{\partial y^2} \tag{1.24}$$

From the equipartition theorem we have

$$S < |u_{q_\perp}|^2 >= \frac{kT}{\kappa q_\perp^4} \tag{1.25}$$

where S is the membrane area. Now, if the membrane is *sandwiched* between two boundary walls, a large number of initially allowed bend conformations is forbidden because the membranes cannot intersect the walls. This constraint in the number of *possible states* is brought in by introducing the cut-off wave length for the fluctuations: this causes a decrease in the configuration entropy and induces a steric repulsive interaction. The energy density of the interaction can be understood from Fig. 1-10. Expressing the displacement as $u(\mathbf{r}) = \int u_q e^{i\mathbf{q}\cdot\mathbf{r}} d\mathbf{q}$, we have from Eq. 1.25

$$< u^2(\mathbf{r}) >= \int |u_{q_\perp}|^2 d^2 q_\perp \tag{1.26}$$

$$= \frac{S}{(2\pi)^2} \int \int_{q_{min}}^{q_{max}} \frac{kT}{S} \frac{1}{\kappa q_\perp^4} 2\pi q_\perp dq_\perp d\theta \tag{1.27}$$

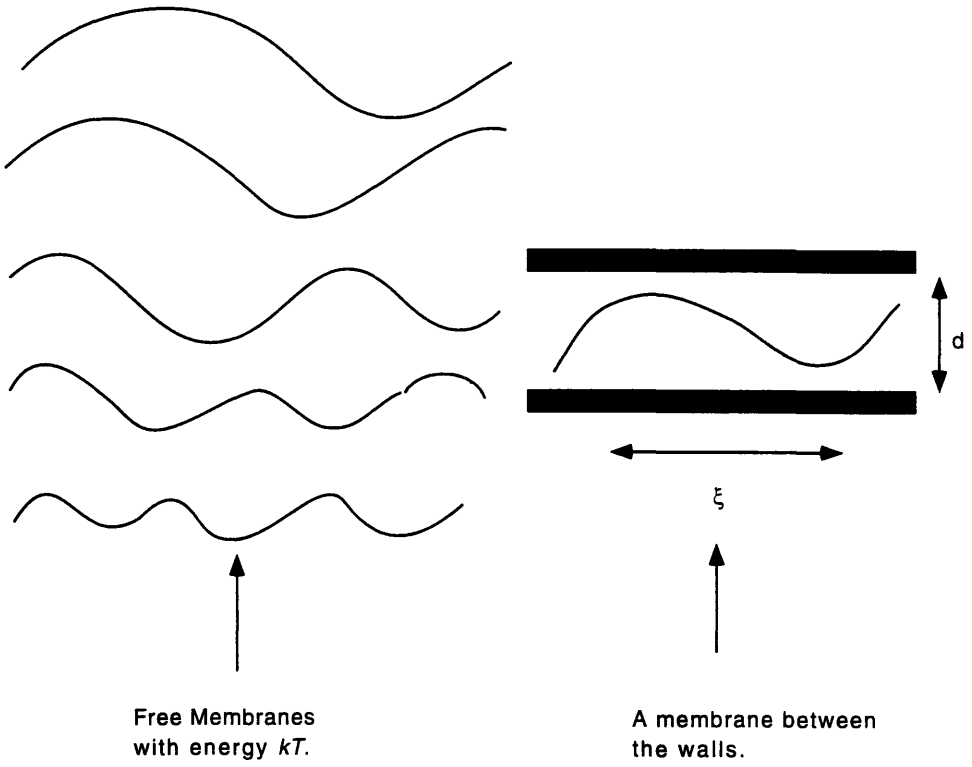

Figure 1-10: The undulating membrane with the given energy *sandwiched* by the walls.

$$= \frac{kT}{4\pi\kappa}\left(\frac{1}{q_{min}^2} - \frac{1}{q_{max}^2}\right) \tag{1.28}$$

where q_{max} and q_{min} are the wave vectors in the in-plane direction of the minimum and the maximum allowed wave length. We call ξ as the largest allowed wavelength at energy kT for the membrane between the walls. By definition, $q_{min} = 2\pi/\xi$. The minimum physically acceptable curvature is related to the mean intermolecular in-plane distance a, and in the case of surfactant membranes, a is typically about $5\mathring{A}$. So $q_{max} = 2\pi/a$ $q_{max} \ll q_{min}$, and we can neglect the term q_{max}. The Eq. 1.28 becomes,

$$< u^2(\mathbf{r}) > \approx \frac{kT\xi^2}{\kappa}$$

The maximum amplitude of the fluctuations d is the separation between the mem-

branes, and it is thus connected to ξ via:

$$|u(r)| \approx \xi\sqrt{\frac{kT}{\kappa}} \approx d$$

We can consider the interactions between membranes as resulting from pressure due to undulations. Using Boltzmann's equation,

$$P = \frac{kT}{V} = \frac{kT}{Nd\xi^2} \approx \frac{(kT)^2}{\kappa d^3} \tag{1.29}$$

This leads to the free energy density per unit area F/S of the form,

$$V_{steric}(d) = \frac{F}{S} = A\frac{(kT)^2}{\kappa d^2} \tag{1.30}$$

The exact calculation using the Landau-de Gennes elastic energy for the smectics gives $A = 3\pi^2/128$[19]. Thus, this is the interaction which works repulsively between membranes, and becomes important only when the membranes are *flexible*, that is when κ is in the range of kT.

This steric interaction is an entropic effect as it costs energy to introduce order (the layer structure), to a disordered system. The free energy is of the order of $1/Kd^2$ Thus, in the case of $\kappa \gg kT$, this effect is not observable except when d is extremely small. This is probably why its discovery had to wait until fluid membranes with large flexibility were studied intensively.

1.4.2 Electrostatic interaction

Nonionic solvent

When ionic surfactants are mixed with nonionic solvents, they form membranes where the total charge is spread uniformly on the surface. As is always the case for the lamellae, the ends of surfactant molecules in adjacent membranes that have the same polarity face each other. Therefore the electrostatic interactions are always repulsive.

The contribution to the free energy per unit area from the electrostatic force, in first order to d, is proportional to $1/d$. It was precisely calculated by D. Roux [20] who obtained

$$V_{elec-nonion} = \frac{\pi^2 kT}{4L_e}\frac{1}{d}(1 - \frac{c}{L_e d} + \cdots). \tag{1.31}$$

Here L_e has units of length and it is defined as $L_e = \pi e^2/\epsilon kT$ [21], c is the surface area per charged polar head, e is the electron charge and ϵ is the surfactant characteristic energy as was introduced before and has typical values of the order of kT. (For pure water at room temperature, $L_e \approx 5$Å.)

Ionic solvent

When the solvent is ionic, the ions screen the charges on the surface of the membranes and the interactions between the membranes become proportional to the ion concentration in the solvent [22]. In this case

$$V_{elec-ion} = E_o exp(-\frac{d}{\lambda_D}) \tag{1.32}$$

Here λ_D is the Debye length which determines the range of the interaction, and is defined as $\lambda_D = 3.04/c$ where c is the ion concentration per $mole^{-1}$, E_o is proportional to σ^2/c, where σ is the surface charge density. Typically, the Debye length λ_D is much shorter than the periodicity. Thus for the system with beyond certain periodicity, addition of salt, which screens the charges of ionic surfactants, can be assumed to create a system without the electrostatic interaction.

1.4.3 Hydration interaction

At the surface of a membrane where the hydrophilic head groups lie, there exist a thin layer of water. As two surfaces approach, *dehydration* of the surface occurs.

The energy cost is the origin of the repulsive force between these surfaces. This force decays quickly and is given empirically as an exponential function of the distance[23].

$$V_H = H_o exp(-\frac{d}{\lambda_B}) \tag{1.33}$$

Here λ_B is a constant, typically $2 \approx 3\mathring{A}$, and H_o is a constant of the order of 2×10^3 erg. cm^{-2} This interaction dominates for distances less that 10 Å but is negligible for distances larger than 30Å.

1.4.4 Van der Waals interaction

The induced dipole-dipole interaction between the surfactant molecules in adjacent membranes is called the Van der Waals interaction. Since the axis of the dipole is perpendicular to the plane of the membrane, the interaction between membranes is attractive. It is well known that the force between the two dipoles is proportional to $1/d^6$. By integrating over the entire plane, we find that the energy of the two membranes which consists of vertically suspended dipoles is

$$V_{VDW} \approx \frac{-H}{12\pi}(\frac{1}{d^2} + \frac{1}{(d+2\delta)^2} - \frac{2}{(d+\delta)^2})$$

Where δ is the thickness of the membrane, d is the periodicity, and H is the Hamaker constant. Ninham et.al. [24] have evaluated this constant to be $\sim kT$, which was confirmed experimentally by Marra et.al.[25]. When $d \approx \delta$, $V_{VDW} \approx H/d^2$, but when $d \gg \delta$, $V_{VDW} \approx H\delta^2/d^4$.

Thus, for $\kappa \approx kT$, the Helfrich interaction is comparable to the VDW interaction for small periodicities, but becomes dominant as the periodicity increases. The electrostatic force decays very slowly with the layer separation. As a lamellar phase is swollen, it is the most intense force. By choosing a non-ionic surfactant, or adding salt to the solvent to screen the charges of the membranes, charge-neutral membranes can be created. In these cases, interactions between the membranes will be doninated

by the steric force, where the fluctuation itself is the origin of the stabilization of the phase. Until recently, charge-neutral membranes with small rigidity had not been studied. Thus the experimental exploration of this theoretically developed system is very interesting, and is the main goal of this thesis.

1.5 Elastic Constants

1.5.1 Non-Ionic Systems

For a non-ionic system, the dominant interaction is the steric interaction. The interaction potential per unit surface has been previously derived Eq. 1.30:

$$V_{steric}(d) = \frac{3\pi^2}{128}\frac{(kT)^2}{\kappa d^2} \tag{1.34}$$

Substituting into Eq. 1.20 we get:

$$\overline{B} = \frac{9\pi^2}{64}\frac{(kT)^2}{\kappa}\frac{d_{peq}}{d^4} \tag{1.35}$$

Using the relation $K = \kappa/d_{peq}$, and η as given in Eq. 1.11 we obtain the universal relation,

$$\eta = \frac{4}{3}(1 - \frac{\delta}{d_{peq}})^2 \tag{1.36}$$

For the dilute bilayer system the expansion around the equilibrium state gives ($d_0 \approx d_{peq} = d$). By substituting Eq. 1.30 into Eq. 1.17, 1.18 and 1.19, and using,

$$\epsilon = \frac{12\pi^2 v\kappa}{(1 - \frac{4}{\pi^2})\delta d^2}$$

as calculated by Lubensky et.al.[18], we find for the elastic constants:

$$\chi^{-1} \approx \frac{12\pi^2\rho^2 v^2\kappa}{(1-\frac{4}{\pi^2})m^2\delta^2 d}, \tag{1.37}$$

$$B \approx \frac{12\pi^2\kappa}{(1-\frac{4}{\pi^2})d^3}, \tag{1.38}$$

$$C_c \approx \frac{12\pi^2\rho v\kappa}{(1-\frac{4}{\pi^2})m\delta d^2},$$

and

$$\overline{B} \approx \frac{9\pi^2}{64}\frac{(kT)^2}{\kappa d^3}, \tag{1.39}$$

$\overline{B}$ only concerns the interaction, while B is related to the intrinsic energy of the bilayer and the interaction. From the relations above,

$$\frac{B}{\overline{B}} \approx \frac{256}{3-\frac{12}{\pi^2}}(\frac{\kappa}{kT})^2$$

In the case where $\kappa \simeq kT$, $B/\overline{B} \simeq 150$

1.5.2 Electrostatically Stabilized Lamellae

In the case of electrostatically stabilized lamellae in a nonionic solvent (Eq. 1.31 above)

$$V(d) \simeq \frac{\pi}{4}\frac{kT}{L_B d}$$

Thus,

$$\overline{B} = \frac{\pi}{2}\frac{kT}{L_B}\frac{d_{peq}}{d^3} \tag{1.40}$$

and

$$\eta = \sqrt{\frac{\pi k T L_B}{2\kappa d}(1-\frac{\delta}{d})^3} \tag{1.41}$$

With an approximation similar to that used for the steric system, we obtain,

$$\chi^{-1} \approx \frac{\rho^2 v \epsilon d}{m^2 \delta},\ B \approx \frac{\epsilon \delta}{v d},\ C_c \approx \rho \epsilon m$$

and

$$\overline{B} \approx \frac{\pi k T}{2 L_B d^2} \tag{1.42}$$

1.6 Dilution of a Lamellar Phase

As we have mentioned before, it is possible to swell a lamellar phase by reducing the concentration of the surfactant. With the swelling of this periodic system, some interesting phenomena have been observed.

The periodicity of the membranes exhibits a logarithmic dependence on the concentration caused by thermal fluctuations [26], [27]. This had, in the case of the bilayer system, allowed the extraction of the membrane bending rigidity k. Within the first order approximation, it is natural to imagine that the periodicity of lamellae is determined only by the concentration of the surfactant, as given by the dilution law,

$$d = \frac{\delta}{\phi}$$

where, δ is the bilayer thickness, and ϕ is the surfactant volume fraction. However, as the fluctuation amplitude increases, because of the difference of the actual surface area of the membranes and the projected area, the increase of the periodicity deviates from being proportional to $1/\phi$. In order to describe this idea, we will again use the model of a membrane between two walls. For an undulating membrane, the relation

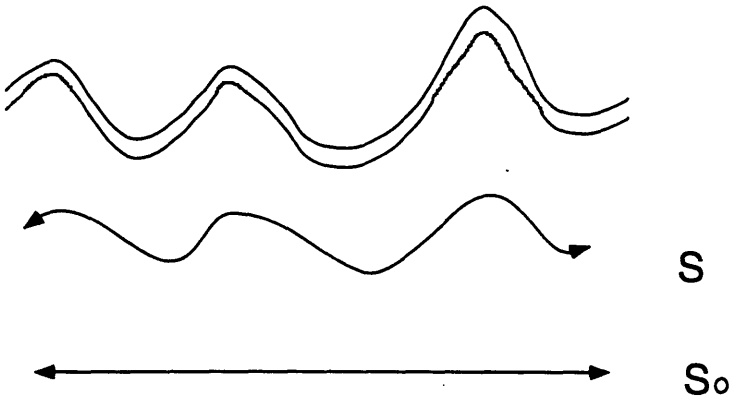

Figure 1-11: The *Actual* membrane area S and the *projected* area S_o

between the projected area(S) and the actual surface area of the membrane(S_o) can be written as,

$$S = S_o[1 + \Delta S]$$

$$S = S_o[1 + \frac{1}{2}(\nabla u)^2]$$

Now, as described before, for a *sandwiched* membrane we have Eq. 1.25,

$$< u_q^2 >= \frac{kT}{\kappa q^4}$$

Thus,

$$\Delta S \sim \frac{1}{2}\int_{qmin}^{qmax} \frac{kTq^2}{\kappa q^4} 2\pi q dq$$

$$\sim \frac{kT}{\kappa} ln\frac{\xi}{\delta} \tag{1.43}$$

As $\xi \approx d$, (Eq. 1.4.1), and $\delta/d = \phi$ to first order, and $S_o = V/d$, $S = \phi V/\delta$, we get:

$$S \sim S_o[1 + \frac{kT}{\kappa} ln\frac{d}{\delta}]$$

$$S \sim S_o[1 + \frac{kT}{\kappa} ln \frac{1}{\phi}]$$

This leads to,

$$d \sim \frac{\delta}{\phi}[1 + \frac{kT}{\kappa} ln \frac{1}{\phi}] \tag{1.44}$$

The exact calculation gives[27],

$$d = \frac{\delta}{\phi}[1 + \frac{kT}{4\pi\kappa} ln(c\frac{\delta}{a}\sqrt{\frac{\kappa}{kT}}\frac{1}{\phi}] \tag{1.45}$$

Here, a is the square root of the area per polar head for a surfactant molecule. Typically $a \sim 5$Å, c is a model dependent constant, and for dilute lyotropic smectic-A phases, Glubovic et.al. [18] have proposed $c = (32/3\pi)^{1/2} \approx 1.84$. δ is the thickness of the membrane. This shows that the periodicity of the fluctuating membranes deviates from the linear dilution law and shows a logarithmic correction, The correction part is proportional to the temperature, and the logarithm of the surfactant volume fraction.

Chapter 2

X-ray scattering : Theory

In this chapter, the theory of x-ray scattering from lamellar phases will be described. X-ray scattering is a powerful technique to probe the structure of materials in the atomic/molecular scale, when the characteristic length of the system is comparable to the wavelength of the x-rays(CuK_α : $\lambda \simeq 1.54$ Å). The x-rays are scattered by the electrons in the matter. Thus, they contain direct information on the positional correlations of the atomic electrons.

One of the features of the interaction between x-rays and atomic electrons is that because of the high energy of an x-rays ($\sim 10KeV$)photon compared to the electronic energy $\sim eV$, the difference in the magnitude of the incoming and the outgoing wave vectors is negligible. The scattering under this condition is called quasi-elastic where,

$$|\mathbf{k_{in}}| \approx |\mathbf{k_{out}}|$$

The scattering vector is defined by the difference between the incident and scattered x-rays,

$$\mathbf{q_{scattered}} = |\mathbf{k_{out}} - \mathbf{k_{in}}|$$

The incident photon is scattered by the electron cloud of the material which has

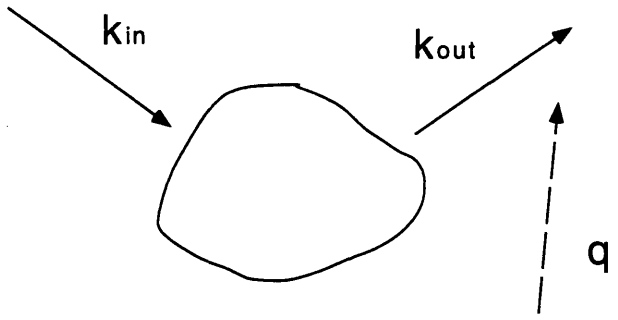

Figure 2-1: The scattering of x-rays by matter.

density $\rho(x)$. The scattering cross section is proportional to ρ. The amplitude of the scattered x-ray can be written as

$$A(\mathbf{q}) = \int_V \rho(\mathbf{x}) \mathbf{e}^{\mathbf{iq \cdot x}} \mathbf{d}^3\mathbf{x} \tag{2.1}$$

The Intensity scattered by the volume V is,

$$I(\mathbf{q}) = < | \int_V \rho(\mathbf{x}) \mathbf{e}^{\mathbf{iq \cdot x}} \mathbf{d}^3\mathbf{x}|^2 > \tag{2.2}$$

The precise derivation of this equation is done in Joel Brock's thesis[28].

2.1 Scattering from a one-dimensional periodic system: Lamellae

Let us model a lamellar system as a one-dimensional periodic order with no fluctuations. Such a system will be a regularly spaced stack of N membranes with periodicity d_p, and thickness δ. The density distribution along the z direction (defined as parallel to the layer normal) of the system is,

$$\rho(\mathbf{x}) = \sum_0^{N-1} \rho_o(z - nd) \qquad \text{for } x_\perp < L \tag{2.3}$$

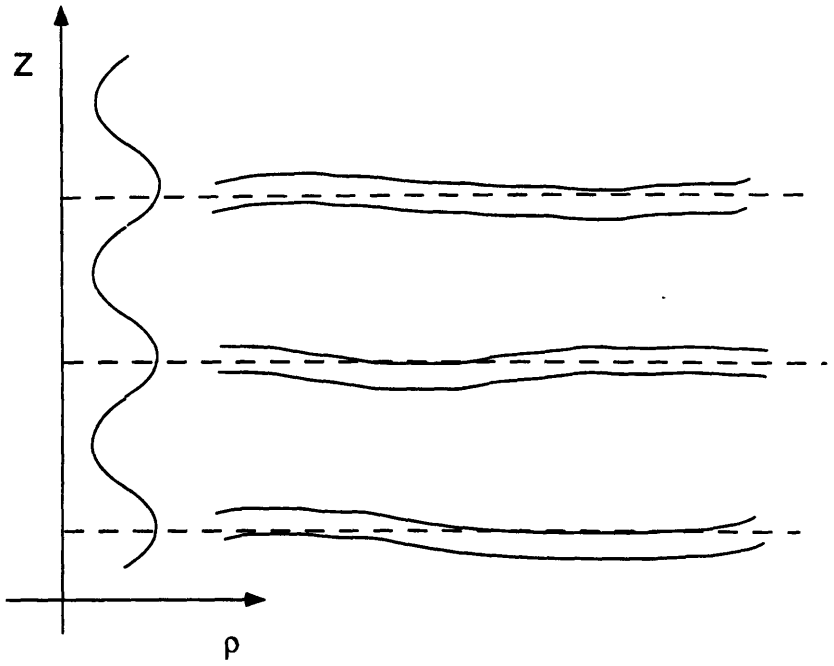

Figure 2-2: The schematic of the surfactant density as a function of z.

Here $\rho(\mathbf{x})$ is the density profile of membranes stack of N within the crystal with transverse size L, and $\rho_o(z) \neq 0$ only when $0 < z < \delta$. Substituting into Eq. 2.2, the intensity profile can be rewritten as,

$$I(\mathbf{q}) =< | \sum_{n,m=0}^{N-1} e^{iq_z(m-n)d} || \int\int\int \rho_o(\mathbf{r}) e^{i\mathbf{r}\cdot\mathbf{q}} d\mathbf{r}|^2 > \tag{2.4}$$

The first factor represents the structure factor$S(\mathbf{q})$:

$$\sum_{n,m=0}^{N-1} e^{iq_z(m-n)d} \tag{2.5}$$

The second part of the Eq. 2.4 is the form factor of a unit cell:

$$|\int\int\int \rho_o(\mathbf{r})e^{i\mathbf{q}\cdot\mathbf{r}}d\mathbf{r}|^2 \tag{2.6}$$

The size of this unit cell in the z-direction is the thickness of the membrane δ and L is the in the in-plane width.

We now introduce a parameter to describe thermal fluctuations. As shown in chapter 1, this is the surface displacement u. The density function Eq. 2.3 can be written as,

$$\rho(\mathbf{x}) = \sum_{0}^{N-1} \rho_o(z - nd + u_n) \qquad \text{for} x_\perp < L \tag{2.7}$$

Where u_n is the displacement of the nth layer from its equilibrium position. Substituting into 2.4, we get as the structure factor,

$$S(\mathbf{q}) = \sum_{n,m=0}^{N-1} e^{iq_z(m-n)d} \int\int d^2r_\perp d^2r'_\perp e^{i\mathbf{q}\cdot(\mathbf{r}_\perp - \mathbf{r}'_\perp)} < exp(iq_z(u_n(r_\perp) - u_m(r'_\perp))) >, \tag{2.8}$$

The structure factor contains the undulation originated from the displacement u_n. If we assume that the thermally undulating membranes have no internal structure, i.e. *infinitesimally thin membranes*, the density profile Eq. 2.4can be written as a δ function. Since the Fourier transform of the δ function is a constant, the intensity is the structure factor multiplied by a constant.

2.1.1 Smectic Structure Factor

Caillé has calculated the structure factor for smectic liquid crystals under the approximation that the density is a continuous function of the positional vector $\mathbf{r}$ in all direction, which corresponds to the approximation that $L = nd_p \rightarrow \infty$. The structure factor can be written as the fourier transform of the density density correlation

function in three dimension:

$$S(q) \sim \int e^{-i\mathbf{q}\cdot\mathbf{r}} g(\mathbf{r}) d\mathbf{r}, \tag{2.9}$$

where $g(\mathbf{r})$ is the density density correlation function:

$$g(\mathbf{r}) = < \rho(\mathbf{r})\rho(\mathbf{0}) >, \tag{2.10}$$

In the case of thermotropic smectics that consist of infinitesimally thin membranes, this correlation function includes only contributions from the thermal fluctuations of the membranes. The electronic density distribution is:

$$\rho(\mathbf{r}) = Acos[q_z(z - u(\mathbf{r}))], \tag{2.11}$$

then within the harmonic approximation, where $u(\mathbf{r})$ is much smaller than the periodicity of the smectic ($< |u(\mathbf{r}) - u(\mathbf{0})|^2 > /d^2 \ll 1$), $u(\mathbf{r})$ can be considered to be a Gaussian variable. It will be shown later that the amplitude of this displacement $u(\mathbf{r})$ caused by thermal fluctuations is a function of temperature. By increasing the temperature, it increases to the point where this condition does not apply anymore. In such cases however, the system undergoes a phase transition from the smectic phase to a more disordered phase. Thus, the density correlation function takes the form,

$$g(\mathbf{r}) = A^2 cos(q_z z) exp(\frac{-q_z^2}{2} < |u(\mathbf{r}) - u(\mathbf{0})|^2 >) \tag{2.12}$$

In order to calculate $< |u(\mathbf{r}) - u(\mathbf{0})|^2 >$, expression for the free energy derived for the thermotropic smectics was used Eq. 1.9. Using the equipartition theorem as it was done in the Chapter 1 for calculating $|u_q|^2$, and by including the phase factor, we obtain

$$< |u(\mathbf{r}) - u(\mathbf{0})|^2 >= \frac{2}{(2\pi)^3} \int < |u(\mathbf{q})|^2 > (1 - e^{-i\mathbf{q}\cdot\mathbf{r}}) d\mathbf{q},$$

Substituting in Eq. 1.10, one finds

$$< |u(\mathbf{r}) - u(\mathbf{0})|^2 >= \frac{2kT}{(2\pi)^3} \int \frac{(1 - e^{-i\mathbf{q}\cdot\mathbf{r}})}{\overline{B}q_z^2 + Kq_\perp^4} 2\pi q_\perp dq_\perp dq_z,$$

where $\overline{B}$ is the compressibility constant and K is the bending constant. Note here that his approximation for $z \to \infty$ results in replacing the summation for each descrete mode in q_z by the integral. By extending the q_z upper limit to ∞, the calculation described in the Appendix gives,

$$< |u(\mathbf{r}) - u(\mathbf{0})|^2 >= \frac{kT}{4\pi\sqrt{K\overline{B}}} (2\gamma + 2ln(\frac{r_\perp^2}{a^2}) + E_1(\frac{r_\perp^2}{4\lambda|z|})) \tag{2.13}$$

where $\lambda = \sqrt{K/\overline{B}}$ is the penetration depth, $\gamma = 0.5772156649...$, is Euler's constant and $E_1(x)$ is the exponential integral function,

$$E_1(x) = \int_x^\infty \frac{e^{-t}}{t} dt$$

$$E_1(x) = -\gamma - lnx - \sum_{n=1}^{\infty} \frac{(-1)^n x^n}{n(n!)}$$

Substituting into Eq. 2.12 we obtain[29],

$$g(\mathbf{r}) = e^{-2M} (\frac{2d}{r_\perp})^{2M} exp(-ME_1(r_\perp^2)/4\lambda z) \tag{2.14}$$

Here M is the Debye-Waller factor:

$$M = q^2 \frac{kT\gamma}{8\pi\sqrt{\overline{B}K}} \tag{2.15}$$

In the vicinity of scattering vector close to $q = q_0$ Eq. 2.14 can be written as,

$$g(\mathbf{r}) = e^{-2\eta} (\frac{2d}{r_\perp})^{2\eta} exp(-\eta E_1(r_\perp^2)/4\lambda z) \tag{2.16}$$

We also define ,

$$\eta_m = \frac{q_m^2 kT}{8\pi\sqrt{K\overline{B}}} = \frac{(q_0 m)^2 kT}{8\pi\sqrt{K\overline{B}}} = m^2\eta \tag{2.17}$$

where m is the integer which determines the higher harmonic terms. From the density density correlation function Eq. 2.14, we can see that the correlation decays with $r_\perp$ and z as a power law with exponent M, rather than exponentially which in the vicinity of quasi Bragg-peak position, M becomes η. This is the characteristic of a two-dimensional system. We can look at the asymptotic limits: $r_\perp = \sqrt{x^2+y^2} \ll z$. or $z \ll r_\perp$,

In these limits, the correlation function calculated from Eq. 2.14 takes the forms,

$$g(\mathbf{r}) = \begin{cases} (\frac{d^2}{\lambda z})^M exp(-M\gamma), & r_\perp \ll (\lambda z)^{1/2} \\ (\frac{2d}{r_\perp})^M exp(-2M\gamma), & r_\perp \gg (\lambda z)^{1/2} \end{cases} \tag{2.18}$$

Here, it is assumed that smectic structure is uniform in the plane, so x and y are treated equally.

The Fourier transform of Eq. 2.14 gives the intensity profile. Because of the E_1 function, it is impossible to perform the integration explicitly, but instead, the asymptotic cases can be again calculated.

$$S(q_\perp, q_z) = \int d^2 r_\perp dz e^{-iq_\perp r_\perp} e^{-i(q_z)z} g(\mathbf{r}) \tag{2.19}$$

In order to see the q dependence close to the quasi-Bragg peak, we substitute $q = q_0$, and by replacing M by η we get,

$\underline{\mathbf{q_\perp = 0}}$

$$S(0, q_z) \sim \int d^2 r_\perp dz e^{i(q_z - q_0)\cdot z} (\frac{4d^2}{r_\perp^2}) e^{-\eta E_1(r_\perp^2/4\lambda z)} \tag{2.20}$$

By changing the variable, $r_\perp^2/4\lambda z = y$ also $d^2 r_\perp = r_\perp dr_\perp d\phi$, this becomes,

$$S(0, q_z) \sim \int dz e^{i(q_z - q_0)} z^{1-\eta} \int dy y^{-\eta} exp(-\eta E(y)) \tag{2.21}$$

where the last integral is a constant. Through dimensional arguments we can get,

$$S(0, q_z) \sim \frac{1}{|q_z - q_0|^{2-\eta}} \tag{2.22}$$

By a similar calculation and by changing $4\lambda z/r_\perp^2 = \tilde{y}$ we get,

$\underline{\mathbf{q_z = 0}}$

$$S(q_\perp, 0) \sim \frac{1}{q_\perp^{4-2\eta}} \tag{2.23}$$

These are the well known asymptotic structure factors of the smectic-A liquid crystals. $\underline{\mathbf{q_\perp = 0}}$

A similar calculation for the correlation function of displacements has been done by Gunter et al[30], and more recently in an unpublished work by Zhang et.al. In their calculations, they use nd_p in stead of z where d_p is the periodicity of the smectics and q_z by $n\pi/L$. Thus, for the calculation of their correlation function, they replaced the z-direction calculation by the summation over n where n is the index of the layer.

The calculation of Gunter et. al. gives,

$$< |u_n(r_\perp) - u_0(0)|^2 > \simeq \frac{kT}{4\pi\sqrt{\bar{B}K}}[ln(\frac{r_\perp}{2a})^2 + 2\gamma + E(\frac{r_\perp^2}{4\lambda|z|}) - f(\frac{\lambda d_p}{\pi a^2})] \tag{2.24}$$

by using Eq. 2.12,

$$g(\mathbf{r}) = (\frac{2d}{r_\perp})^{2X} e^{-2B} exp(-XE_1(r_\perp^2)/4\lambda z) \tag{2.25}$$

$E(x)$ is the same integral function which was introduced for the Caillé's function. X, B are defined by,

$$X \equiv \frac{q_z^2 kT}{8\pi\sqrt{K\bar{B}}} \quad , \quad B = \frac{X}{2}(2\gamma - f(\frac{\lambda d_p}{\pi a^2})) \tag{2.26}$$

Here $f(x)$ is

$$f(x) = \frac{2}{\pi}\int_0^x dy \frac{tan^{-1}y}{y} \tag{2.27}$$

Their result differs from Caillé's function by the introduction of the function $f(x)$.

As $x \rightarrow \infty$, $f(x)$ diverges logarithmically:

$$f(x) \rightarrow ln(x) \tag{2.28}$$

The calculation by Zhang et.al gives:

$$< |u(r_\perp, z) - u(0,0)|^2 >= \frac{2\eta}{q_0^2}(\sum_{n=0}^{N} \frac{1 - cos(n\pi z/L)}{n} + \frac{r_\perp^2}{4\lambda z}) \tag{2.29}$$

Very close to the m-th order peak, the approximation $q_z = q_m$ was made in Eq. 2.12 where q_m is defined as $q_m = mq_0$. Also by employing the relation $\eta_m = m^2\eta$, they get,

$$g(\mathbf{r}) = exp(-\eta_m \sum_{n=0}^{N} \frac{1 - cos(n\pi z/L)}{n}) exp(\frac{-\eta_m r_\perp^2}{4\lambda z}) \tag{2.30}$$

The difference between the two is that Zhang accounts for the finite size of the system, Gunter et.al.'s calculation is done for an infinite size approximation. The calculation of these two density density correlation functions shows however, a close agreement by substituting $q_z \sim q_m$ in the calculation by Gunter et.al. except of very large z where the infinite size approximation deviates from the calculation done for the finize size sample. The comparison was done by Zhang et.al. along with the comparison with the Caillé's correlation function. They showed that both of them have a significantly higher value than Caillé's correlation function Eq. 2.14. The ratio was shown to be,

$$\frac{g(\text{Gunter, Zhang})}{g(\text{Caillé})} = (\frac{4\pi\lambda d_p}{a^2})^{\eta_m} > 1 \tag{2.31}$$

For lipid bilayers, $d_p\lambda > a^2$, where λ is the penetration depth, d_p is the periodicity, and a is the intermolecular distance between the surfactants. η_m is positive by definition.

2.1.2 Fluctuations of the Concentration

As we have seen in the first chapter in the case of lyotropic lamellae, we have to take into account the concentration fluctuations. The electronic density is a function of both concentration and displacement $u(\mathbf{r})$ From Eq. 2.11, we have ,

$$\rho(\mathbf{r}) = \rho(c+ < \delta c(\mathbf{r}) >) + A < cos[q_z z - u(\mathbf{r})] > \tag{2.32}$$

In order to calculate the correlation functions of the concentration and the displacement, we can start from the free energy expression, Eq. 1.12.

Using the equipartition theorem, and the calculation done in the Appendix, we get, [31], [32]

$$< |u_{\mathbf{q}}|^2 >= \frac{kT}{\overline{B}q_z^2 + Kq_\perp^4} \tag{2.33}$$

$$< \delta c(\mathbf{q})\delta c(-\mathbf{q}) >= -\frac{\chi(q)kT(Bq_z^2 + Kq_\perp^4)}{\overline{B}q_z^2 + Kq_\perp^4} \tag{2.34}$$

$$< |\delta c(\mathbf{q})u_{-\mathbf{q}}| >=< |u_{\mathbf{q}}\delta c(-\mathbf{q})| >= i\frac{kT\chi C q_z}{\overline{B}q_z^2 + Kq_\perp^4} \tag{2.35}$$

The density-density correlation function, which contributes to the intensity profile, can be written as [32],

$$g(\mathbf{r}) = \rho^2 < \delta c(\mathbf{r})\delta c(\mathbf{0}) > + A^2 cos(q_z z) exp[-\frac{q_z^2}{2} < |u(\vec{r}) - u(\vec{0})|^2 >] \tag{2.36}$$

The Fourier transform of the density correlation, Eq. 2.36, gives the expression for the intensity scattered by a two-component smectic-A. It contains two terms: The first term comes from the concentration fluctuations $< \delta c(\vec{r})\delta c(\vec{0}) >$ and the second term is the quasi-Bragg part, related to the smectic ordering. Thus

$$I(\mathbf{q}) = \rho^2 < \delta c(-\mathbf{q})\delta c(\mathbf{q}) > + \int d\mathbf{r} e^{-i\mathbf{q}\cdot\mathbf{r}} cos(q_z z) exp[-\frac{q_z^2}{2} < |u(\vec{r}) - u(\vec{0})|^2 >] \quad (2.37)$$

Scattering at $q \to 0$

While the intensity profile originating from concentration fluctuation was given by the correlation function in the Eq. 2.34, in fact χ is a decreasing function of q [32]. In order to calculate explicitly the intensity increase at small q, we have to include the higher order terms for the concentration fluctuations in the free energy. As it was calculated in [32],

$$\chi(q) = \frac{\chi}{1 + \xi_z^2 q_z^2 + \xi_\perp^2 q_\perp^2} \quad (2.38)$$

where χ is the osmotic compressibility of the membrane as defined in Chapter 1, and ξ_z , $\xi_\perp$ are the correlation lengths for the concentration fluctuations along and perpendicular to the layer normal respectively. This gives the small angle excess scattering. From Eqs. 2.34 and 2.37, it can be shown that the intensity increases anisotropically at low q in q_z direction and $q_\perp$ directions.

$$< \delta c(q_z, 0)\delta c(-q_z, 0) > \to \ kT\frac{\chi B}{\overline{B}} \quad \text{as } q_z \to 0 \quad (2.39)$$

$$< \delta c(0, q_\perp)\delta c(0, -q_\perp) > \to kT\chi \quad \text{as } q_\perp \to 0 \quad (2.40)$$

Quasi-Bragg peak

The second term in Eq. 2.37 which originates from the quasi-Bragg scattering is the same as the classical structure factor of the one-component smectic-A. It also diverges anisotropically as a function of q in the vicinity of the Bragg peak position as shown in Eqs. 2.22, 2.23.

It had been shown[30] that the intensity of the first order Bragg peak scales as $\lambda^{1-\eta}/d^2$, where λ the penetration length that was introduced before, can be written as $\lambda = (K/\overline{B})^{1/2}$. Substituting for K and $\overline{B}$ from Eqs. 1.35 and 1.22, for a sterically interacting system, λ can be written as, $\lambda = (8/3\pi)(\kappa d/kT)$. Thus, the quasi Bragg peak intensity decreases as $d^{-1-\eta} \sim q_0^{1+\eta}$, i.e., with the increase of the periodicity. On the other hand, for the scattering at $q \to 0$, the intensity is proportional to $\chi(q)$ which, at $q = 0$ is proportional to d_p, which is the periodicity of the smectics.

Experimentally, it is not possible to separate the scattering at $q \to 0$ from the tail of the quasi-Bragg peak, and to date there exist no quantitative measurements of the the small angle scattering($q \to 0$) without the contribution from quasi-Bragg peak.

Safinya et.al. [2] have constructed the structure factor by using Caillé's expression in the vicinity of the Bragg peak position, taking into account the finite size effects and the powder averaging, while neglecting the scattering at low q. Starting with the definition of the structure factor,

$$S(q) \propto \int d\mathbf{r} g(\mathbf{r}) e^{-i\mathbf{qr}}, \tag{2.41}$$

where $g(\mathbf{r})$ is given above 2.14. We introduce the average crystalline size of the powder sample L, as it was introduced by Dutta and Sinha [33], where they have modeled finite size effects by a Gaussian function. In order to perform the powder averaging the scattered intensity was averaged over the sphere of equally probable orientations with q being fixed in space, which in fact is equivalent to averaging the scattering vector over all possible directions. Taking the real part of the exponential and using $q_\perp = qsin\theta$ $q_z = qcos\theta$, we find

$$e^{-i\mathbf{q}\cdot\mathbf{r}} = \frac{sinqr}{qr} \tag{2.42}$$

$$S(q) \propto \int_{-\infty}^{\infty} dz \int_0^{\infty} dr_\perp g(r_\perp, z) exp(-\frac{\pi r^2}{L^2}) \frac{sinqr}{qr} e^{-izq_o} \tag{2.43}$$

where $q_o = 2\pi/d_p$

2.1.3 Scattering From the Finite Size Thickness Bilayer

For all of the above, we considered membranes that were infinitesimally thin. In reality, membranes have a finite size. Therefore, a zero thickness description is inadequate for describing the lineshape of the scattered x-rays, especially when the bilayer thickness becomes comparable to the periodicity itself.

Nallet et al.[34] have recently modeled the scattering spectrum of lyotropic bilayers of finite thickness by taking into account both the structure factor and the form factor and also by including harmonic effects in the structure factor expression.

Under the assumption that the the displacement of the nth layer u_n around its equilibrium position $z = nd_p$, is a function of only z and it is independent of the transverse coordinates, which corresponds to the case where the curvature energy is negligible compared to the compression energy, the electronic density distribution Eq. 2.3 can be written as,

$$\rho(\mathbf{x}) = \sum_{0}^{N-1} \rho_o(z - nd + u_n), \qquad x_\perp < L_\perp \tag{2.44}$$

$$\rho(\mathbf{x}) = 0, \qquad \text{otherwise} \tag{2.45}$$

Substituting into Eq. 2.4, and by similar calculation as for Eq. 2.4 we obtain,

$$I(\mathbf{q}) = < \sum_{n=0}^{N-1} e^{iq_z n d_p} < exp(iq_z(u_n - u_0)) > | \int_0^\delta \int_0^L dr_\perp \rho(\mathbf{r}) e^{i\mathbf{q}\cdot\mathbf{r}} dz dr_\perp |^2 > \tag{2.46}$$

$$I(\mathbf{q}) = \sum_{0}^{N-1} cos(nq_z d_p) e^{-\frac{q_z}{2} < |u_n - u_0|^2 >} < | \int_0^\delta \int_0^L \rho(\mathbf{r}) e^{i\mathbf{q}\cdot\mathbf{r}} dz dr_\perp |^2 > \tag{2.47}$$

The intensity can be described as the product of the structure factor and the form factor. Assuming the in-plane form factors in the x and y-direction to be equal, and $P(q_x)P(q_y) = P(q_\perp)$, and

$$I(\mathbf{q}) = NS(\mathbf{q})P_z(\mathbf{q_z})P_\perp(\mathbf{q}_\perp) \tag{2.48}$$

$S(\mathbf{q})$, is the structure factor with the higher order harmonic terms , $P_\perp(\mathbf{q}_\perp)$, and $P_z(\mathbf{q_z})$ are the form factors of lamellae, in-plane and in the z direction respectively.

Form factor :along the z-axis

The form factor in the z-direction is the mean square of the Fourier transform of the density profile of the membrane in that direction:

$$P_z = |\int_0^\delta \rho(z)e^{iqz}dz|^2 \tag{2.49}$$

where δ is the thickness of the bilayer, and $\rho_(z)$ is the electronic density difference between water and oil. In a simplistic bilayer model, the density profile is modeled as follows: The electronic density of the *head* is assumed to be the same as that of water, while the density of the *tail* is assumed to be the same as that of oil. This assumption should not be too far from the reality since the chemical composition of the *tails* is $C_{12}H_{25}$. The electronic density of the molecule which is the closest to this structure is that of $C_{12}H_{26}$ (0.26 $e/\mathring{A}^3$) while octane is C_8H_{18} and the electronic density is (0.24 $e/\mathring{A}^3$). For the *head* part, the electronic density for the ether $[CH^2 - CH^2 - O]^n$ is 0.37, while it is 0.33 for water.

Using the model shown schematically in Fig. 2-3,

$$\rho(z) = \begin{cases} \rho_{water} - \rho_{oil}, & 0 \leq z \leq \delta \\ 0, & \text{otherwise} \end{cases} \tag{2.50}$$

This leads to,

$$P_z = \frac{4}{q_z^2}(\rho_{water} - \rho_{oil})^2 sin^2(q_z\delta/2) \tag{2.51}$$

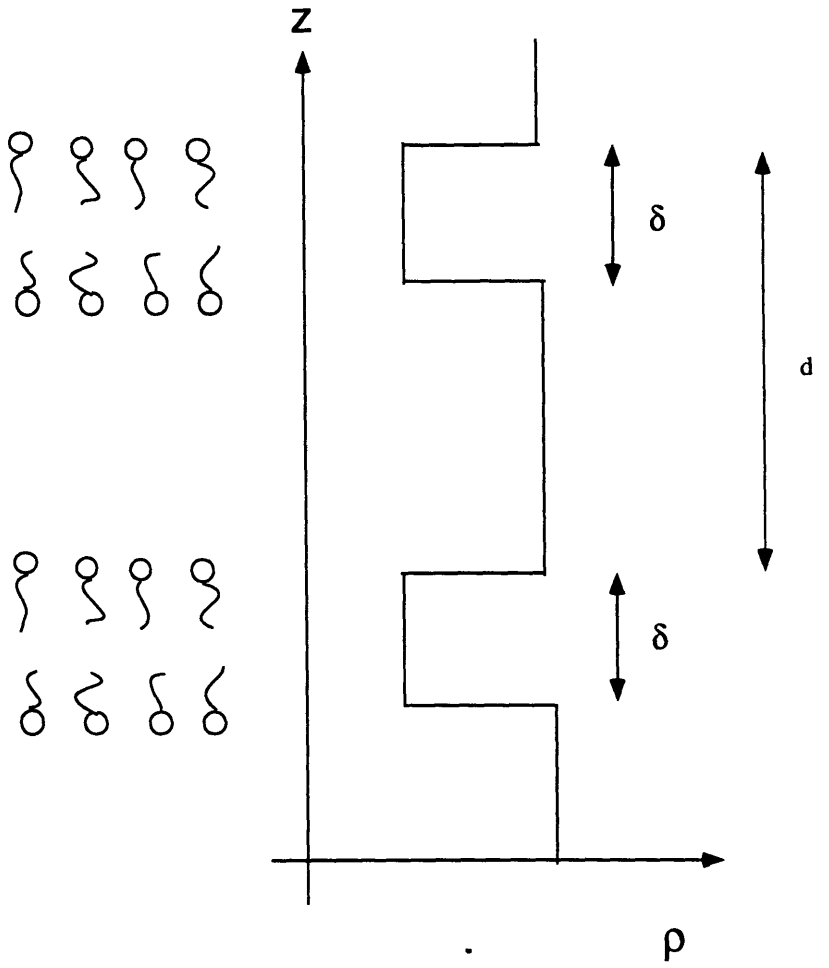

Figure 2-3: The density profile modelled for the L_α phases

Form factor: in-plane

The form factor in the in-plane ($\perp$) direction, which is correlated to the domain size L, is not as obvious as for the z-direction form factor. We can model the unit cell for the electronic density of the membrane for in-plane direction to have a disk-like shape and of radius L. We can also assume that the density is uniform inside this unit cell. From a calculation similar to that done for P(z), but with L instead of δ, we get,

$$P_\perp = |\int_0^L e^{iqx}dx \int_0^L e^{iqy}dy|^2 \tag{2.52}$$

where we have assumed that the density is uniform in the in-plane direction for the membrane. This leads us to

$$P_{\perp} = \frac{4}{(q_x q_y)^2} sin^2(q_x L/2) sin^2(q_y L/2) \tag{2.53}$$

Structure factor

Using 2.24 for the calculation of the structure factor, and assuming we can ignore the transverse correlation, ($r_{\perp} \rightarrow o$, and $z = nd$) the correlation function of only n $< (u_n - u_0)^2 >$ can be shown to be

$$< |u_n(r_{\perp}) - u_0(0)|^2 >= \frac{\eta}{2\pi^2}[ln(\pi n) + \gamma + ln\frac{\lambda d_p}{a^2} - f(\frac{\lambda d_p}{\pi a^2})] \tag{2.54}$$

By approximating $f(\lambda d_p/\pi a^2) = ln(\lambda d_p/a^2)$ under the assumption $\lambda d_p \gg a^2$, we can rewrite this as,

$$< (u_n - u_0)^2 >= \frac{\eta}{2\pi^2}[ln(\pi n) + \gamma] d_p^2 \tag{2.55}$$

From Eq. 2.48 the structure factor can be written as,

$$S(q_z) = 1 + 2\sum_{1}^{N-1}(1 - \frac{n}{N})cos(nq_z d_p) e^{-\frac{q_z^2}{2}<(u_n - u_0)^2>}$$

Note that we did not make the approximation $q_z = q_m$ to get the structure factor.

Convolution with the Resolution function

In the detection of the scattered intensity, the finite instrumental resolution must be taken into account. Calling $R(q)$ the resolution function, we can express the convoluted intensity as

$$I_r(\mathbf{q}) = \int I(\mathbf{q}') R(\mathbf{q} - \mathbf{q}') d^3\mathbf{q}' \tag{2.56}$$

The resolution funcion $R(q)$ can modeled as a Gaussian function of width ∇q,

$$R(q) = (2\pi \nabla q^2)^{-2/3} e^{-\frac{q^2}{2\nabla q^2}} \tag{2.57}$$

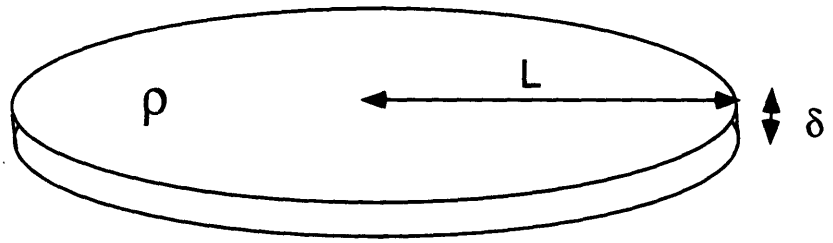

Figure 2-4: The disk-like electron density model used for the derivation of the form factor

with ∇q (Full width at half maximum:FWHM) .

In the in-plane direction, normally the resolution is much wider than the inverse of the size of the crystals. (From microscopy observations the crystal size in the powder sample is typically $\approx 5\mu m$, which corresponds to $\approx$ 1e-5 Å^{-1} for the powder sample, and much larger for the oriented sample: $L_\perp \nabla q \gg 1$ and $Nd\nabla q \gg 1$). Since $P_\perp(q_\perp)$ is a much sharper function of $q_\perp$ than the resolution function, we can approximate the form factor by a δ function. Thus, convoluting the resolution function, modeled as a Gaussian function, we get

$$P_{r\perp}(q_\perp) = \frac{2\pi L^2}{\nabla q^2} exp(-\frac{q_\perp^2}{2\nabla q_\perp^2}) \tag{2.58}$$

In the z direction, the structure factor varies much more rapidly with q_z, than the form factor P_z. Therfore, we approximate the convolution of the resolution function *only* with the structure factor.

$$S_r(q_z) = 1 + 2\sum_1^{N-1}(1-\frac{n}{N})cos(\frac{nq_z d_p}{1+2\nabla q^2 d_p^2 \alpha(n)})\ exp(\frac{2q_z^2 d_p^2 \alpha(n) + \nabla q^2 d_p^2 n^2}{2(1+2\nabla q^2 d_p^2 \alpha(n))}) \times$$

$$\times \frac{1}{\sqrt{1+2\nabla q^2 d_p^2 \alpha(n)}} \quad (2.59)$$

Where $\alpha(n) \equiv < (u_n - u_0)^2 > /2d_p^2$. Thus, the intensity convoluted with the resolution can be written as.

$$I_r(\mathbf{q}) = P_{r\perp}(q_\perp) S_r(q_z) P_z(q_z)$$

Powder averaging

For a randomly oriented "*powder*" sample, we have to integrate the scattering vector over all possible directions in space. Since $P_{r\perp}(\mathbf{q}_\perp)$ is a much more rapidly varyng function of $q_\perp$ than $P_z(q_z)$ or $S(q_z)$ are of q_z, we can assume P_z and S to be constants, taken at the point where $P_{r\perp}$ is maximum. Thus the powder average becomes,

$$< P_{r\perp}(q_\perp) >_{powder} = \int\int \frac{sin\theta d\theta d\phi}{4\pi} P_{r\perp}(\mathbf{q}_\perp) \quad (2.60)$$

With $\mid q_\perp \mid = |\mathbf{q}| sin(\theta) \equiv q sin(\theta)$, the form factor integrated over entire space takes the form,

$$< P_{r\perp}(q_\perp) >_{powder} = 2\int_0^{\pi/2} \frac{sin\theta d\theta}{2} P_{r\perp}(q sin(\theta)) \quad (2.61)$$

Substituting Eq. 2.58 into Eq. 2.61 and with $x = cos(\theta)$ we get,

$$< P_{r\perp}(q_\perp) >_{powder} = \frac{2\pi L^2}{(\nabla q)^2} \int_0^1 dx\ exp(-\frac{q^2}{2(\nabla q)^2}(1-x^2)) \quad (2.62)$$

This is the powder averaged form factor in the in-plane direction. For q much larger than ∇q, we notice that the integrand is always very small except at $x \approx \pm 1$, thus, by approximating $(1-x^2) \approx 2(1-x)$, and changing the variable $1-x = u$ we get,

$$< P_{r\perp}(\mathbf{q}_\perp) >_{powder} = \frac{2\pi L_\perp^2}{(\nabla q)^2} \int_0^1 du\ exp(-\frac{q^2}{(\nabla q)^2} u) \quad (2.63)$$

$$\simeq \frac{2\pi L_\perp^2}{(\nabla q)^2}\int_0^\infty du\ exp(-\frac{q^2}{(\nabla q)^2}u) \tag{2.64}$$

$$= 2\frac{L_\perp^2}{q^2} \tag{2.65}$$

Note that this approximation is only valid with the condition $q/\nabla q \gg 1$, because of the assumption we made above.

Finally, using the relation $N = V/dL^2$, we can write the intensity as,

$$I(\mathbf{q}) = 2\pi\frac{NL^2}{q^2}P(\mathbf{q})S(\mathbf{q}) \tag{2.66}$$

Chapter 3

Experimental Techniques

In this chapter, we will describe the system which was investigated. The description of the sample preparations will be given first, followed by a description the techniques used for the characterization of the samples. Then, the established phase diagrams will be given. Finally, we will describe the various x-ray scattering techniques used for data acquisition.

The system we studied is a mixture of surfactant, water and oil. The surfactant was is $C_{12}E_5$ (Pentaethylene-glycol-monododecyl-ether). The chemical structure is given in Fig. 3-2. The essential character of this surfactant is that it is non-ionic. By comparison with the more commonly studied surfactants which are ionic, the special interest of our system is its total suppression of the electrostatic effects so that we can study a purely sterically stabilized system. In order to study the steric interaction, in a system with an ionic surfactant, salt must be added to screen the electrostatic interaction. This makes the system at least ternary, or quaternary if there are two solvents. In our case, the number of components is kept minimal, and its physical chemistry becomes simpler to describe.

The second and even more important reason for which the present system attracted our interest is related to its phase diagram: Various phases are stable within an accessible range of temperature. Moreover in certain regions of the phase diagram: it is possible to go continuously from an oil rich region to a water rich region while remaining in the same type of phase. In particular the lamellar phase ranges

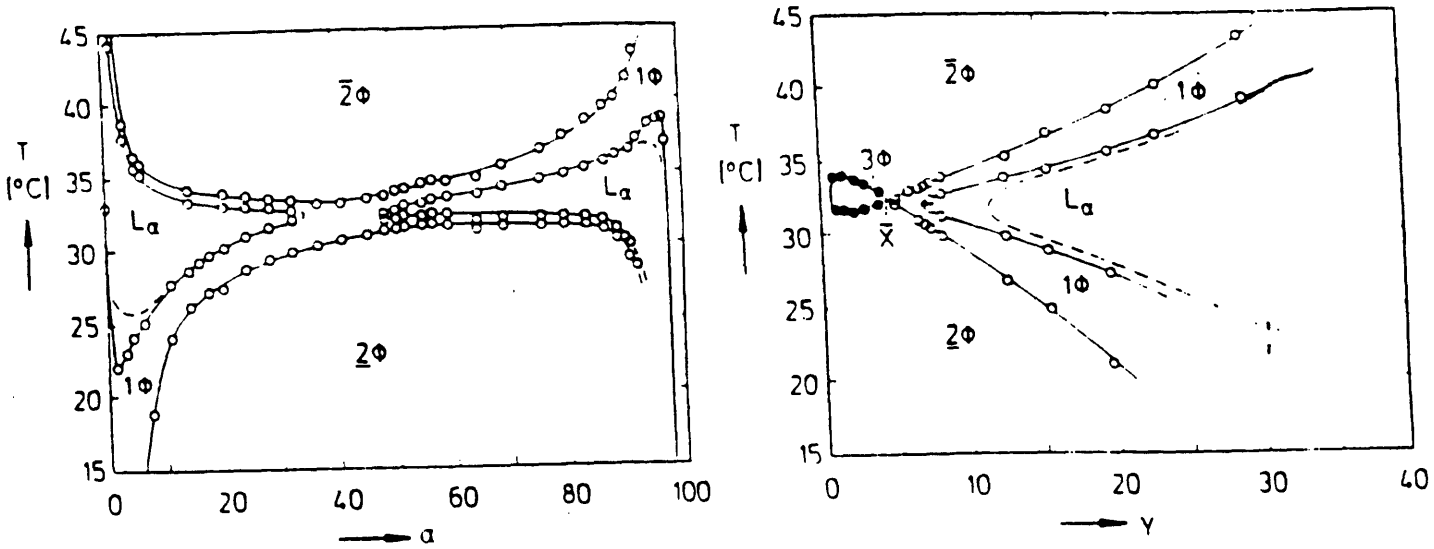

Figure 3-1: Phase diagram of $C_{12}E_5$ studied by Strey et.al. The surfactant fraction and water to oil ratio was measured in weight%

from a water bilayer embedded in oil to an oil bilayer embedded in water, through a symmetric phase with similar amount of oil and water separated by a monolayer of surfactant. This unique feature of our system allows us to study the cross over from an asymmetric to a symmetric system.

Another special feature of our system is that the lamellar phases can be well aligned by methods described later. This allows us to perform x-ray scattering studies on oriented samples.

3.1 $C_{12}E_5$: Sample Preparation

The chemical form of this surfactant is shown in Fig. 3-2 $C_{12}E_5$ was synthesized by Fluka Chemical Co. with a purity > 98%. An important concern of the study has been the stability of the surfactant, which can be easily oxidized by air. In order

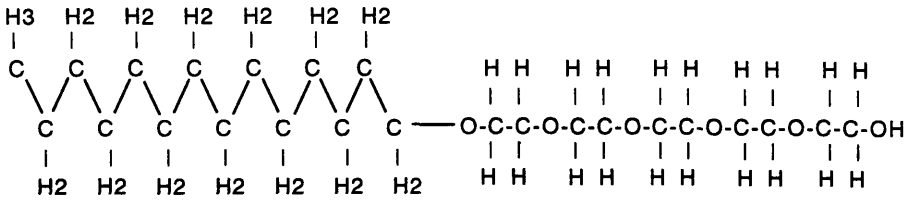

Figure 3-2: The chemical structure of $C_{12}E_5$

to minimize its degradation, several precautions were taken, and its stability was followed over time.

The bottles, which are hermetically sealed, have always been stored in a refrigerator well below the melting point ($23°C$). After a container was opened, the surfactant was stored in a nitrogen environment. Under these conditions, it was still found that the surfactant did not remain stable for more than a month. Moreover, during the actual preparation of samples, contact with air could not be avoided, and the surfactant started to degrade more rapidly. For this reason, new samples were made every few days.

The level of the degradation was checked by the shifts in the isotropic to lamellar transition temperature, as well as by the changes in the critical (clouding point) temperature, (the 2 % solution of $C_{12}E_5$ becomes biphasic at $32°C$).

The octane was also made by Fluka, with a purity of $> 99.5\%$. The water used was deionized. For the samples used in the experiment at MIT, millipore purified water was used, while for the powder sample experiments, tridistilled water was used.

The samples were prepared by mixing the components directly in glass test tubes in order to minimize the number of transfers. They were weighed using a Mettler balance with a precision of $0.1mg$. Once prepared, they were tightly sealed with teflon caps. Because of the low vapor pressure of octane, it is crucial to have a good seal in order not to change the composition due to evaporation.

The volume composition of samples that were made were:

$$\gamma \equiv \frac{V_{\text{surfactant}}}{V_{\text{surfactant}} + V_{\text{water}} + V_{\text{oil}}} = 0.15,\ 0.20,\ 0.25,\ 0.30.$$

$$\alpha \equiv \frac{V_{\text{oil}}}{V_{\text{water}} + V_{\text{oil}}} = 0.20,\ 0.30,\ 0.40,\ 0.50,\ 0.60,\ 0.70,\ 0.80.$$

We also made $\alpha = 0.10$ and 0.90 samples, but these did not exhibit a lamellar phase at temperatures comparable with the others. Since it was essential that we perform the experiments at the same temperature in order to measure the characteristic constants which depend both on temperature and concentration, we could not use them.

In order to plan the scattering experiments, it was crucial to construct the phase diagrams of the system that shows the transition temperatures and the temperature range of the lamellar phase. Because of the strong birefringence as well as the high viscosity of the lamellar phases, optical characterization could be used for these studies.

3.2 Phase Diagrams

Glass vials containing the samples were placed in a flat acrylic cell which can contain up to 12 vials. The inner dimensions of the cell are $12cm \times 12cm \times 1.5cm$. Water flows through the cell from a Neslab heat bath, which regulates the temperature of the water within $\pm 0.2°C$. Two rotating polarizing filters were placed on each side of the cell. This allowed us to observe the texture and the birefringence with polarized, and nonpolarized light, .

The basic features of the phase diagram of the C_iE_j, series which have been established by Strey et.al.[35], are more or less common to all the studied systems. There exists a two phase region at high temperatures, where both phases are isotropic, One of the phases looks turbid while the other phase is transparent. The structure

of the turbid phase has not been studied to date. As the temperature is lowered, the transparent phase region expands, and . the system enters a one-phase isotropic phase. This transition is not shown in our phase diagram: in the case $\alpha = 0.6$, this transition occurs at around $47°C$ for $\gamma = 0.30$, and around $40°C$ for $\gamma = 0.15$. Since our interest lies in the L_α phase, we did not perform any further investigations of this phase. Also, in order to avoid phase separation, we were careful not to heat the samples up into this two-phase region. The one-phase region which lies under the two phase region is transparent and nonbirefringent at rest. This phase turns out to be a *sponge* phase L_3, as determined by an NMR study[36]. As we approach the lamellar L_α phase by cooling, the system goes through a two-phase coexistence region. The lamellar phase which is birefringent first appears at the bottom of the vial. It expands in volume until it takes over the entire sample space. The temperature range of the one-phase lamellar region depends on the composition. As shown in the phase diagram 3-3, it ranges from $\sim 1.5°C$ for the $\gamma = 0.15$, to $\sim 15°C$ for $\gamma = 0.30$. In general, the lamellar temperature range is larger for the more concentrated (larger γ) samples and for the asymmetric bilayer configuration ($\alpha \approx 0.2$, or 0.8). By cooling further, another two-phase coexistence region appears in a similar way as at the higher temperatures.

Because the isotropic to lamellar transition is a first order transition, there will always be a two phase coexistence region at the phase boundary. For the present system, this region is about 1.5 $°C$ wide, and does not seem to depend much on the surfactant fraction γ nor the oil to water ratio α. A technical problem with this transition is that since the densities for the lamellar and the isotropic phases are quite different, and also the viscosity of the lamellar phase is large, during the slow cooling from the isotropic phase, they phase-separate due to gravity, and once they are separated, even after we reach the temperature of one-phase lamellar phase, the inhomogeneity of the sample does not disappear even after several days.

This unhomogeneity is a serious problem. We need to have an homogeneous sample in order to carry out the optical or scattering experiments. Therefore, we developed several procedures to bypass this problem depending on the experiment

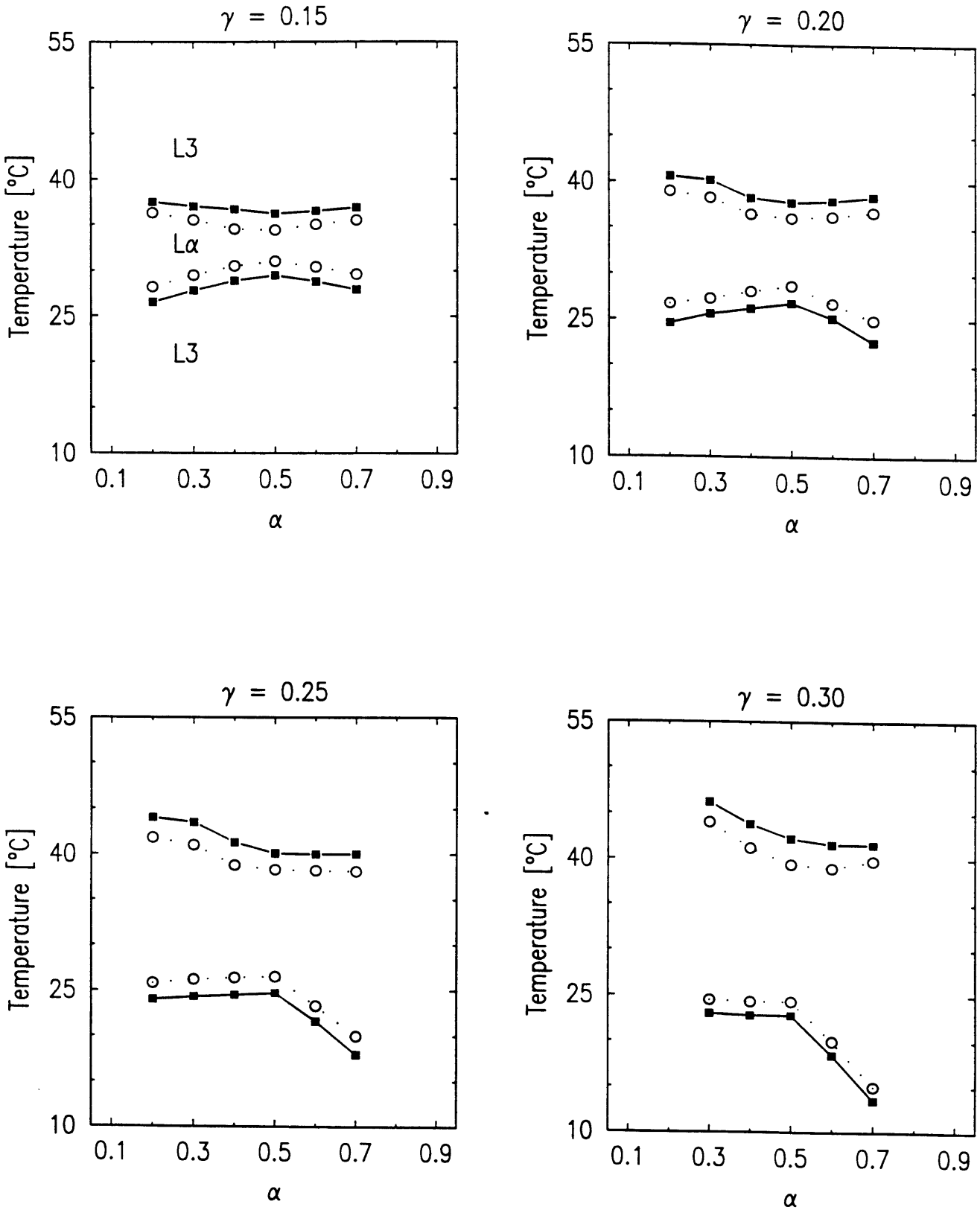

Figure 3-3: The phase diagram for $C_{12}E_5$ - water - octane system at constant γ's.

we wished to perform. When we wanted to get homogeneous, randomly-oriented samples, we found the best way was by *quenching*. From the isotropic L_3 phase, the system is cooled rapidly ($> 10°C$ per minute) into a temperature in the middle of the lamellar phase. This way we do not allow time for the two phases to separate. Occasionally, the sample was also mechanically shaken while cooling from the isotropic phase. However, this latter procedure is not good when we want to *align* a sample or to determine the transition temperature. Another way to reduce the gravity effect is to reduce the sample-cell's vertical height when the system is cooled through the two-phase coexistence. This way, a more uniform sample is achieved.

3.2.1 Microscope

The flat glass cells used for the optical microscopy studies were purchased from Vitro Dynamics Co. They have a inner thickness of either $100\mu m$ or $200\mu m$, a width of either $1mm$ or $2mm$, and a length of either $5cm$ or $10cm$.

The cells were cleaned either with Chromic acid, or a glass cleaning solution RBS pF, and then rinsed throughly with the distilled water. Before loading, the samples were kept at the temperature which corresponds to one-phase L_α. The loading was done by the use of a syringe. The samples were sealed by flame, taking caution to assure that they were not burned.

Two microscopes, both with polarizers, were used for the observation with a magnification of 10× 10. One was a Leitz Wetzler microscope equipped with a polaroid camera. The temperature of the sample on the stage of the Leitz microscope was regulated by a Mettler hot stage FP52, which allows for temperature scans of 0.2 to 10 deg/min. The other microscope was a Nikon (Optiphoto-Pol): pictures were taken with a Nikon camera. The temperature of the sample at the Nicon microscope was regulated by an Instec programmable hotstage HS-1. This allowed cooling rates as slow as $\sim$ 0.05 deg/min. In this configuration, we could investigate the effect of the cooling rate and also the step size of the cooling on the alignment of the lamellae.

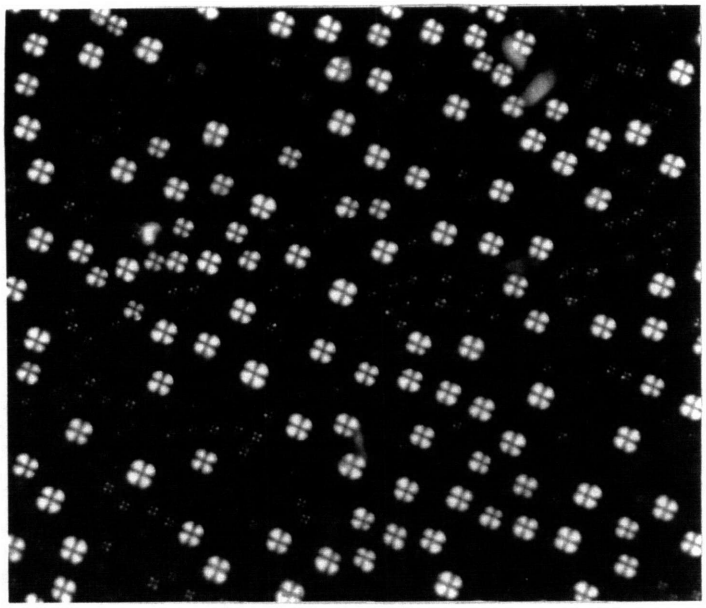

Figure 3-4: Spherulite defects observed between the crossed polarizers

Rapid Cooling

As we cool down from the isotropic phase, which shows complete darkness under crossed polarizer, into the two phase coexisting region, we start to observe interesting defects. These defects are spherical and have a dark cross in the center. The direction of the cross depends on the direction of the two polarizers Fig. 3.2.1. This defect was named *Spherulites*, by Benton et.al.[37]. and is a known structure of defect lamellar phases, and has an onion-like texture[38]. The layers are formed in a concentric manner, with a dislocation in the center caused by the finite curvature allowed by lamellar membranes. Fig. 3.2.1

The core size of the defects increases as the temperature is lowered deeper into the lamellar phase. This may indicate that the allowed curvature for the lamellae is smaller away from the sponge-lamellar transition. As we go into the one-phase lamellar region, the stars increase in number as well as in the diameter, and eventually, the entire sample is covered with them.

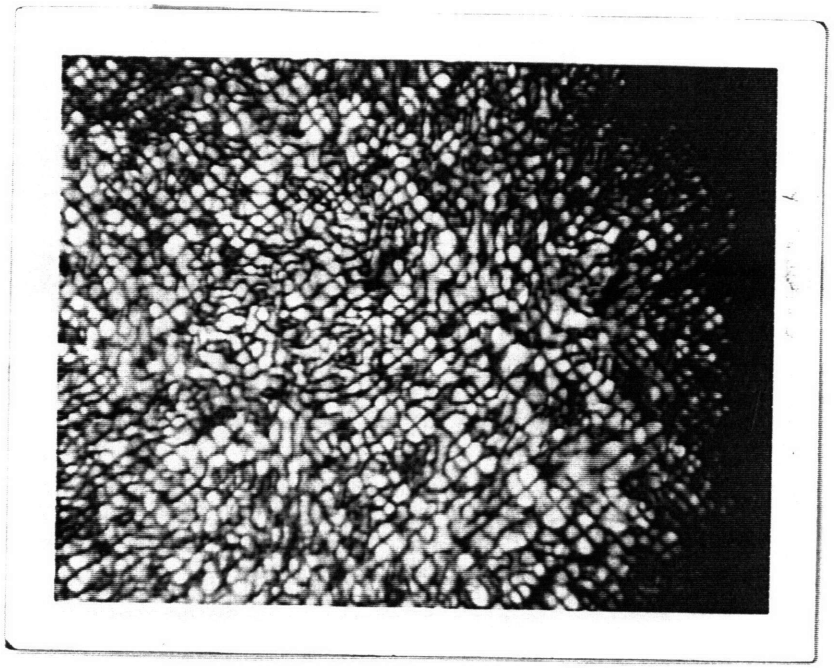

Figure 3-5: Spherulite defects covering the entire sample

Slow Cooling

By cooling slowly, we could achieve well aligned samples. We start cooling from high temperatures where we have the dark isotropic region. As we enter the two phase coexistence region, we first see a bright birefringent line appearing along the glass edge for about $0.3°C$ Fig. 3-8. This is a perfectly oriented lamellar phase of only a few-layer thickness, in contact with the glass surface that causes the alignment. Very few *star* defects (spherulites) can be seen, and by cooling to the one-phase lamellar region, these *stars* disappear. The sample becomes completely dark. This indicates that the lamellae are aligned parallel to the glass surface: When the lamellae are aligned paralell to the glass surface the axis of the molecules is perpendicular to the polarization of the incoming light. Thus the evidence of good alignment is to see a completely black sample except at the edge of the cell where, because of the curvature of the glass, dislocations are found Fig. 3-9. These defects are called oily streaks, and have been studied by Boltenhagen et.al.[39].

By these optical observations, we determined that the rate of cooling needed in order to achieve good alignment is$\leq 0.1°C/\text{min}$ for the $200\mu m$, and $\geq 0.2°C/\text{min}$

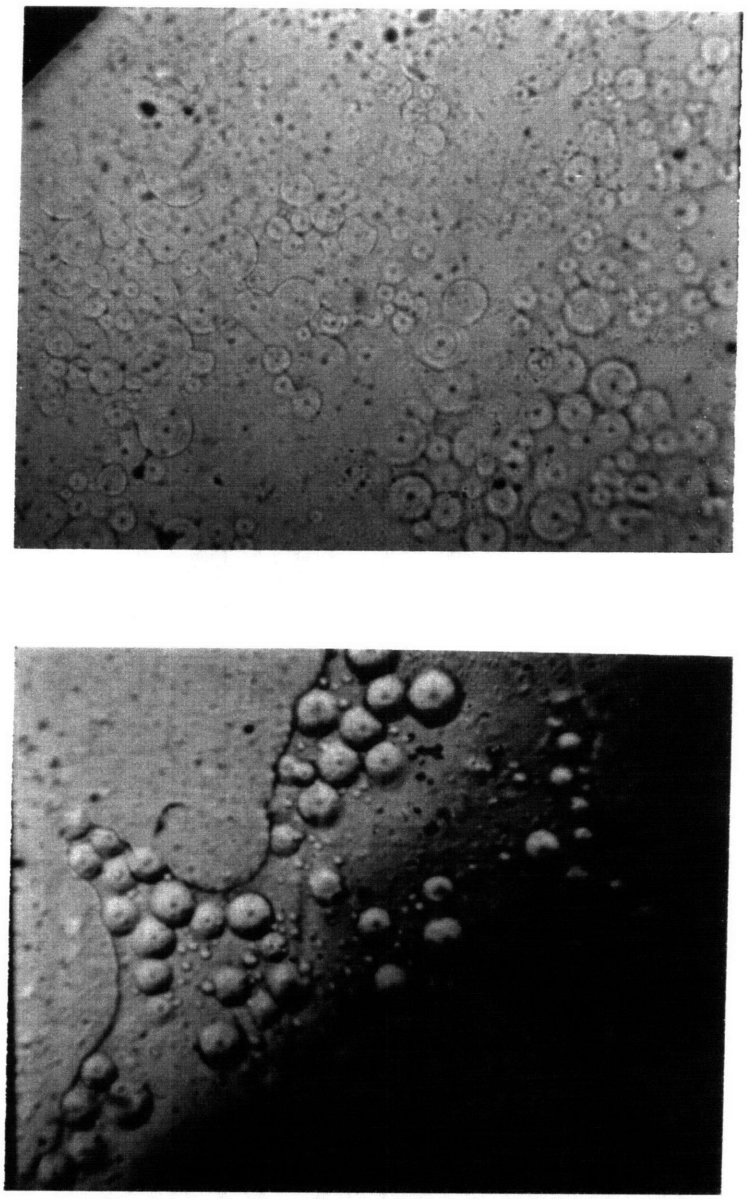

Figure 3-6: Spherulite defects observed without the crossed polarizers. The dislocation cores in the center can be observed.

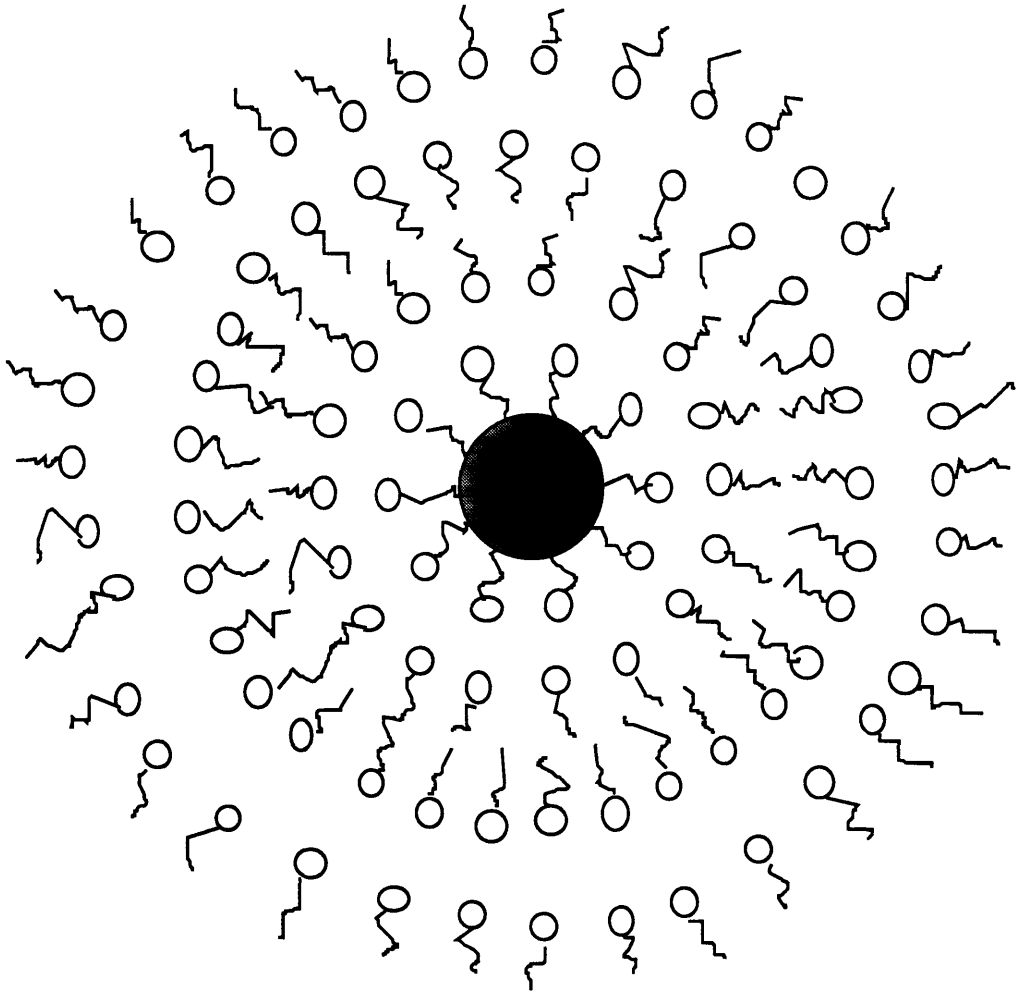

Figure 3-7: The schematic of Spherulites. As it can be seen, towards the center, the curvature increases and creates a dislocations

for the $100\mu m$ cell, the best results were achieved. With the cooling rate slightly above the *good alignment rate* another pattern appears, *the snake skin-like pattern* Fig. 3-10. This was theoretically modeled by Clark et.al.[40] for the smectic-A liquid crystals, and corresponds to a periodic network of dislocations caused by the applied strain. In the biphasic region, the periodicity of the lamellae changes with the change of temperature until the temperature reaches that of the one-phase region, and the

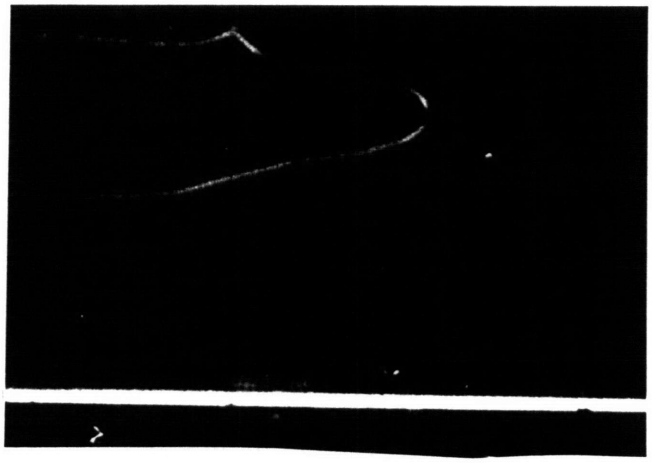

Figure 3-8: Crystalline layers directly at the surface of the glass capillary

periodicity of the lamellae reaches the final the one-phase periodicity determined by the concentration and the thermodynamics. However, this increase causes a strain, and when the rate of the temperature change is faster than the lamellae can adjust their periodicity, it causes the periodic dislocations.

In fact, there is a slight uncertainty in the determination of the transition temperature of the two phase coexistence to one phase lamellae, since we cannot see the lamellae growing when the sample is cooled down slowly (both are black). The lamellae are extremely hard to see. On the other hand, when we cooled down fast, we do not really see the equilibrium state for each temperature. In order to optimize the equilibrium, we stayed at every $0.2°C$, for about a day, and looked at it with the non-polarized light. The boundary between the *stars* caused by the biphasic coexistence disappeared in the one phase region. But, since the speed of the phase separation, increases at the transition temperature, it was never quite clear where exactly the borderline was. In the phase diagrams 3-3, these lines are presented as a dotted line.

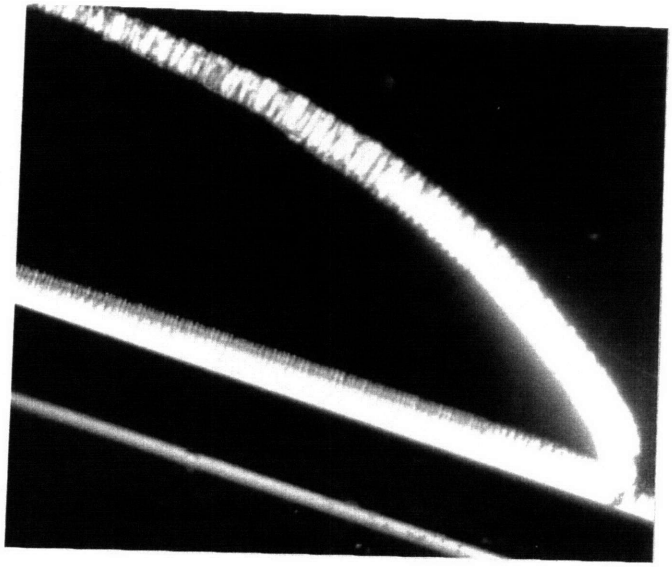

Figure 3-9: An *Oily streak* at the edge of glass

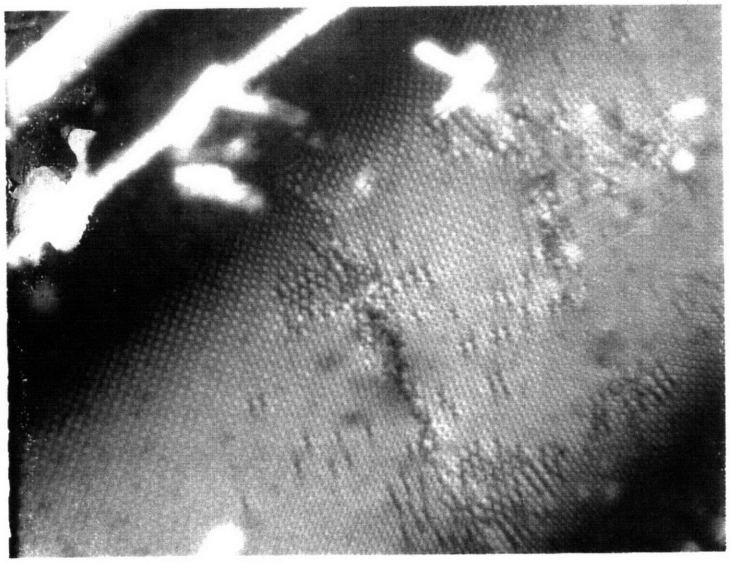

Figure 3-10: Snake skin-like pattern of the dislocation caused by the strain

3.3 X-ray scattering, experimental setup

We have used two different x-ray scattering setups in order to perform high-resolution and low-resolution scattering. In both cases we used the Rigaku rotating anode source (Rigaku RU2000) that produces the C_u K_α lines ($\lambda_{K_\alpha} = 1.54\mathring{A}$)

3.3.1 X-ray scattering from powder samples

The Rigaku RU2000 source was operated at 1kW (25mA, 40kV). The output was collimated by a gold-plated quartz mirror. A nickel plate was placed at the output in order to eliminate the K_β lines. The detector was a linear detector with 512 channels (99 channels $/cm$) and was placed 81 cm from the sample position. The beam path was in vacuum. The resolution of the direct beam was measured to be $\Delta q = 1.7 \times 10^{-3}\mathring{A}^{-1}$ full width at half maximum (FWHM) The schematics of the low resolution apparatus are shown in Fig. 3-11

The samples were loaded into 1 mm diameter glass capillaries and six of them at a time were placed in a sample holder. They could be moved horizontally, which made data aquisition easier and faster.

The temperature within the sample holder was controlled by a Neslab heat bath with a temperature accuracy of $\pm 0.1°C$. The glass capillaries were bought from Mark-Roehrchen. Because the capillaries had a size destribution, their diameters were remeasured at the lab and only the ones with diameters of 1 mm $\pm$ 5% were used. The thickness of the glass was chosen to be 10μm in order to minimize the attenuation of x-rays, they were thus, extremely fragile. To fill these capillaries, we made tiny pipets out of the glass tubes, that fit inside the capillaries. Once filled, they were sealed by flame. To make sure of the tightness of the seal, they were also covered by epoxy. The sealed capillaries were then put in the sample holder. The peak intensity was normalized by the transmission of the direct beam. In order to subtract the background, we measured the scattering from the pure solvent and the glass and subtract it from the signal.

. The most important technical difficulties involved the production of homogeneous

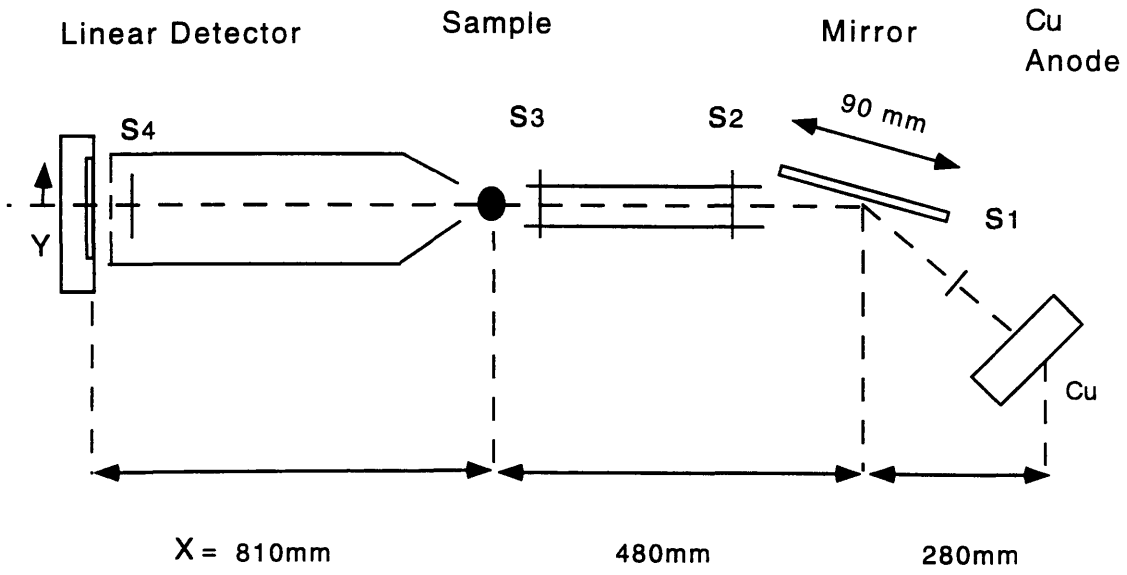

Slit size (mm)	horizontal	Vertical
S1	0.3	
S2	1.0	0.6
S3	1.5	0.5
S4	2.0	

Figure 3-11: The experimental setup for the x-ray scattering of the powder samples.

samples and their protection from evaporation. An inhomogeneous sample gives rise to multiple x-ray peaks and evaporation causes a shift of the x-ray peak-position as a function of time. Thus, the samples must be well mixed and in the one-phase lamellar phase when we put them into the cells. The cells should be as filled as possible and the seals must be perfectly tight.

The gravity inside the one-phase lamellar did not have and important effects. No difference in the periodicity of the lamellae between the top and the bottom of the sample cell was observed as we scanned across the 4 cm of sample height. Slow

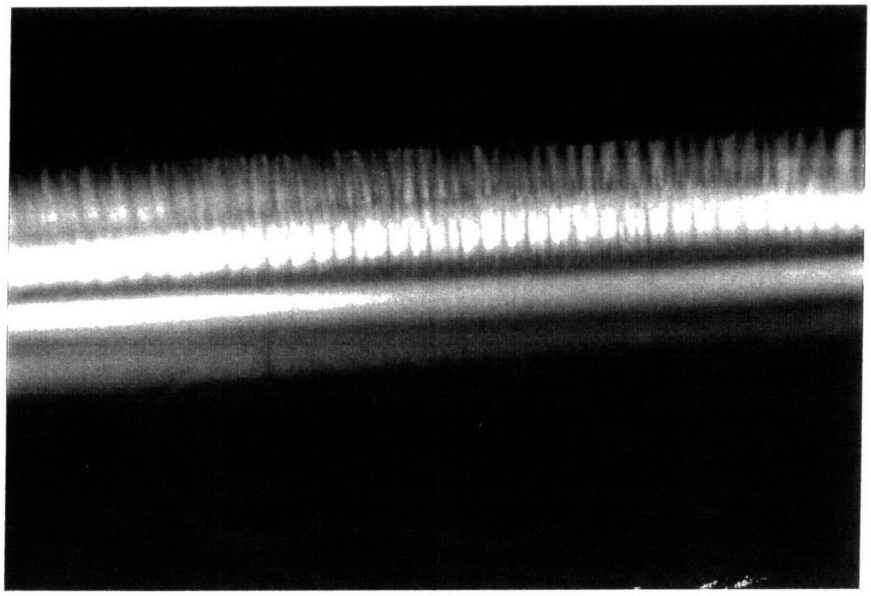

Figure 3-12: Leek-like alignment

cooling through the two-phase coexistence region will cause phase separation. As all of the samples turned out to be in one-phase lamellar phase, at temperature $33C°$, the samples were stored at $33C°$, and the experiments were also carried out at the same temperature.

If the samples remained within the capillaries for long periods of time, (3 days) leek-like alignment was produced due to the contact with the capillary walls Fig. 3-12. So fresh samples had to be made every so often, since we wanted randomly oriented samples without any prefered long-range orientations. We also checked the *powderness* using the microscope before and after the scan to make sure that the sample did not orient during the data acquisition.

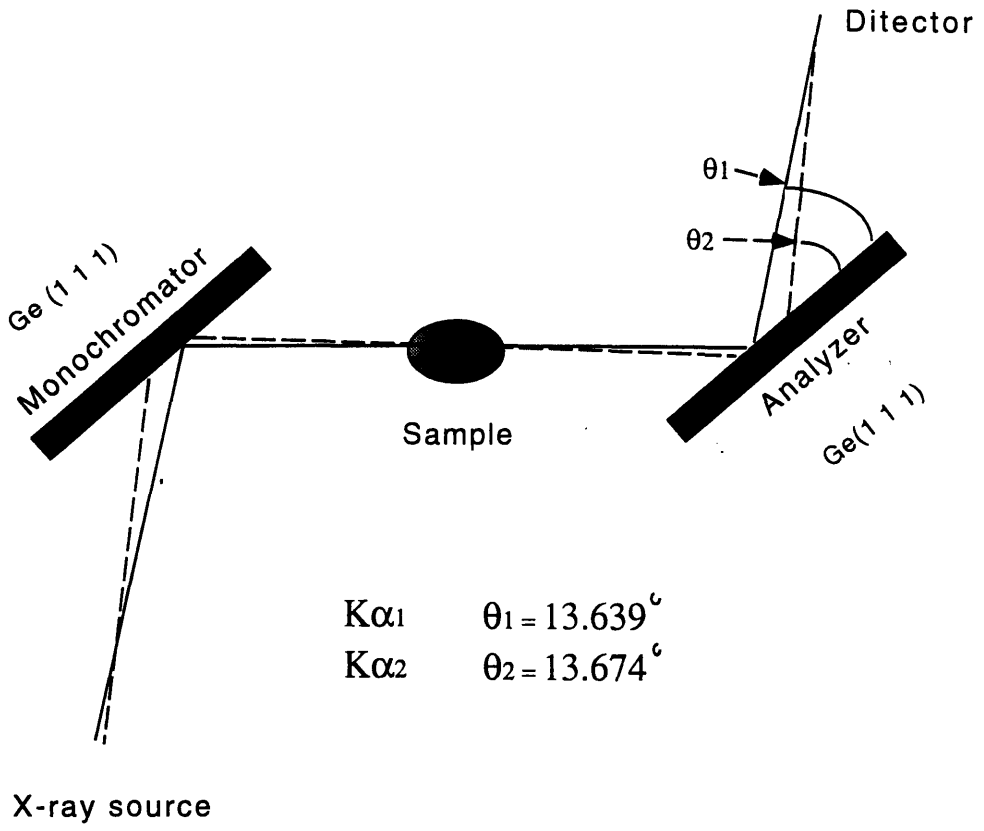

Figure 3-13: The geometry of the non-dispersive orientation of the monochromator and analyzer crystals and sample.

3.3.2 High-Resolution X-ray Scattering from Well Oriented Samples

For these experiments, the Rigaku was operated at 7.42 kW (140 mA, 53 kV). Germanium (111) crystals were used as monochromator and analyzer in the nondispersive mode as shown Fig. 3-13[16]. Both $K_{\alpha_1} = 1.54051\mathring{A}$ and $K_{\alpha_2} = 1.54433\mathring{A}$ lines were used in order to gain intensity. The longitudinal resolution could be modeled as a Lorenzian with $\Delta q = 4.5 \times 10^{-4}\mathring{A}^{-1}$ full width at half maximum. The technique is illustrated in Fig. 3-14

The sample was placed at the center of rotation of a four-cycle Huber goniometer inside a homemade sample holder Fig. 3-15. In order to orient the samples, two pieces

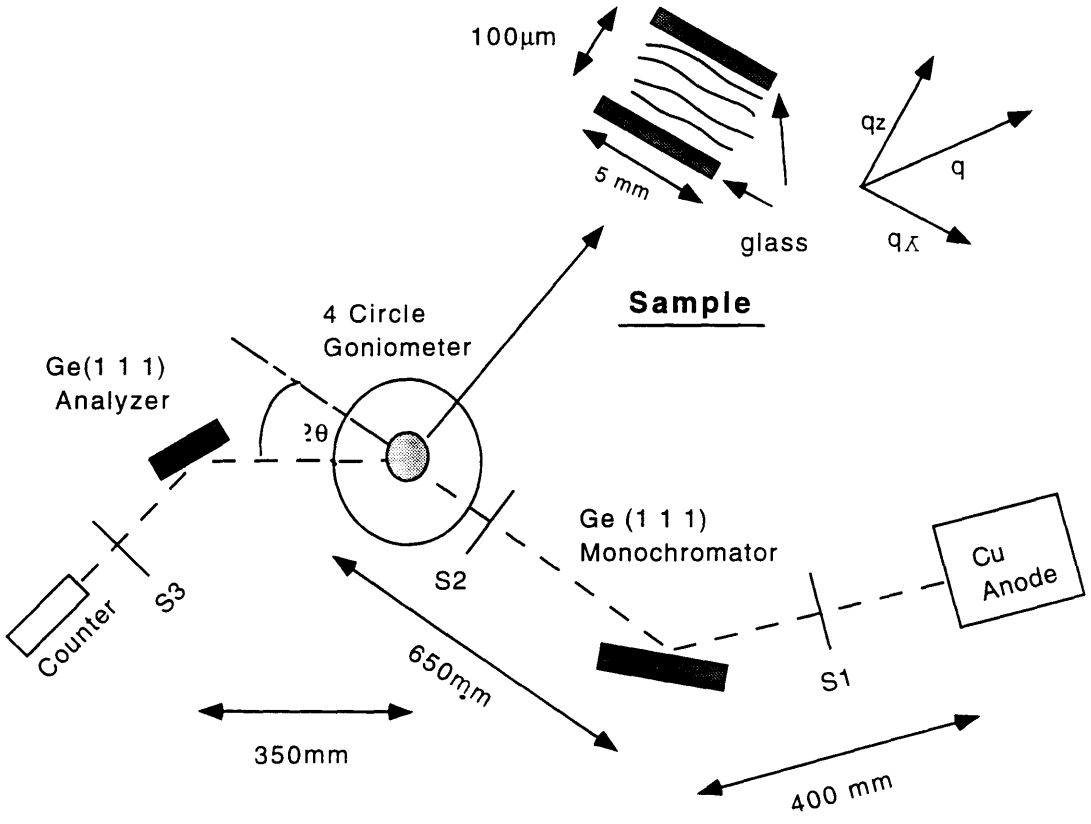

Slit size	horizontal	Vertical
S1		0.4 mm
S2	3.0 mm	1.0 mm
S3		1.0 mm

Figure 3-14: High-resolution set-up for the x-ray scattering

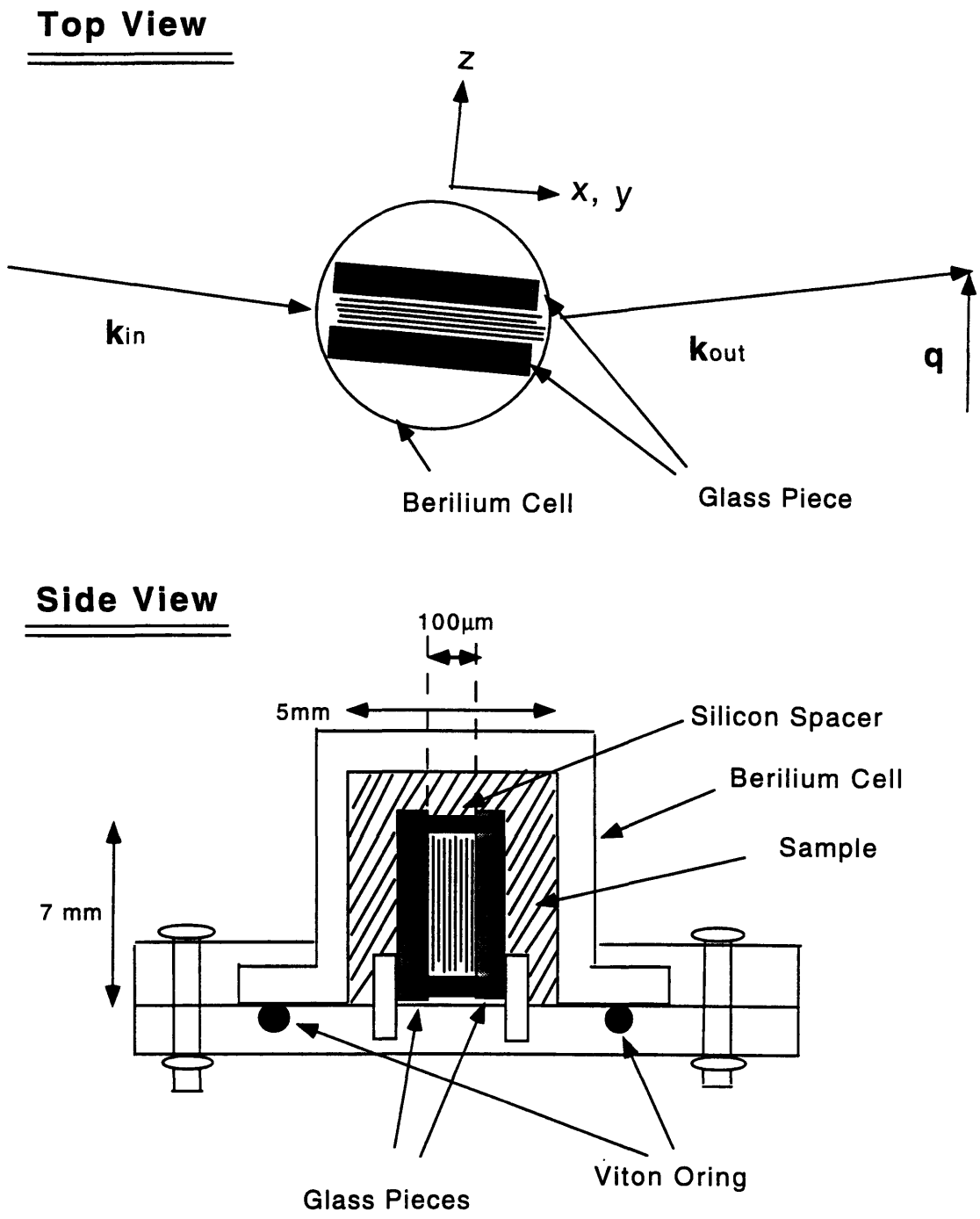

Figure 3-15: The Sample Cell configuration

of glass $8mm \times 4mm \times 1mm$ glued upon each other with a separation of $100\mu m$ were used. As the absorption of x-rays by the glass is high, we developed a technique in which the x-ray does not have to pass through the glass. The two pieces of glass are attatched through the silicon separator, only at the top and the bottom, and are open on both sides where the x-ray beam comes in and goes out. This sample cell

is housed inside a beryllium cell, which is also the sample reservoir. Beryllium was chosen because it is highly transparent to x-rays.

Temperature stability and homogenity and slow temperature scan rates were essential for good alignment . Heating was produced by a Minco heater (R = 37.5Ω) A $300k\Omega$ (YSI 44014) silicon thermistor was used to measure the temperature. A Lakeshore 93C controller was used for the temperature control and was operated by a GateWay Computer through Camac to achieve scan rates of $\sim$ 0.1 deg/min. To keep the homogenity of the temperature, the oven was covered with the acrylic holder, except for the beam path, also the entire goniometer was covered with a big sheet of paper which seemed to efficiently decreased the temperature fluctuation. The temperature stability was $\pm 5mK$. Also as it has been emphasized before, having a large sample height during the slow cooling down in the biphasic region, enhances the phase separation. Because of the configuration of the setup, we had to have the sample in the vertical position as the scattering experiment was performed. So we established the procedure where the cooling was done while the sample holder was kept in the horizontal position(minimum height), and we changed to the vertical position only during the data acquisition. As a measure of the homogenity, we used the reproducibility of the periodicity when we heat up and cooled down in cycle. With the cautions mentioned above, the difference of the periodicity of the cycle was < 0.5Å.

To orient the samples, we used a thermal treatment. The samples were kept at the temperature where the system was isotropic, for about one hour, then they were cooled down very slowly, $\sim$ 0.05 deg/min. Different speeds were required for the different phases: at the isotropic phase, it is not necessary to cool down so slowly ($\sim$ 0.1 deg/min), inside the two-phase coexistent region however, we found it to be critically important to slow down (for 0.02 deg/min). Any instablity in this region can cause the inhomogenity of the lamellae, thus, causes the multiple peaks. Once the system is in the lamellar phase, one can increase the speed to $\approx 0.1°C$ per minute.

The glass pieces were placed at the center of rotation, and after the calibration of the zero positions for $2\theta, \theta$ and the translational position, the scattering in L and K directions were recorded . With the $q_\perp = 0$, q_z was rocked, for the L scan, with $q_z = 0$.

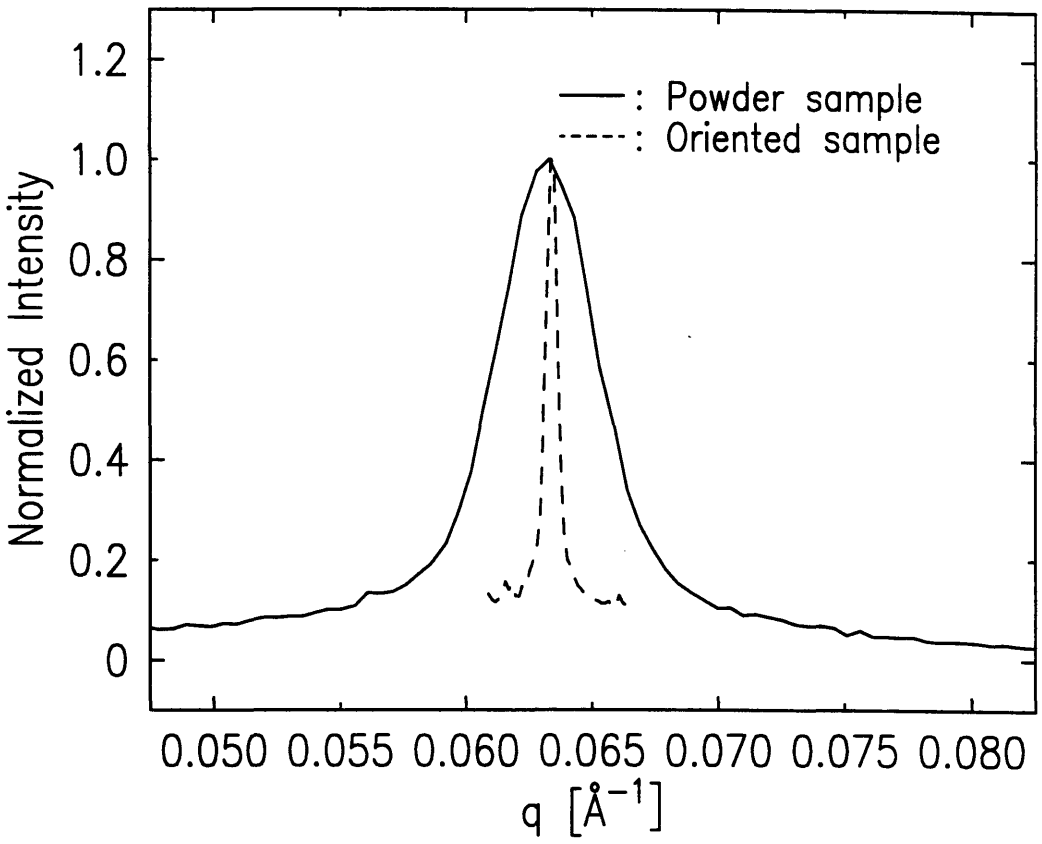

Figure 3-16: The intensity profiles from the two scattering techniques.

$q_\perp$ was rocked for the K scan. The typical periodicity of the lamellae studied was $\approx 100\mu m$. The scattering angle was around 0.4°. As the lamellae are aligned along the glass surface, two non-parallel glass slides can cause the dislocation lines. The glass pieces were glued together by hand, and after numerous practices, we managed to get them parallel as $\leq 0.1°$. For the good alignment, the glass surface has to be completely oil-free. So, we were especially careful to clean the surface of the glass every time we load the samples with a glass cleaning solution RBS pF.

The peak width of the oriented sample was much smaller than that of the powder scattering. Therefore, we could determine much more accurately $\leq 1\mathring{A}$ the peak position, However, the glass which we were using to orient the samples reflects x-ray at low angle i.e. below the critical angle of the glass-water interface, thus, we chose samples which had Bragg peak far from the critical angle: i.e. $\gamma = 0.30$.

Chapter 4

Powder Samples:Data Analysis

In this chapter, the data obtained from x-ray scattering measurements from powder samples are presented. The experiment was carried out for the following concentrations that were also studied by optical microscopy:

$$\gamma \equiv \frac{V_{\text{surfactant}}}{V_{\text{surfactant}} + V_{\text{water}} + V_{\text{oil}}} = 0.15,\ 0.20,\ 0.25,\ 0.30.$$

$$\alpha \equiv \frac{V_{\text{oil}}}{V_{\text{water}} + V_{\text{oil}}} = 0.2,\ 0.3,\ 0.4,\ 0.5,\ 0.6,\ 0.7,\ 0.8.$$

The typical data acquisition time for each spectrum was 600 seconds, in order to get the good signal to background ratio. The temperature was set at $33. \pm 0.1°C$ for which all the samples are in the one-phase lamellar phase. All the intensity were normalized by the intensity of the directly transmitted beam. In order to make sure that there was no evaporation of the octane, we made time-series measurements in order to check that the peak position did not shift with time. Within the data acquisition time of about 5 hours, the peak shift was less than $1e^{-4}\mathring{A}^{-1}$ which is negligible.

4.1 Lineshape Analysis

4.1.1 Scattering spectrum of the lamellar phase

The x-ray intensity profiles are shown in Figs. 4-1 - 4-4. As can be seen from these figures, the sharpness of the peaks as well as the peak intensity are largest for $\alpha = 0.5$ and decrease for $\alpha \neq 0.5$, for all γ's. The very interesting feature of the spectra is that they clearly show two contributions. The Bragg-like part at $q_0 = 2\pi/d_p$, where d_p is the smectic periodicity, and an intensity increase as $q \rightarrow 0$. These two contributions have been discussed in Chapter 2. The Bragg-like peak is due to the quasi-long-range smectic ordering, while the intensity increase as $q \rightarrow 0$ is due to concentration fluctuations in the correlation function.

In the analysis of the data, we will attempt to separate the two contributions.

4.1.2 Scattering at $q \rightarrow 0$

We have seen in Chapter 1 that the concentration fluctuations can cause anisotropic scattering peaked at $q = 0$. For powder samples, we have to average over all directions. In spherical coordinates we get:

$$I_{SAXS} = \int_0^{2\pi} d\phi \int_0^{\pi} < \delta c(q)\delta c(-q) > \frac{2\pi q^2 sin(\theta) d\theta}{4\pi q^2} \tag{4.1}$$

$$I_{SAXS} = \pi \int_0^{\pi} < \delta c(q)\delta c(-q) > \frac{2\pi q^2 sin(\theta) d\theta}{4\pi q^2} \tag{4.2}$$

Here I_{SAXS} ($I_{small\ Angle\ X-ray\ Scattering}$ is the intensity originated from the concentration fluctuations. Substituting $q_z = qcos(\theta)$, and $q_\perp = qsin(\theta)$ into Eq. 2.34 in, we get

$$I_{SAXS} = \frac{kT\chi}{2} \int_0^{\pi} \frac{Bcos^2(\theta) + Kq^2 sin^4(\theta)}{\overline{B}cos^2(\theta) + Kq^2 sin^4(\theta)} sin(\theta) d\theta \tag{4.3}$$

Here, as it was mentioned in Chapter 1, K is the bending constant of the smectic layers, B is the compressibility modulous at constant surfactant concentration, $\overline{B}$ is

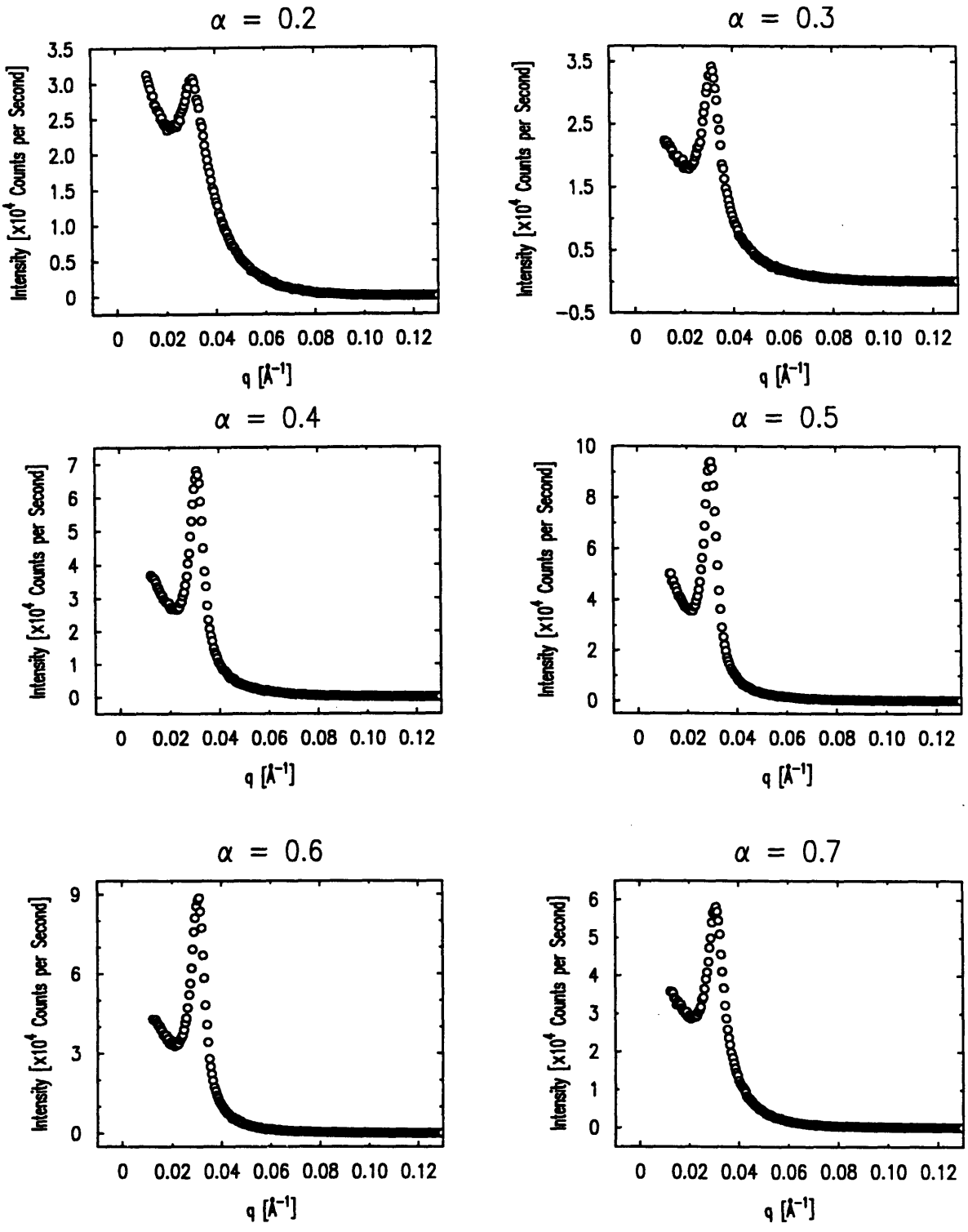

Figure 4-1: Intensity profiles: $\gamma = 0.15$

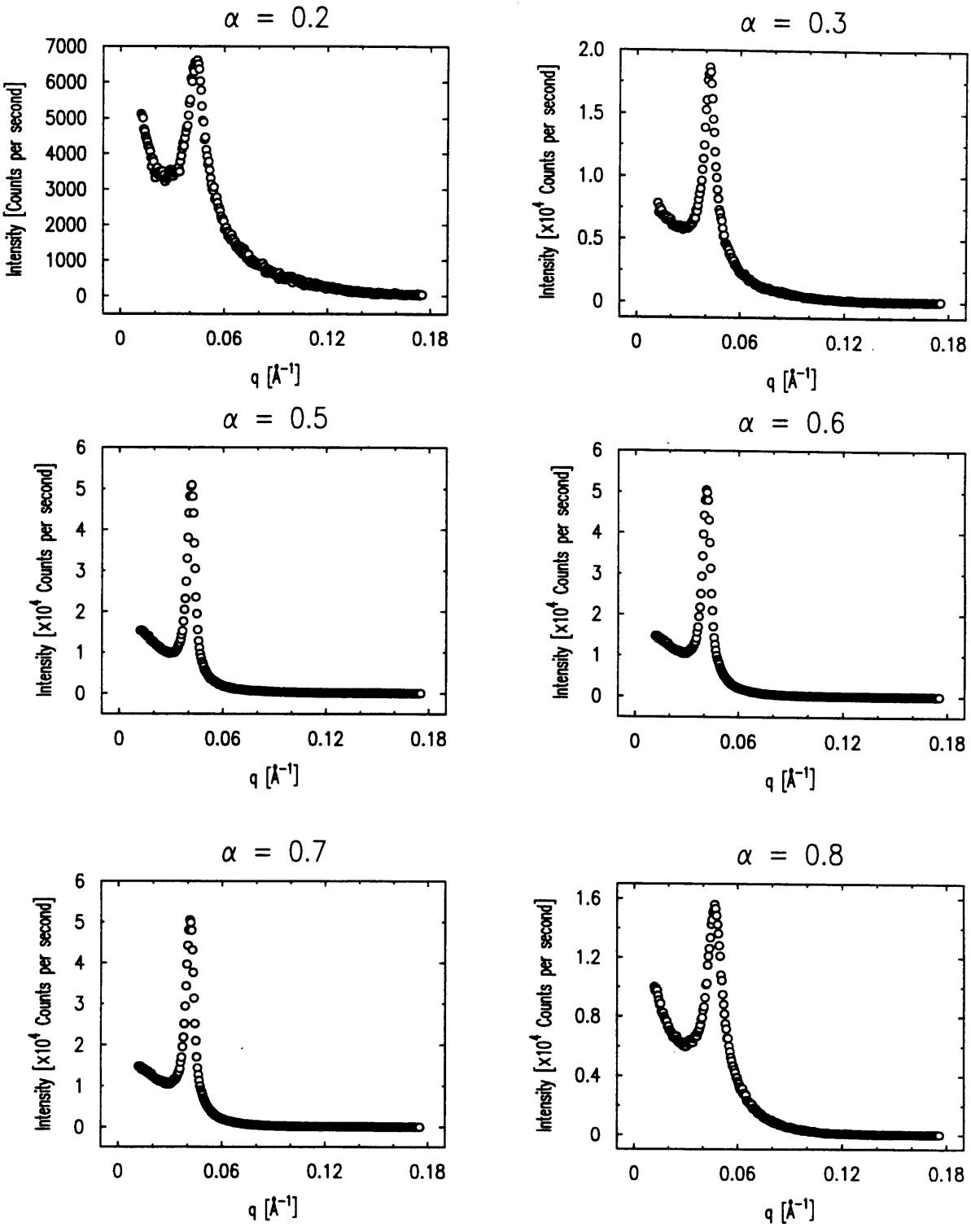

Figure 4-2: Intensity profiles: $\gamma = 0.20$

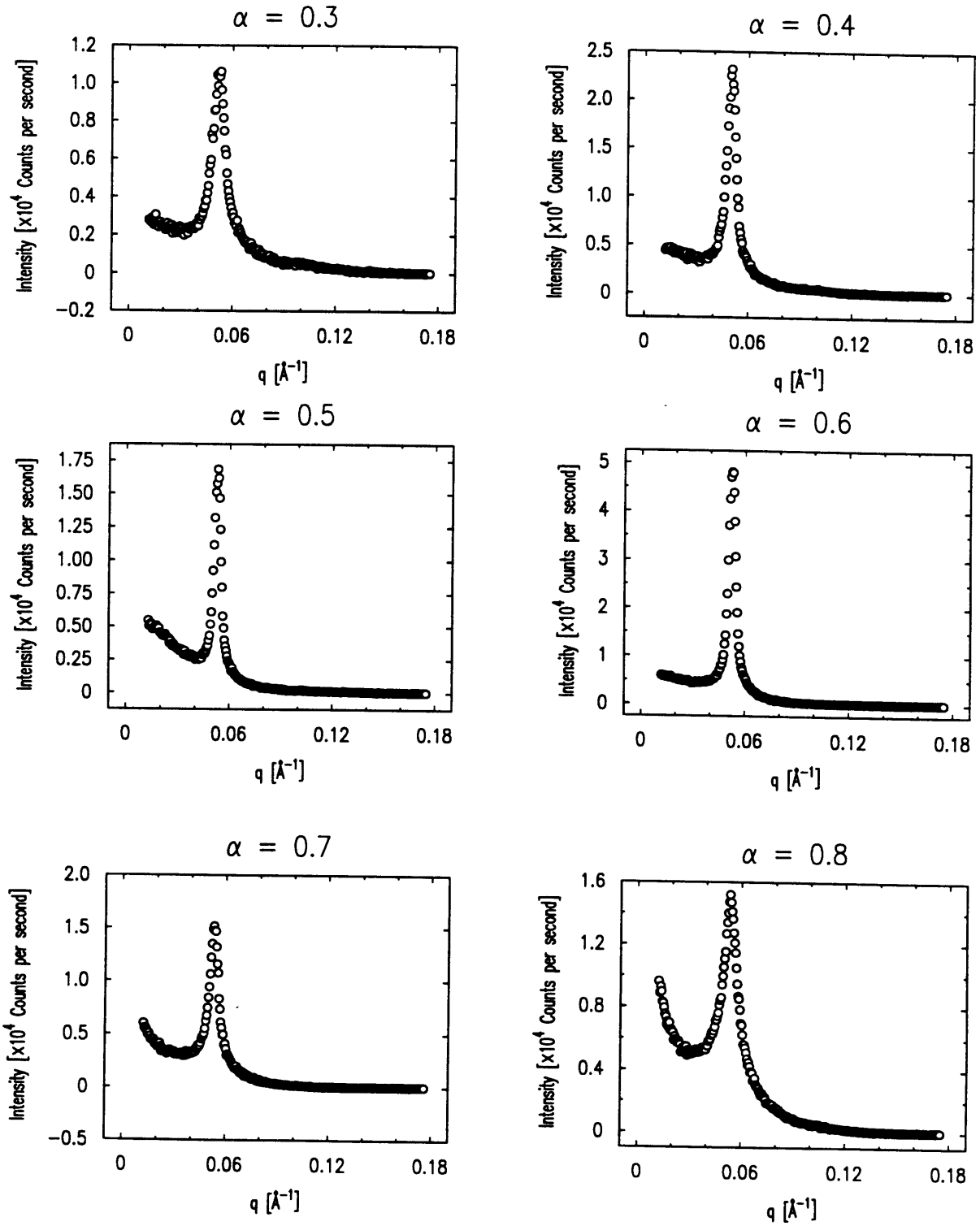

Figure 4-3: Intensity profiles: $\gamma = 0.25$

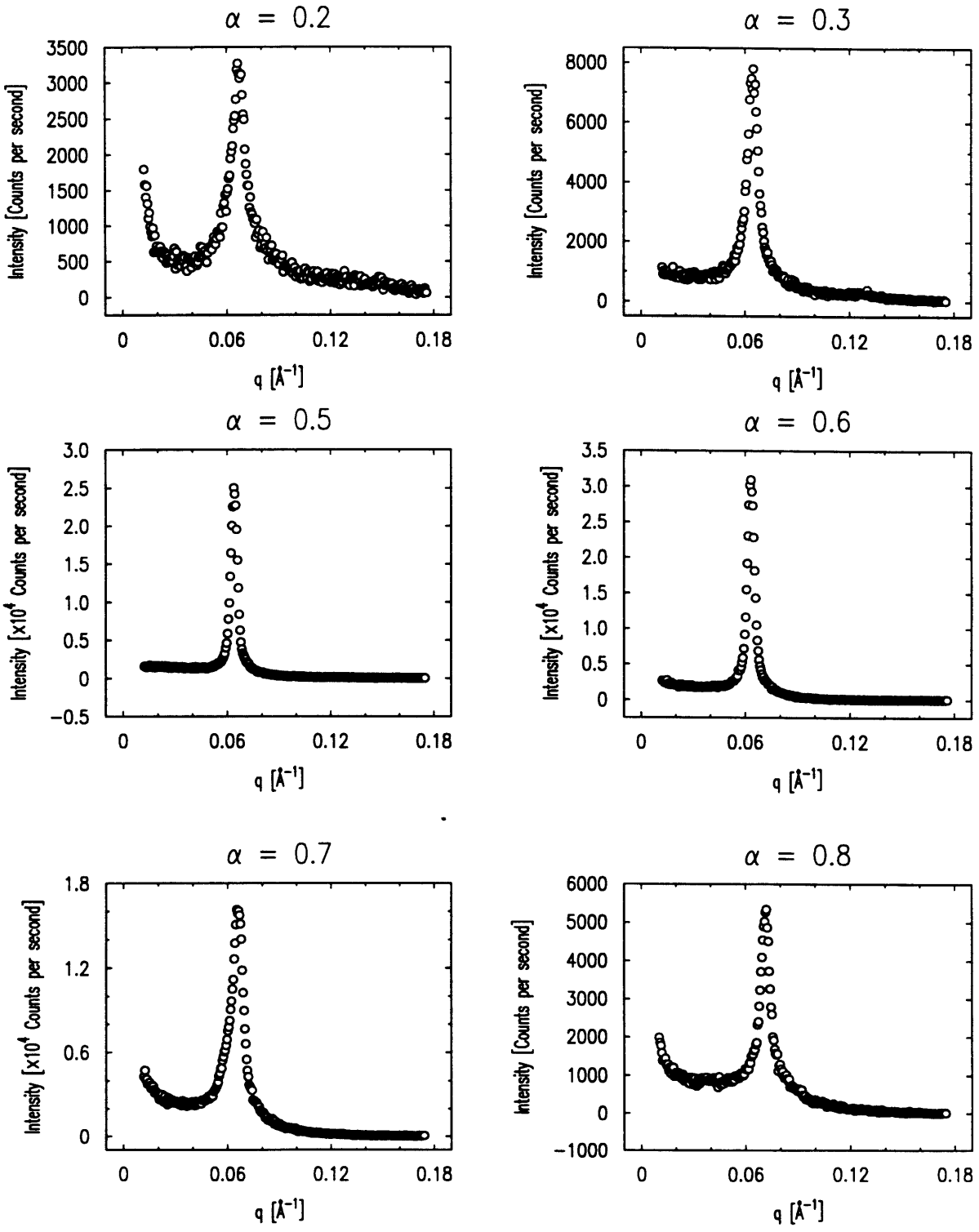

Figure 4-4: Intensity profiles: $\gamma = 0.30$

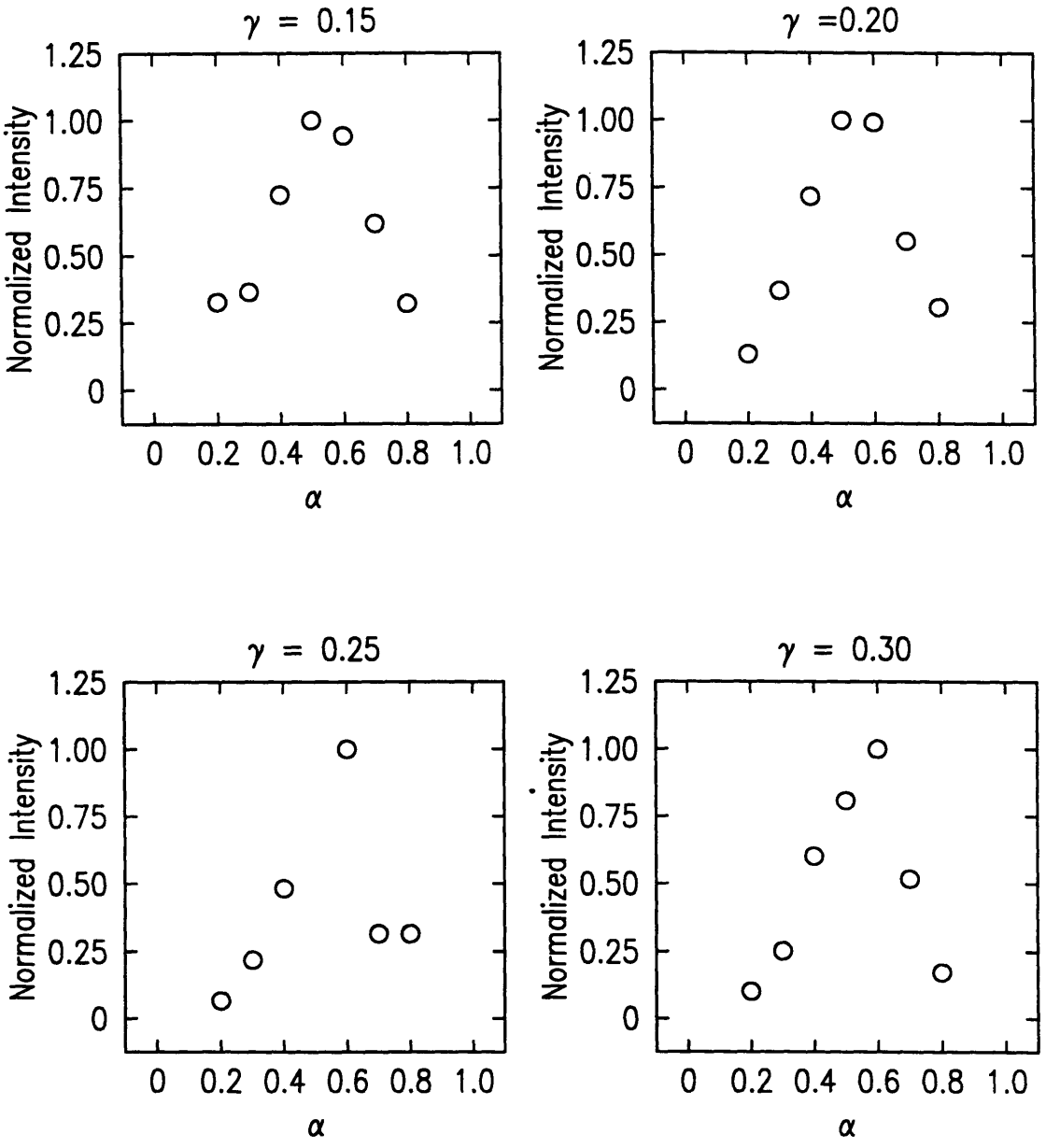

Figure 4-5: The Normalized Intensity(I/I_o)vs α for each surfactant concentration γ.

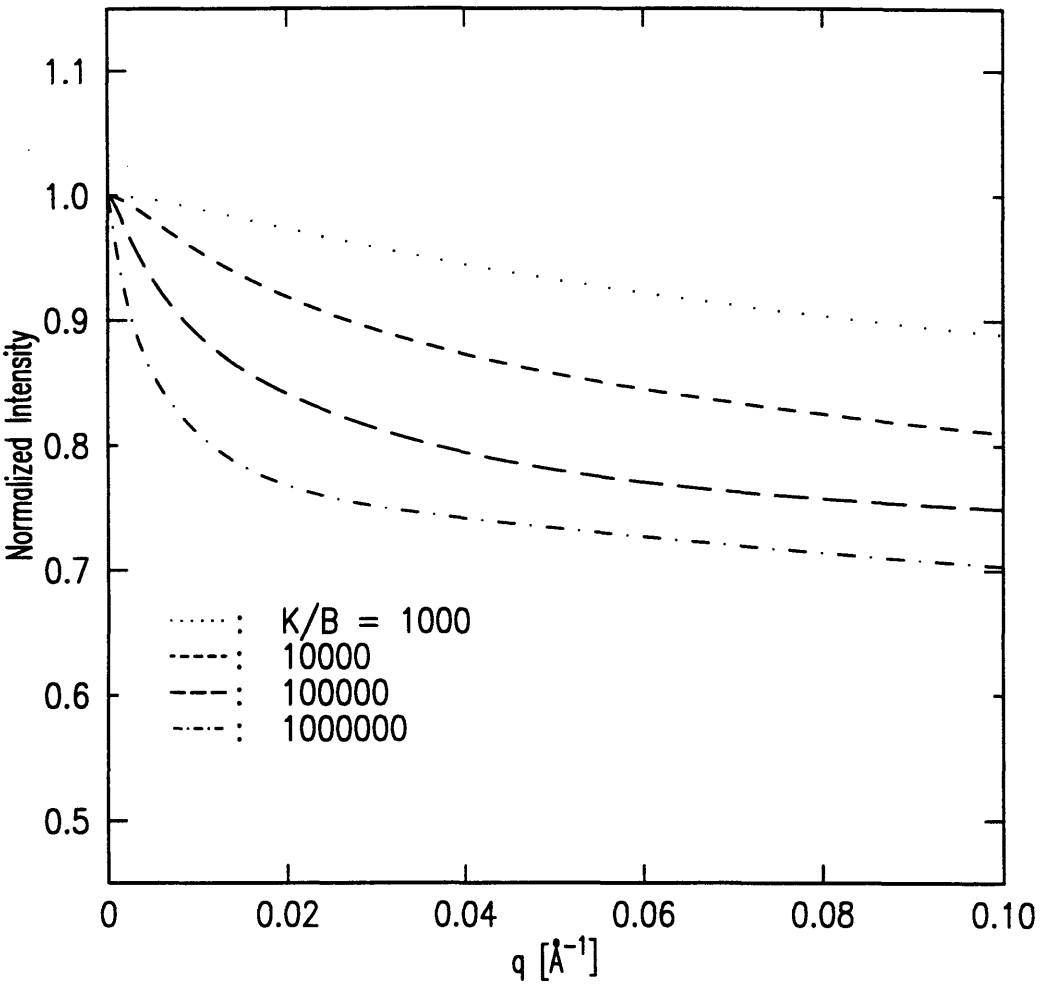

Figure 4-6: The excess scattering as $q \to 0$ originating from the concentration fluctuations. Here $B/\overline{B} = 100$

the compressibility modulous at constant membrane thickness, and χ is the osmotic compressibility of the membrane. This integration turns out to be nonanalytical. We performed a numerical computation in order to estimate the general behavior and the results are shown in Fig. 4-6. From Chapter 1, we have seen that $B/\overline{B} \approx 100 \gg 1$. The intensity profiles are shown in figure 4-6 for several values of $K/\overline{B}$ where we have chosen the value $B/\overline{B} = 100$. More precisely, χ is also a function of q that converges to the expression given in Chapter 1, as $q \to 0$

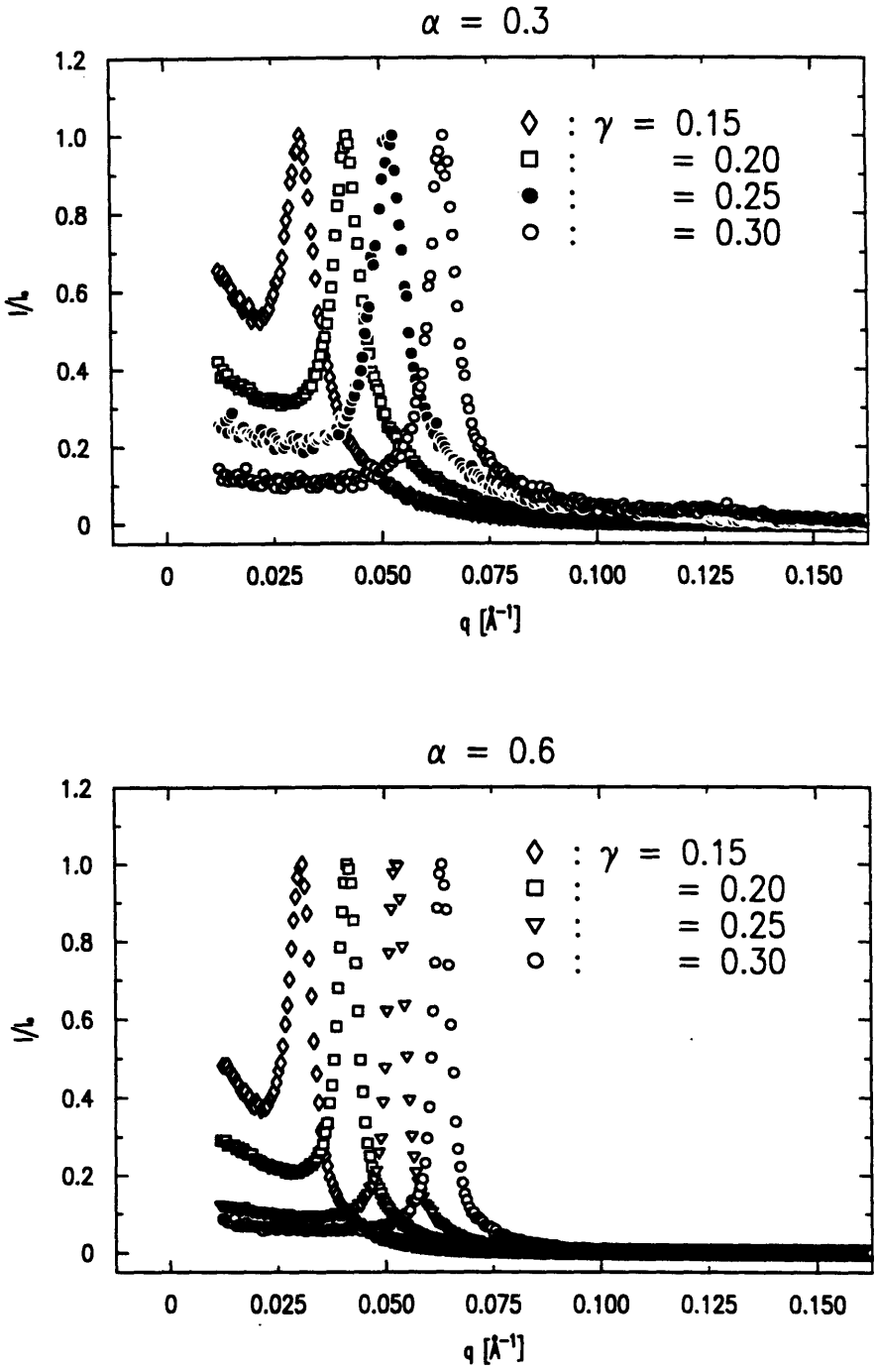

Figure 4-7: The normalized intensity profiles vs surfactant concentrations at the same oil to water ratios. I_o is the peak intensity

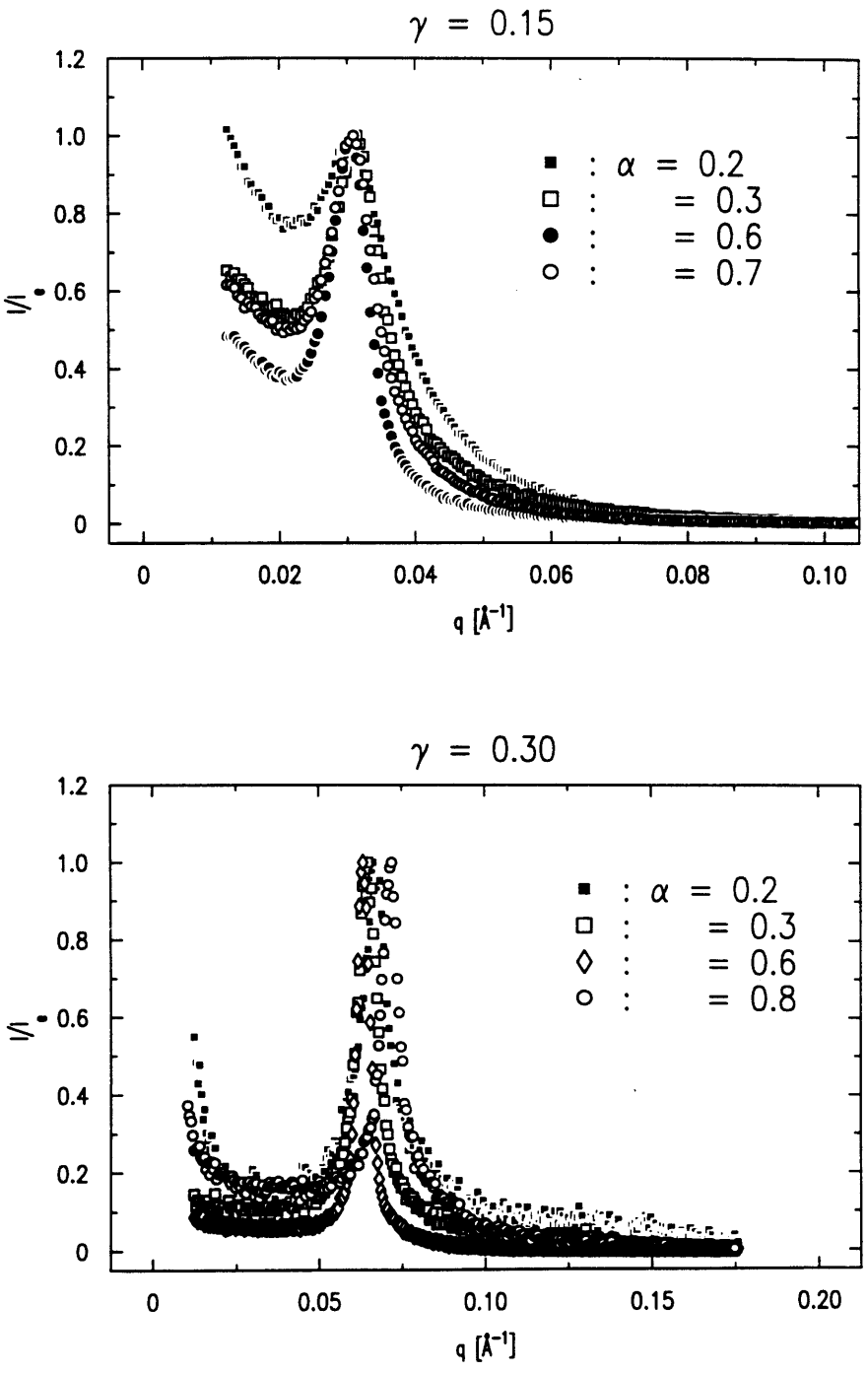

Figure 4-8: The normalized intensity profiles for various oil to water ratios. and for the same surfactant concentrations. I_o is the peak intensity

In reality, the scattered intensity as $q \rightarrow 0$ is superimposed on the intensity of the direct beam. However, we will still be able to make several qualitative arguments.

We have obtained in Chapter 1, the value for $B, \overline{B}$, as well as χ, for the lamellar phases which are stabilized by steric interactions. Using 1.38, 1.37 and 1.39 we get,

$$I_{\mathrm{SAXS}_{(q=0)}} = kT\chi\frac{B}{\overline{B}} \approx \frac{1}{kT}(\frac{m}{v\rho})^2\kappa d\delta^2 \tag{4.4}$$

Now, let us see how the small angle x-ray scattering(SAXS) intensity depends on α and γ separately. In order to be able to compare the intensity, the intensities at a given q are normalized by the Bragg peak intensity, and q was chosen safely away from the Bragg-like peak position q_o, ($q = 0.01\mathring{A}^{-1}$). From the data, Figs. 4-7, 4-8, we can observe that the intensity is larger for the lower surfactant concentrations i.e. smaller γ, and also for the more single-solvent-type system, ($\alpha = 0.20$ or 0.80).

Dilution at constant oil to water ratio

When, α is fixed and γ is varied, that is when we keep the oil to water ratio constant and change the surfactant concentration, we can see Fig. 4-7, that by decreasing the concentration of the surfactant, the periodicity d_p increases, and from Eq. 2.34, this will cause an increase in the intensity I_{SAXS}. Also the mass density of $C_{12}E_5$ is 0.963 g/ml, for water it is 0.998 g/ml and octane is 0.703 g/ml. By deducing the electronic density to be correlated to the mass density, thus the decrease of the volume fraction of $C_{12}E_5$ which causes a decrease in the total mass density ρ, which in turn will cause an increase of the intensity. The other varying parameters here κ and δ. For these parameters, there are two possible scenarios.

Monolayer System

In the first scenario, the oil and water are equal in volume, thus the system consists of a stack of monolayers separated by the same thickness of either oil or water. Now, we are going to make the following assumption: In this system, it is not clear

whether monolayers interact with each other via the Helfrich (steric) interaction. Since Helfrich-type interactions require the absence of any spontaneous curvature, consequently, the lowest-energy equilibrium geometry for the membrane will be the flat configuration. Thus the bending energy can be calculated from deviations from the flat position. This assumption is valid for a bilayer because of its symmetry. However, when we deal with a stack of monolayers, it is not clear whether we can neglect the spontaneous curvature and apply the steric law. Nevertheless, for the analysis presented here, the monolayer-case will be treated as a membrane with zero spontaneous curvature and half the bilayer thickness. In this case, neither κ nor δ change with the decrease of the surfactant concentration(γ decrease), since they are associated with the bending rigidity of a single surfactant layer. So, when $\alpha \approx 0.5$, the intensity is mainly controlled by changes in d and ϕ.

Bilayer System

For the case of the bilayer system, where the ratio oil/water is much larger, or smaller than one, by increasing γ at fixed α, we are increasing the membrane thickness. Now, the relation between the bending rigidity of a monolayer and a bilayer without any swelling(in single solvent) has been theoretically modeled by Porte et al. [5],

$$\kappa_{bilayer} = 2\kappa_{monolayer} \tag{4.5}$$

Note here that this result does not agree with the usual law of strain on a two dimensional solid board [15] where the rigidity increases as the cubic power of the thickness. This difference comes from the assumption that the two monolayers slide on each other so we can ignore the shearing force between them.

In our case, we are not dealing with a bilayer system with a single solvent. Nevertheless, we can use the qualitative argument that the rigidity of the membrane κ, increases with the thickness of the membrane. Considering that the thickness of the membrane is proportional to $d_p\gamma$, we can conclude that κ increases as γ increases. Thus from Eq. 4.4, the SAXS intensity should decrease with increasing surfactant concentration γ . This is in agreement with the results that are shown in Fig. 4-7.

Therefore, in the almost-bilayer cases, the intensity I_{SAXS} with the dilution at fixed α, is controlled by δ, κ, d and ϕ, and all of them contribute towards increasing the intensity. This is indeed the case with our results as $\alpha \rightarrow 0$ or $\alpha \rightarrow 1$ as shown in Fig. 4-7

Variation of oil to water ratio at constant surfactant concentration:

We will now look at the changes in the SAXS intensity as α changes at fixed γ. In this case, we will also examine two extreme cases, i.e. $\alpha \rightarrow 0$ or 1 (bilayer), or when $\alpha = 0.5$, (monolayer). The periodicity for a monolayer is half the periodicity of a bilayer d, the bending rigidity is κ_{mono} with $\kappa_{mono} = \kappa_{bilayer}/2$. The membrane thickness is δ for the monolayer and 2δ for the bilayer. From Eq. 4.4 , we expect the highest intensity for the bilayer case. The data are in agreement with this, Fig. 4-8.

4.1.3 Quasi-Bragg Scattering

As we have seen in Chapter 3, the scattering intensity can be expressed as the product of the structure factor and form factor.

$$I(\mathbf{q}) = \sum_{0}^{N-1} cos(nq_z d) e^{-\frac{q_z}{2}<(u_n-u_0)^2>} < |\int_0^{\delta} \rho_o(z) e^{iqz} dz|^2 | \int_0^{L} \rho(r_\perp) e^{i\mathbf{q}\mathbf{r}_\perp} d\mathbf{r}|^2 > \quad (4.6)$$

Form Factor

By using the density profile introduced in Chapter 2, the form factor for the bilayer system can be calculated as,

$$P_z = \frac{4}{q^2}(\rho_{water} - \rho_{oil})^2 sin^2(q\frac{\delta}{2}) \quad (4.7)$$

Usually, the lineshape analysis of a smectic system is done by assuming the form factor to be constant. [2] [16] If the thickness of the bilayer is much smaller compared to the repeating periodicity, one can approximate the form factor to be constant.

As it is shown in Figs. 4-9 and 4-4, this is not a good assumption for the present

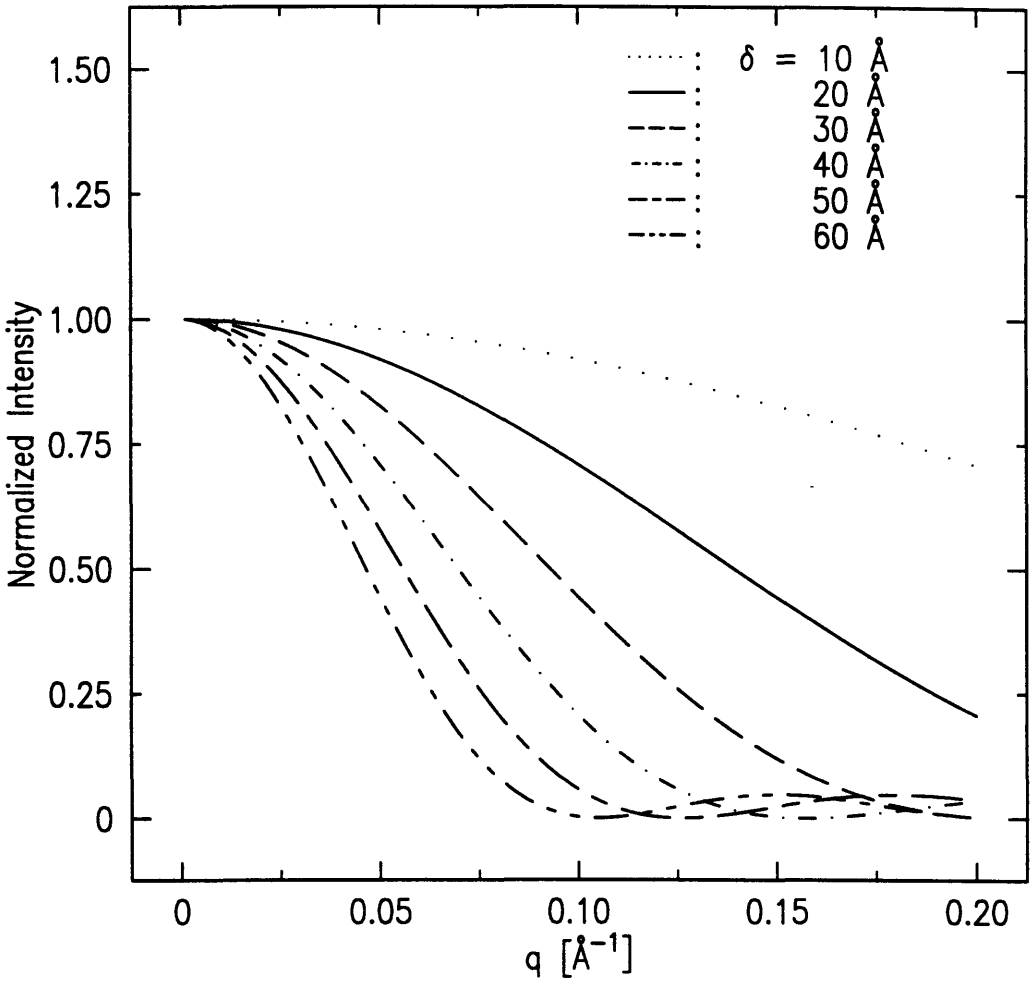

Figure 4-9: Variation of formfactor with bilayer thickness

system. It is important not to neglect the form factor particularly as we increase the thickness of the bilayer at constant surfactant concentration: i.e. constant periodicity, especially when the periodicity of the order parameter is comparable to that of the bilayer thickness. In Fig. 4-9 we show the dependence of the form factor on the bilayer thickness δ.

Structure Factor

The dependence of the lineshape for the quasi-Bragg peaks on η, for the three structure factors derived in Chapter 2, Eqs. 2.43, 2.30 2.59 and are shown in Figs. 4-10, 4-11 and 4-12.

(1) The structure factor proposed by Safinya et.al.[2] originated from a Caillé-type correlation function as was modified by Kaganer et.al.[41].The density correlation function $g(\mathbf{x})$, is calculated with the integration over q_z with $q_z^{max} \rightarrow \infty$ This model is expected to be valid only in the near vicinity of peak position because of the approximation $q = q_0$ done in order to get the correlation function

$$S(q) = \int_{-\infty}^{\infty} dz g(0,z) exp(-iq_z z) \tag{4.8}$$

In order to get Eq. 4.8 from Eq. 2.43, the following approximation was done. Since the powder averaging part in Eq. 2.43, $sinqr/qr$, is a rapidly oscillating function and the only considerable contribution to the integral comes in near the z axis , where $r_\perp \ll z$, by approximating $r_\perp = 0$ leads to a one-dimentional integral in Eq. 4.8.

(2) The structure factor proposed by Gunter et. al.[30]

The correlation function was calculated with the summation in q_z direction replacing q_z by $n\pi/L$ This model also uses the approximation $q = qm$ in calculating the density density correlation function.

$$S(q) = 1 + 2\sum_{1}^{N-1}(1 - \frac{n}{N})cos(nq_z d_p)e^{-\eta_m[ln(\pi n)+\gamma]} \tag{4.9}$$

(3) The structure factor proposed by Nallet et.al.[34] originated from the same correlation function model of Gunter et.al. [30]. The approximation $q = q_m$ is not made and the model should work well away from $q = q_m$.

$$S(q) = 1 + 2\sum_{1}^{N-1}(1 - \frac{n}{N})cos(nq_z d_p)e^{-\frac{q_z^2}{2}\frac{\eta}{2\pi^2}(ln(\pi n)+\gamma)d_p^2} \tag{4.10}$$

As it can be seen, the difference between Eq. 4.8 and Eq. 4.9. Eq. 4.10 is the absence in the higher harmonics in 4.8, and also that the summation over n in

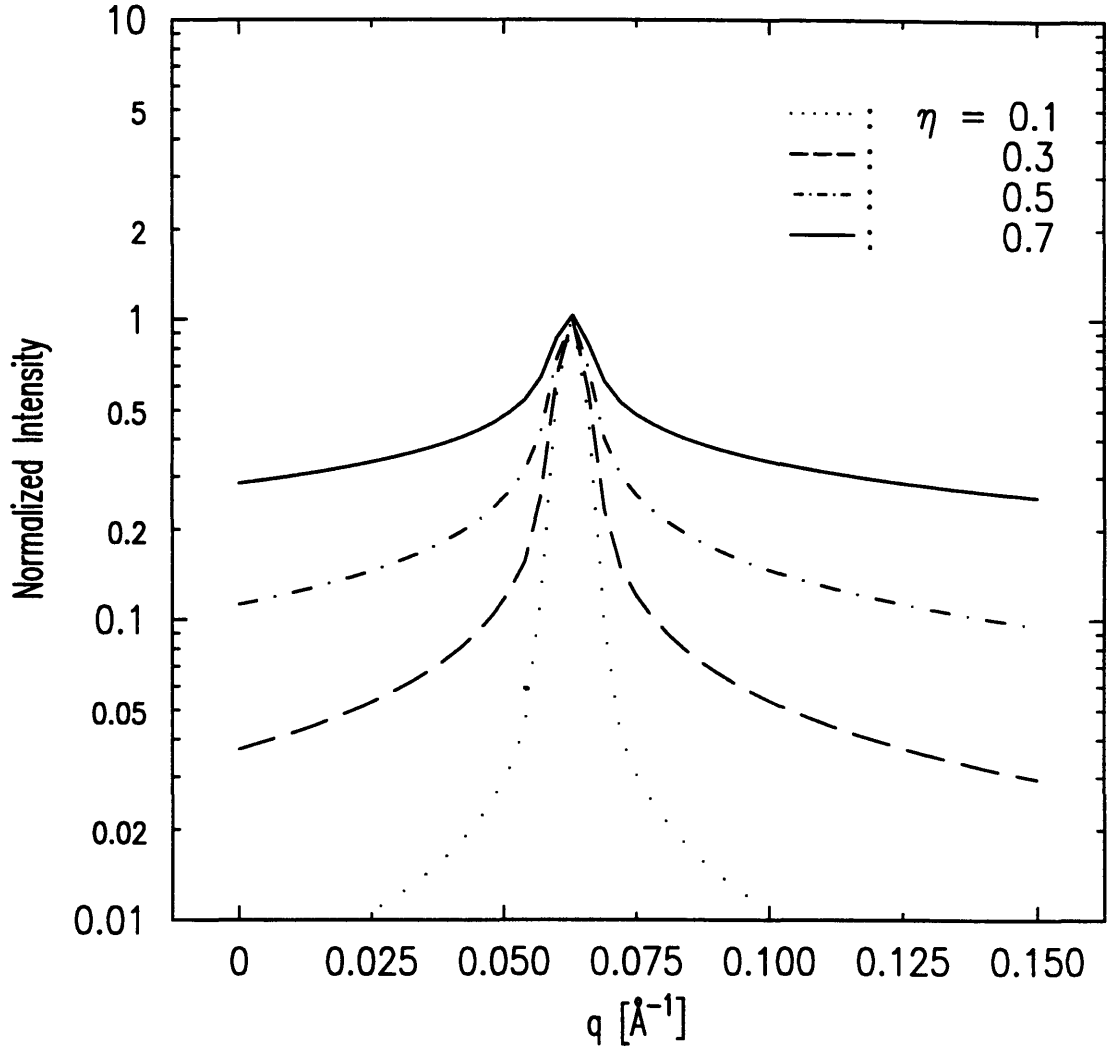

Figure 4-10: The structure factor Eq. 4-8, for various η, from 0.1, to 0.7, for the case $z \gg x, y$

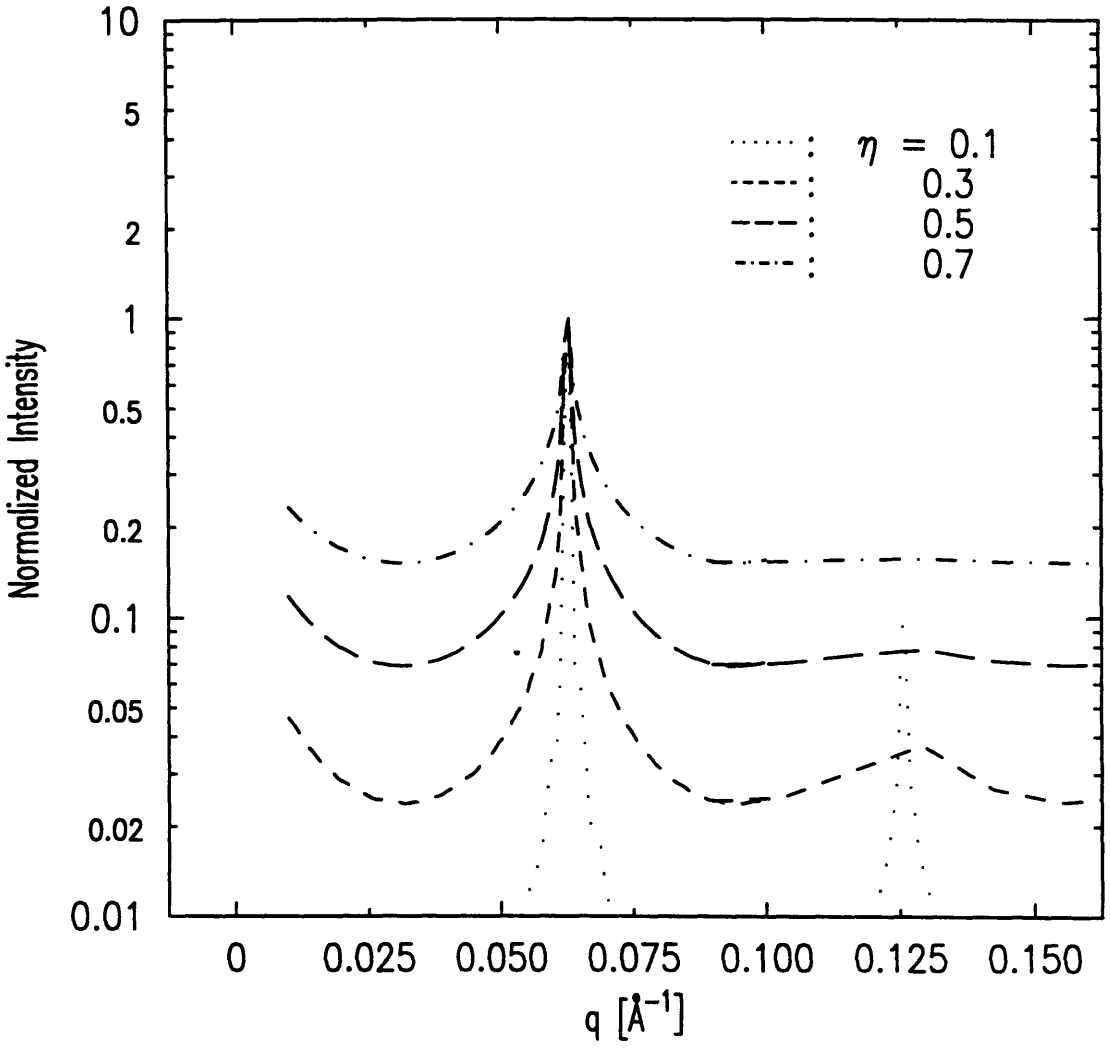

Figure 4-11: The structure factor Eq. 4-9, for various η, from 0.1, to 0.7, for the case $z \gg x, y$

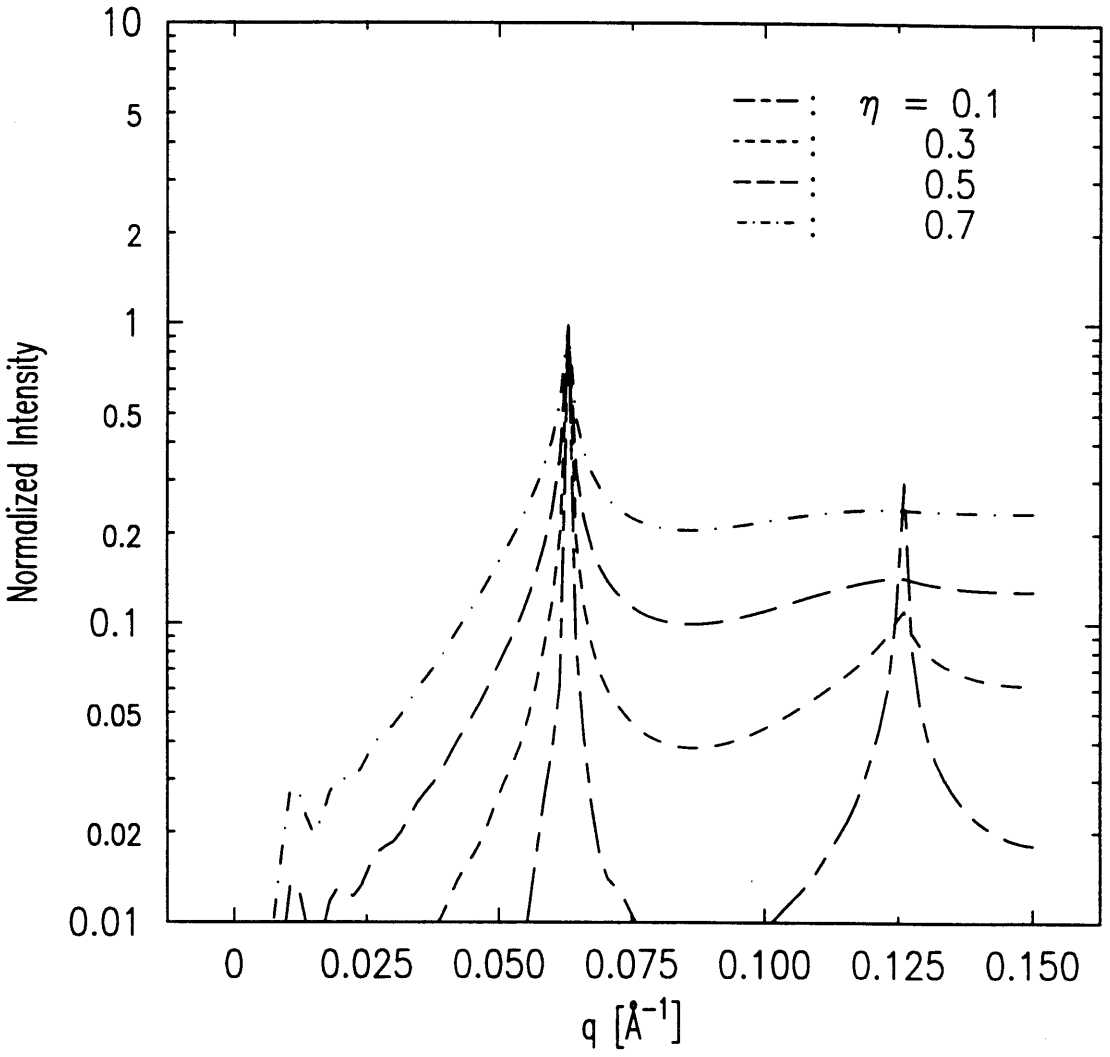

Figure 4-12: The structure factor Eq. 4-10, for various η, from 0.1, to 0.7, for the case $z \gg x, y$

z direction with $z = nd_p$ is taken place by the integral, thus the . The difference between Eq. 4.9 and Eq. 4.10 is that while Eq. 4.9 is valid only close to the quasi-Bragg peaks, 4.10 can continuously describe the behavior of the intensity profiles away from q_0 since the approximation $q = q_0$ is not made.

4.2 Fitting of the Data and the Variation of the Parameter

4.2.1 The Comparison of the Three Structure Factors

We fitted the data with the three expressions for the structure factors. The fitting of the data was done by using Certified Scientific Software's C-PLOT data analysis program with non-linear squares fitting routines. The spectra were fit to the structure factors multiplied by the form factor 4.7. In the case of 4.8 and 4.10, the resolution was convolved only with the structure factor with the approximation that the structure factor is a much faster varying function, while in the case of 4.9, the convolution was done to the product of the structure factor and the form factor, because of the relatively simpler structure factor.

1)

$$I(q) = A_0 \int_{-\infty}^{\infty} dz g(0,z) exp(-\frac{\pi \mathbf{r}^2}{L^2}) exp((-\nabla q)^2 \mathbf{r}^2) exp(-iq_z z) \frac{1}{q^4} \nabla \rho^2 sin^2(q\frac{\delta}{2})) \quad (4.11)$$

2)

$$I(q) = \frac{A_0}{q^4}(1 - e^{-(\delta \nabla q_z)^2/2} cos(\delta q_z) + \sum_{n=1}^{N-1}(1 - n/N)(2e^{2\gamma}(1 - cos(n\pi/N)))^{-\eta/2}$$
$$\times (2e^{-(nd_p)^2 \nabla q^2/2} cos(nd_p q_z) - e^{-(nd_p - \delta)^2 \nabla q^2/2} cos((nd_p - \delta)q_z)$$
$$- e^{-(nd_p + \delta)^2 \nabla q^2/2} cos((nd_p + \delta)q_z)) \quad (4.12)$$

3)

$$I(q) = A_0(1 + 2\sum_{1}^{N-1}(1 - \frac{n}{N})cos(\frac{nq_z d}{1 + 2\nabla q^2 d^2 \alpha(n)})\ exp(\frac{2q_z^2 d^2 \alpha(n) + \nabla q^2 d^2 n^2}{2(1 + 2\nabla q^2 d^2 \alpha(n))}) \times \frac{1}{\sqrt{1 + 2\nabla q^2 d^2 \alpha(n)}})\frac{1}{q^4}\nabla\rho^2 sin^2(q\frac{\delta}{2})) \quad (4.13)$$

where $\alpha(n) =< (u_n - u_0)^2 > /2d^2$.

For the fitting range, we chose $q_{min} = q_0/2$ to avoid the excess scattering at $q \rightarrow 0$. For q_{max}, in the case of Eqs. 4.11 and 4.12, it was chosen to be $q_{max} = 1.8q_0$, while for Eq. 4.13, since it was possible to fit simultaneously of the first and second harmonics, it was chosen to be $q_{max} = 2.5q_0$. The density difference ρ was chosen to be the electronic density difference between water and octane which is $0.09e\mathring{A}^{-3}$ and $\nabla q = 0.0017\mathring{A}^{-1}$ was the half width half maximum of the measured resolution function.

The fitting was attempted for all three functions Eqs. 4.11 4.12 and 4.13, the fitting for two of the peaks are shown in Figs 4-13. Fig. 4-13 shows, the two functions Eq. 4.11 and 4.12 which use the approximation $q_z = q_0$, do not fit the tail of the broad peaks. Therefore, finally, we chose the function Eq. 4.13 to be the most adequate fitting function for our system, In Figs. 4-14 $\sim$ 4-20, and Tables 4.1 $\sim$ 4.4, the fitted intensity profiles as well as the fitted parameters with the function (3), Eq. 4.13 are given.

4.3 Discussion

First of all, from the Fig. 4-18, we can see the trend of the membrane thickness δ. It has a maximum at $\alpha = 0.50$, as the membrane thickness is the maximum when the oil-water ratio is 1:1. It can be defined that $\delta(\alpha > 50\%) \equiv$ water bilayer thickness, $\delta(\alpha < 50\%) \equiv$ oil bilayer thickness,

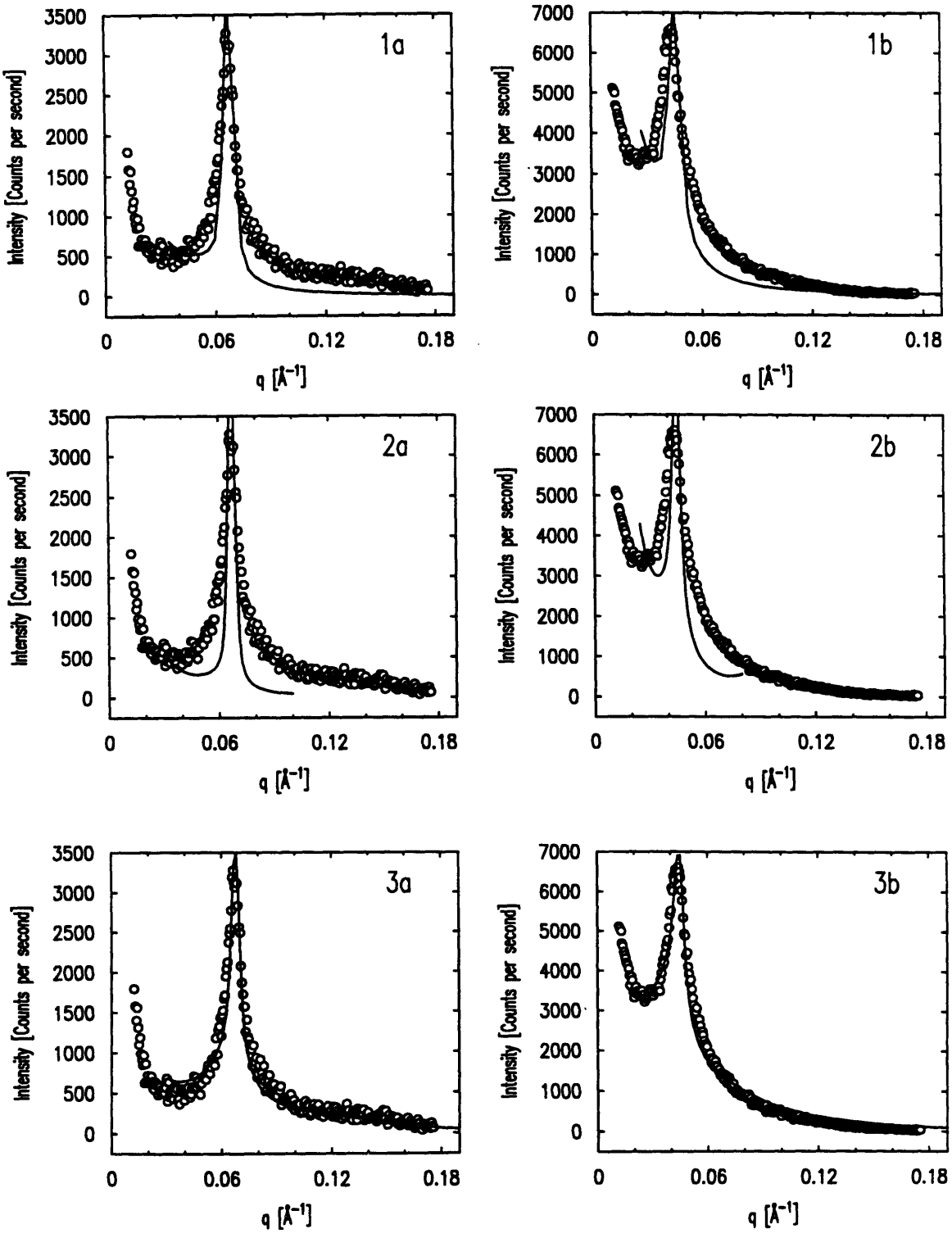

Figure 4-13: The three fitting functions are shown for the fitting of the spectra $\alpha = 0.2$ $\gamma = 0.30$ and $\alpha = 0.2$ $\gamma = 0.20$. 1a and 1b are Eq. 4-11, 2a and 2b are Eq. 4-12, 3a and 3b are Eq. 4-13

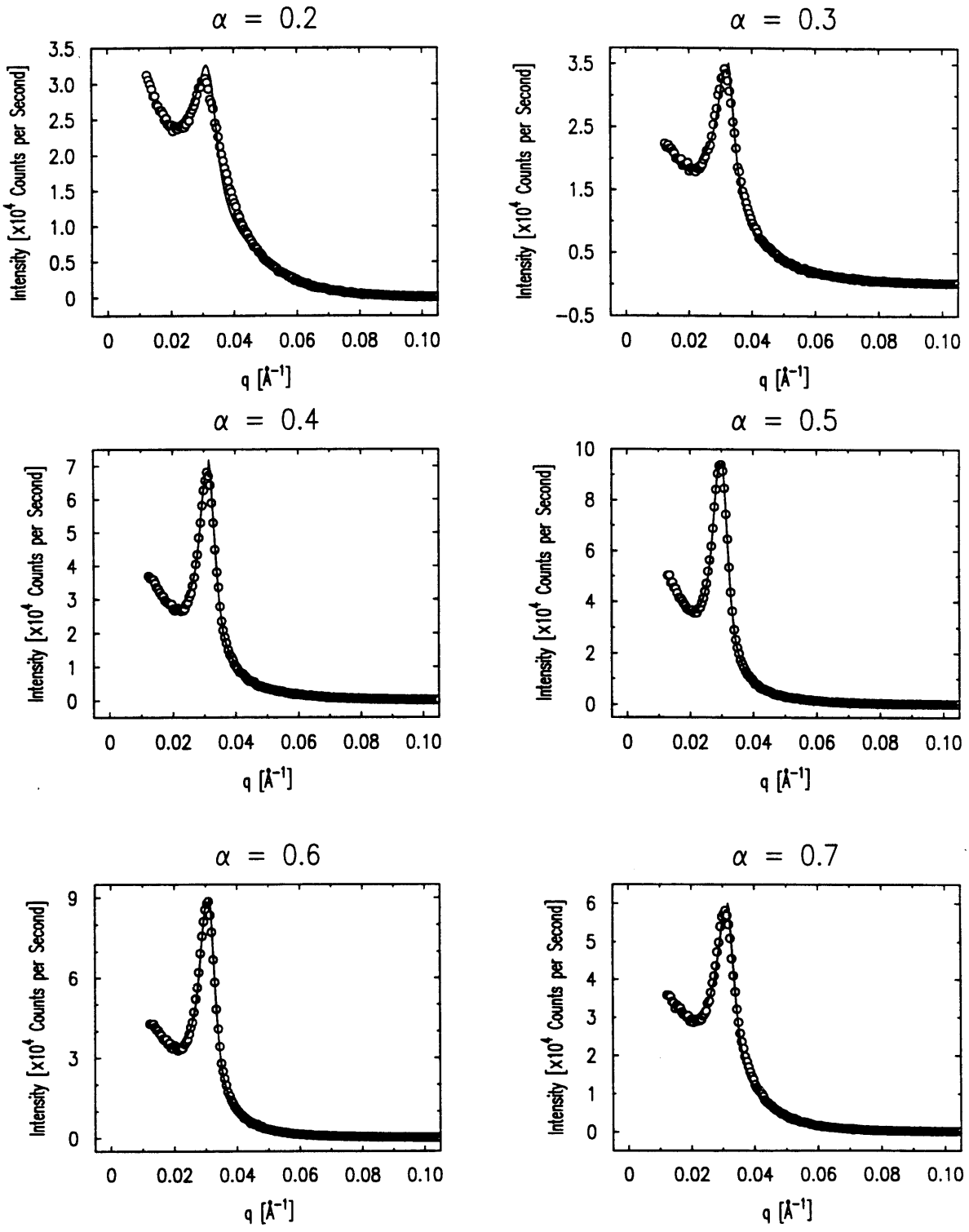

Figure 4-14: The fitting of the intensity profiles (open circles), fitting done by Eq.(solid line) : $\gamma = 0.15$

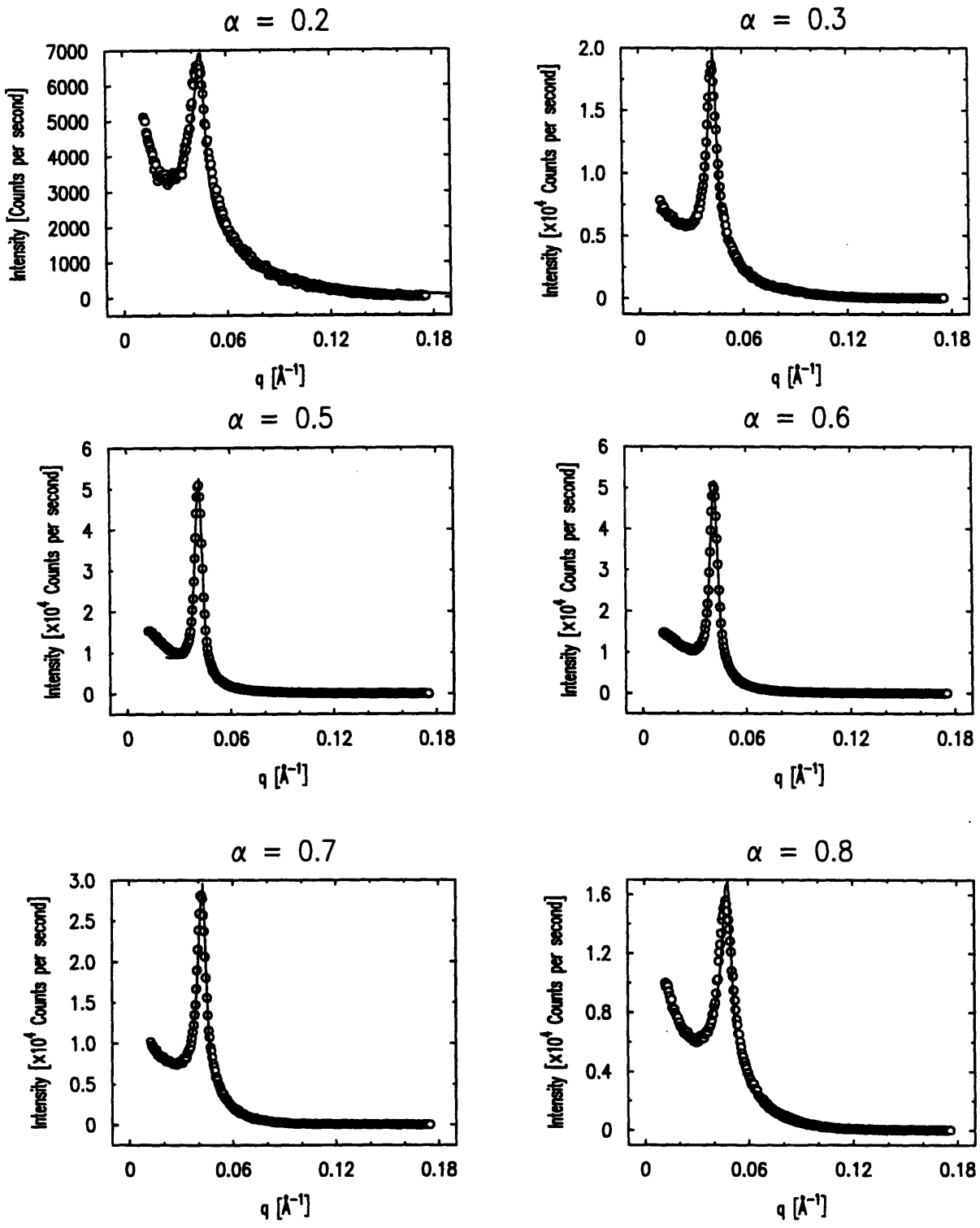

Figure 4-15: The fitting of the intensity profiles (open circles), fitting done by Eq.4-13 (solid line) : $\gamma = 0.20$

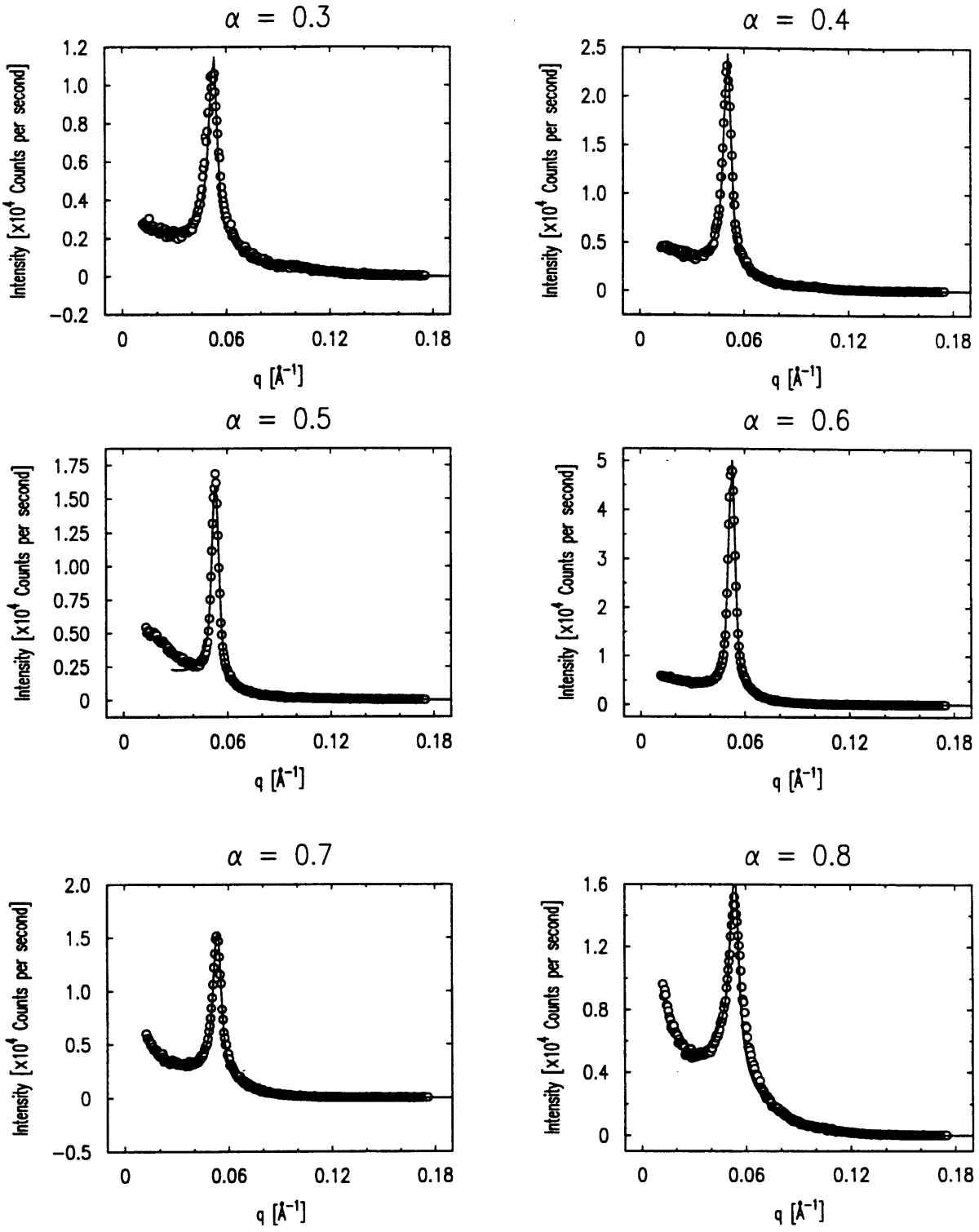

Figure 4-16: The fitting of the intensity profiles (open circles), fitting done by Eq. 4-13(solid line) : $\gamma = 0.25$

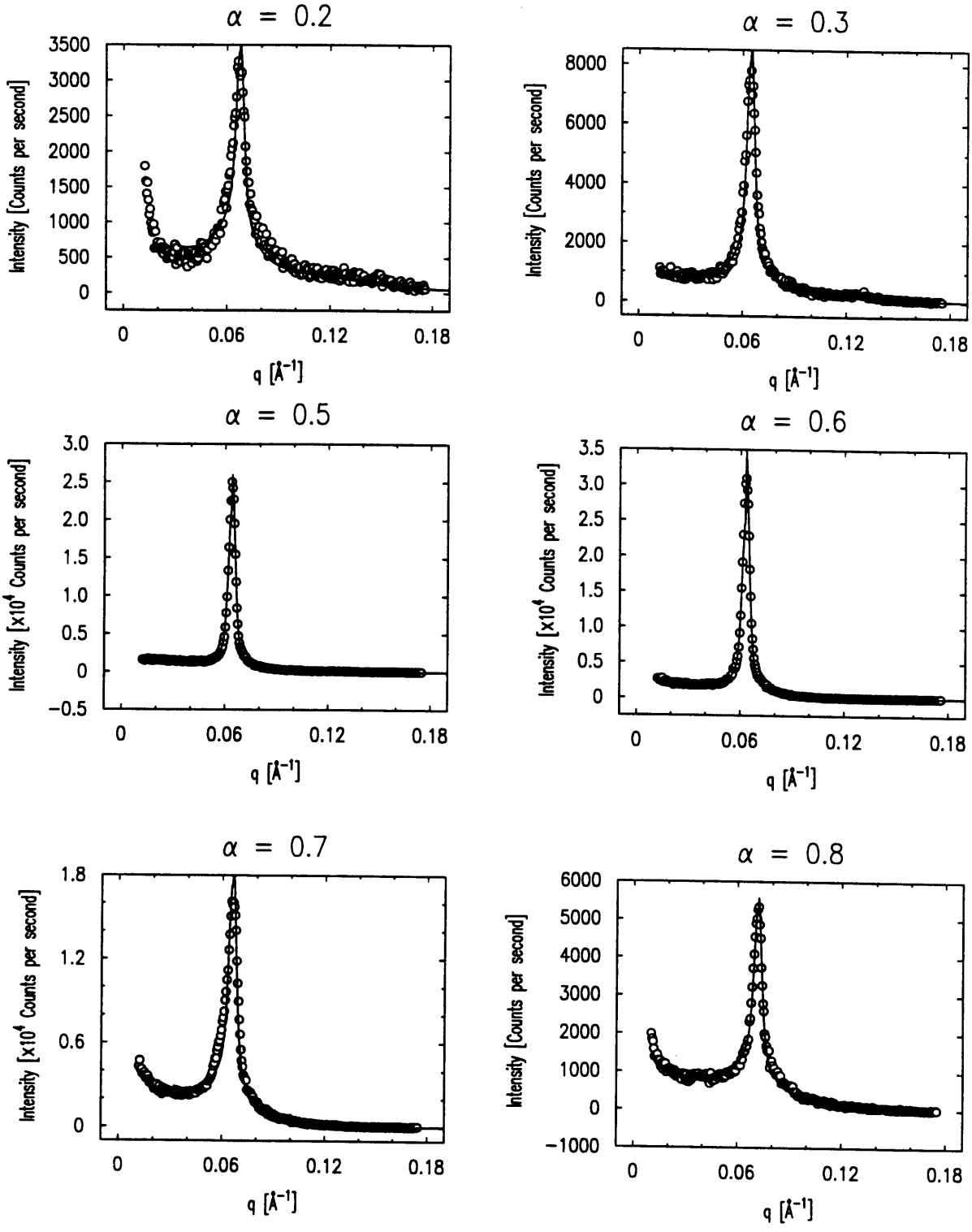

Figure 4-17: The fitting of the intensity profiles (open circles), fitting done by Eq. 4-13 (solid line) : $\gamma = 0.30$

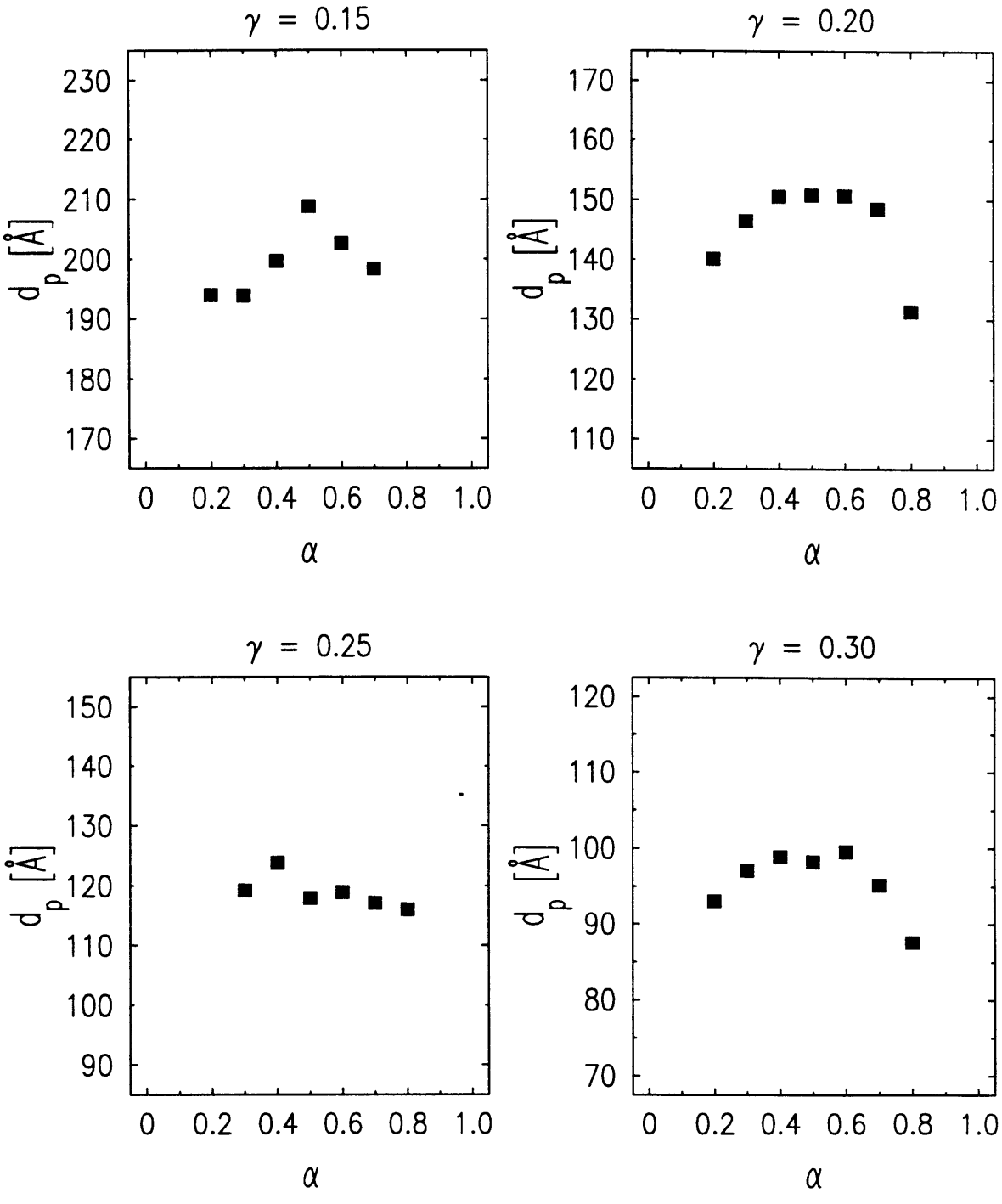

Figure 4-18: The periodicity $d_p$vs α

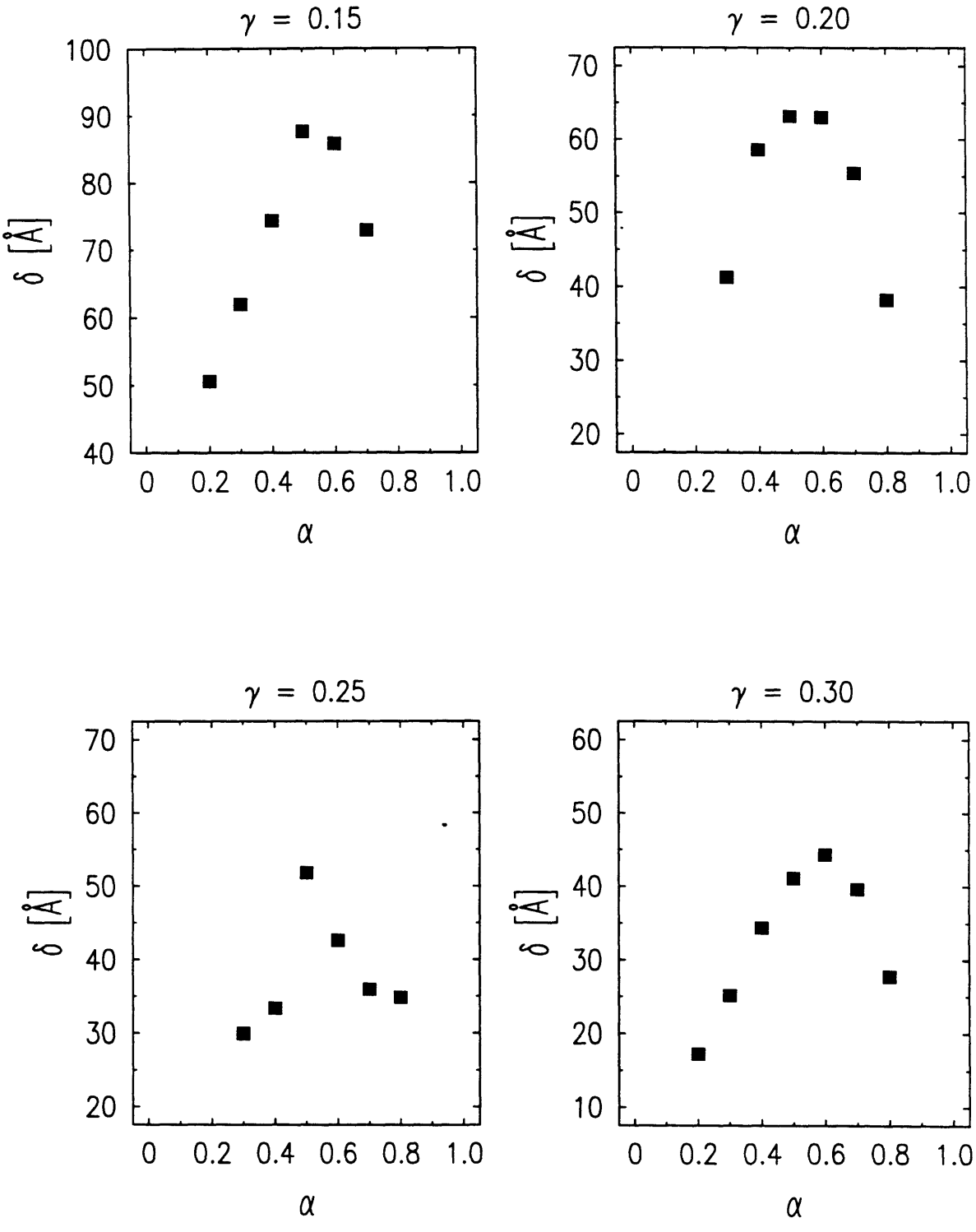

Figure 4-19: The membrane thickness δ vs α

$\gamma = 0.15$	α	η	$\delta\mathring{A}$	d_p (Å)	A_0
	0.2	0.976	52.2	194	0.0369
	0.3	0.757	60.1	192	0.0272
	0.4	0.551	71.4	199	0.0317
	0.5	0.496	79.8	208	0.0325
	0.6	0.517	79.4	202	0.0341
	0.7	0.685	70.2	197	0.0333

Table 4.1: Fitted parameters for $\gamma = 0.15$

$\gamma = 0.20$	α	η	$\delta(\mathring{A})$	d_p (Å)	A_0
	0.2	0.849	23.9	138	0.0553
	0.3	0.602	39.3	146	0.0419
	0.4	0.458	52.9	149	0.0409
	0.5	0.367	61.8	150	0.0405
	0.6	0.395	61.9	150	0.0430
	0.7	0.505	54.5	148	0.0338
	0.8	0.684	36.4	131	0.0588

Table 4.2: Fitted parameters for $\gamma = 0.20$

$\gamma = 0.25$	α	η	$\delta(\mathring{A})$	d_p (Å)	A_0
	0.3	0.515	29.9	119	0.0509
	0.4	0.403	33.4	124	0.0649
	0.5	0.357	51.8	118	0.0269
	0.6	0.271	42.6	119	0.0781
	0.7	0.467	36.0	117	0.0484
	0.8	0.636	34.9	116	0.0738

Table 4.3: Fitted parameters for $\gamma = 0.25$

$\gamma = 0.30$	α	η	$\delta(\mathring{A})$	d_p (Å)	A_0
	0.2	0.510	8.99	92.8	0.218
	0.3	0.380	23.3	96.7	0.0622
	0.4	0.219	32.2	98.5	0.0554
	0.5	0.197	39.6	97.9	0.0551
	0.6	0.217	42.0	98.9	0.0698
	0.7	0.394	37.9	94.7	0.0774
	0.8	0.446	29.1	87.4	0.0414

Table 4.4: Fitted parameters for $\gamma = 0.30$

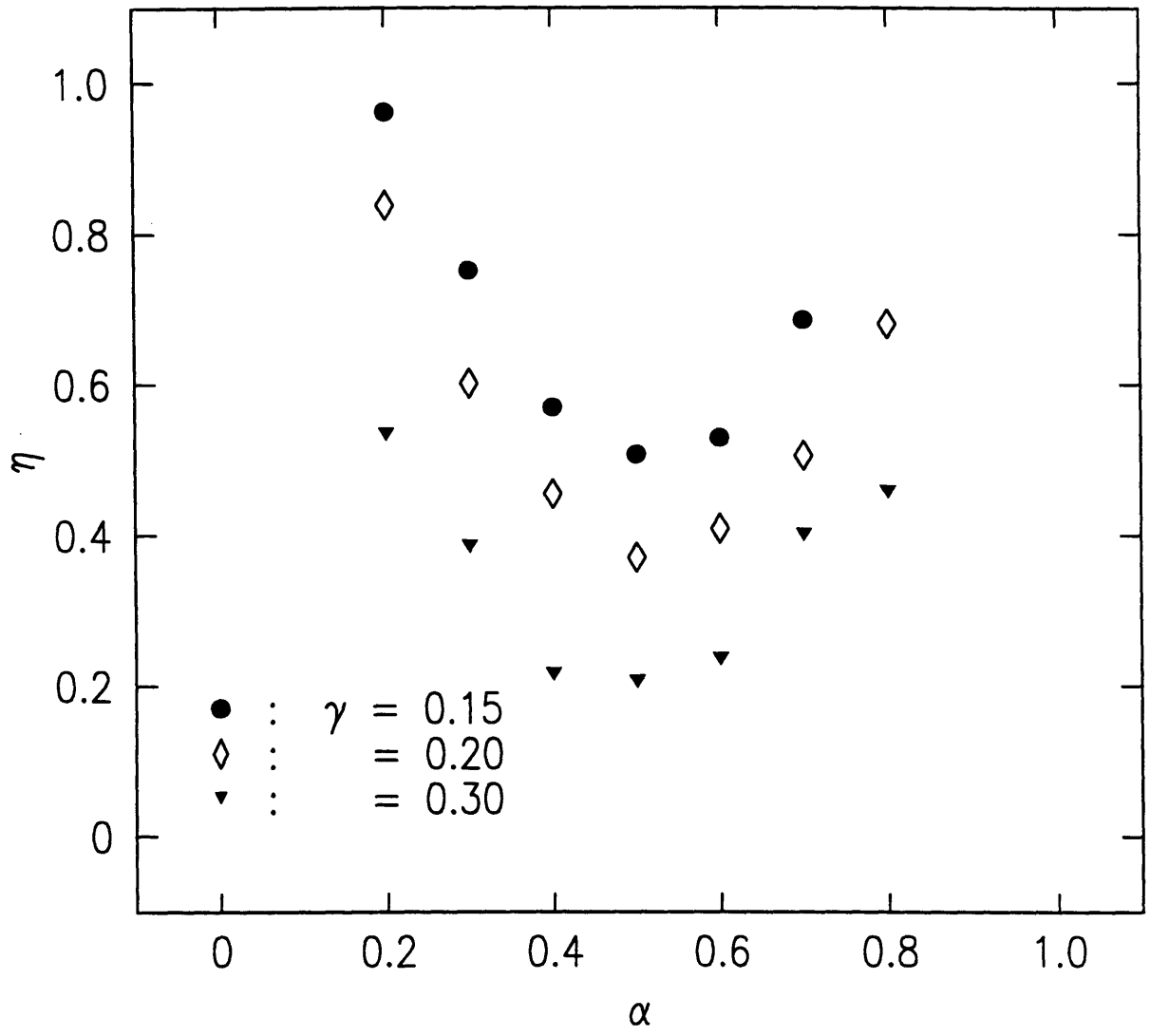

Figure 4-20: η vs γ for various γ's

The periodicity as $\alpha \rightarrow 0$ or 1 is smaller than for $\alpha = 0.5$. although the surfactant concentration γ is fixed. We will discuss this phenomenon in detail in the next chapter focused on aligned samples.

Another interesting feature which is quite striking is the intensity variation with the change of α. As we have mentioned in Chapter 2, the first order Bragg peak intensity scales as $\lambda^{1-\eta}/d^2$ [30] where $\lambda = \sqrt{K/B}$: λcharacterizes the decay of an undulation distortion at the surface of the smectic. Using the elastic constants

derived in Chapter 1 in the case of sterically interacting lamellae, this relation can be reduced to be $I_{Bragg} \sim d^{-\eta}$. Therefore an increase of η should lead to a decrease of the intensity at constant periodicity. From Figs. 4-20 and 4-5 we can see the agreement.

4.3.1 Bilayer Model

To deal with a lamellar system as mode of three components with different densities and characteristics will require an enormous mathematical computation. Instead, one can perform several approaches with reasonable approximations in order to simplify the problem, one of which is to apply the bilayer model and take the case of the $\alpha = 0.50$ to be the extreme case of a thick bilayer.

First, we want to discuss the variation of η with γ, as well as α. Here we introduce the notation ϕ_o, ϕ_w, ϕ_s for the volume fraction of oil, water, and surfactant respectively,

$$\phi_o + \phi_w + \phi_s = 1 \tag{4.14}$$

By definition,

$$\alpha = \phi_o/(\phi_o + \phi_w), \ \gamma = \phi_s \tag{4.15}$$

We can rewrite Eq. 1.36 derived for the bilayer lamellar system, where either $\phi_o = 0$ or $\phi_w = 0$ by noting that the intermembrane distance $d = d_p\phi_w$ or $d = d_p\phi_o$ we get:

$$\overline{B} = \frac{9\pi^2}{64}\frac{(kT)^2}{\kappa}\frac{1}{d^3\phi_w^4}, \qquad \text{for} \qquad \phi_o = 0 \tag{4.16}$$

$$\overline{B} = \frac{9\pi^2}{64}\frac{(kT)^2}{\kappa}\frac{1}{d^3\phi_o^4}, \qquad \text{for} \qquad \phi_w = 0 \tag{4.17}$$

By using $K = \kappa/d$, these lead to,

$$\eta = \frac{4}{3}\phi_w^2 \ or \ \eta = \frac{4}{3}\phi_o^2 \tag{4.18}$$

Combining with Eq. 4.15, we get,

$$\eta = \frac{4}{3}\alpha^2(1-\gamma)^2 \qquad \alpha \approx 1 \tag{4.19}$$

$$\eta = \frac{4}{3}(1-\alpha)^2(1-\gamma)^2 \qquad \alpha \approx 0 \tag{4.20}$$

In Fig. 4-21 we show the η values from the fitting and also the theoretically predicted values for η using Eq. 4.19 and 4.20, for each γ as a function of α. The data show not only a good qualitative agreement with the theory for the decrease as $\alpha \rightarrow 0.5$, we also see a reasonably good quantitative agreement.

However, this theory clearly breaks down as $\alpha \rightarrow 0.5$, since the derivative of Eq. 4.19 and 4.20 is discontinuous at $\alpha = 0.5$.

4.3.2 Swelling of the lamellae with monolayers

We have also checked the deviation of the periodicity from the linear dilution law. We have discussed in Chapter 1 that the excess area caused by the thermal fluctuations gives a logarithmic correction to the linear dilution law. [27]

$$d = \frac{\delta}{\phi}[1 + \frac{kT}{4\pi\kappa}\log(\frac{c\delta}{a}\sqrt{\frac{\kappa}{kT}}\frac{1}{\phi})] \tag{4.21}$$

Where $2\pi/a = q_{max}$ is the shortest possible wavelength of the fluctuation which is taken to be the distance between the molecules in the smectic plane, $a \approx 5\mathring{A}$, c is a proportionality constant between the periodicity and the longest allowed wave-length of the fluctuations ξ.

$$\xi = c\sqrt{\frac{\kappa}{kT}}d \tag{4.22}$$

Here the exact value of the constant c is model-dependent. According to the unified microscopic theory for a dilute lyotropic smectic-A phase proposed by Golubovic and Lubensky [18] $c = (32/3\pi)^{1/2} = 1.84$

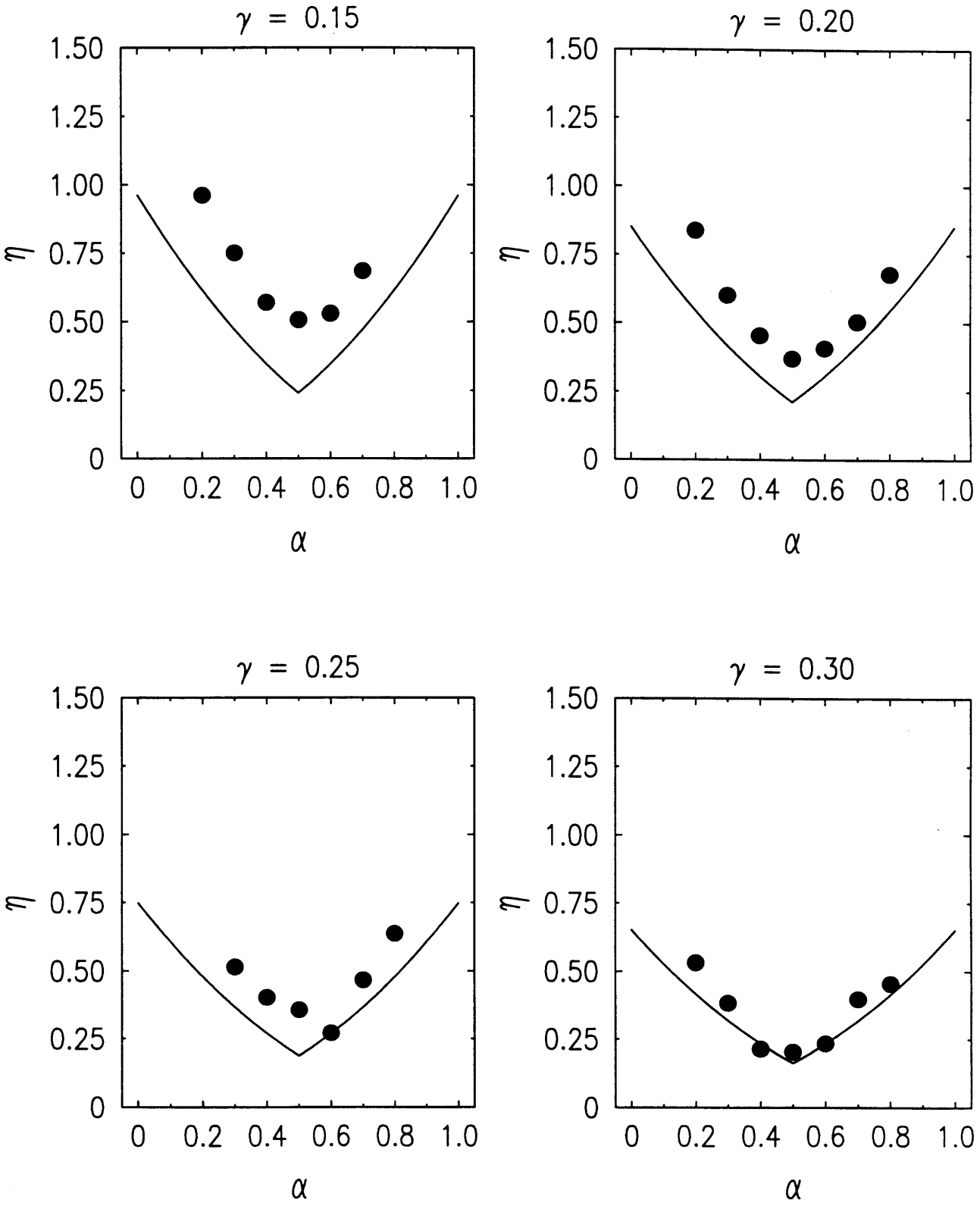

Figure 4-21: η measured (filled circle) is shown along with the theoretically predicted values (solid line)

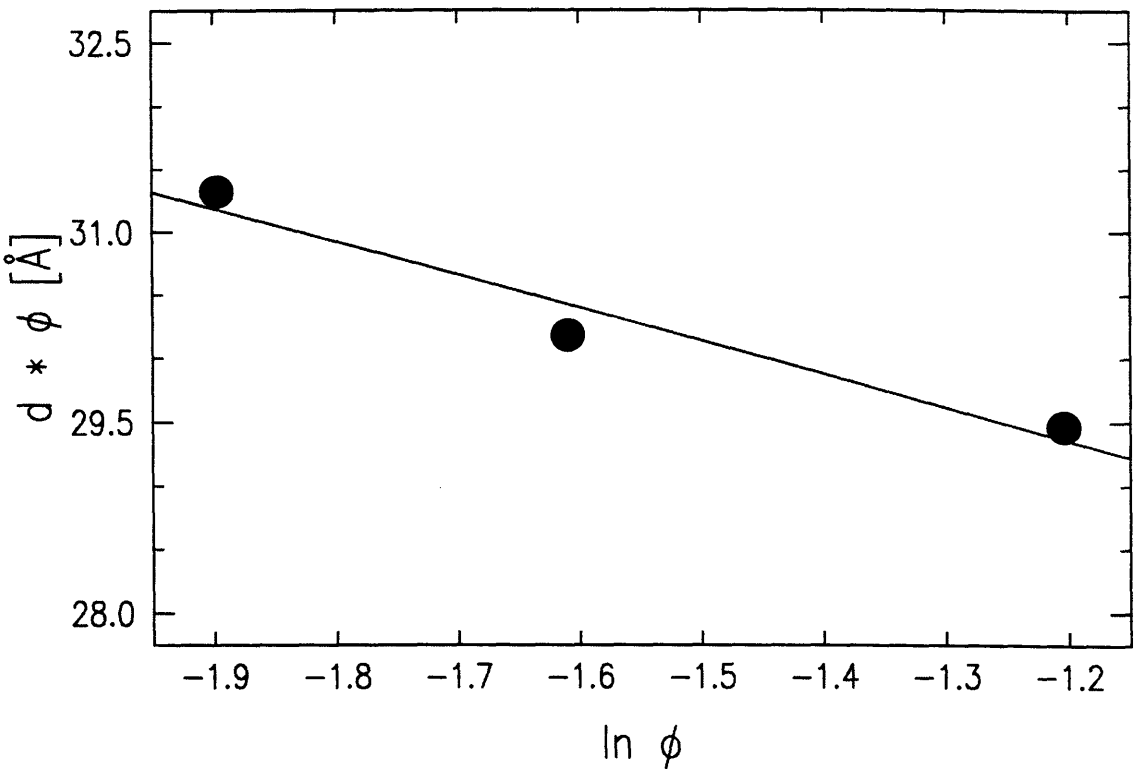

Figure 4-22: Experimentally derived valued of $d_p\phi$ vs ln ϕ for $\alpha = 0.5$. The solid line is the fit with the theoretically predicted Eq. of the logarithmic correction

In our case, neither δ nor δ/ϕ is constant as γ is increased. Moreover, the change in the membrane thickness δ will also affect the value of κ. However, in the case of $\alpha = 0.5$, on the assumption that the interactions between the monolayers are Helfrich-like, we can assume a constant monolayer thickness and carry on the theory of swelling from the bilayer system to the monolayer case. In Fig. 4-22, we show $d_p\phi$ vs $ln\phi$. From a least-square fit to 4.21 we get

$$\delta\frac{kT}{4\pi\kappa} = 2.61 \pm 0.61 \tag{4.23}$$

From the first order approximation, $d_p = \delta/\phi$. By substituting $d_p \approx 100$Å, as measured for $\phi \equiv \gamma = 0.30$ we get, $\delta_{bilayer} = 30$Å. We speculate that the thickness of

a monolayer in the lamellar phase is $\delta_{mono} \approx \delta_{bilayer}/2 \approx 15$ Å. Using 4.23 we get for the monolayer bending rigidity:

$$\kappa_{mono} \approx 0.45kT \tag{4.24}$$

4.3.3 Monolayer Model

We can also approach the problem by modeling a monolayer as a bilayer membrane with the bending rigidity of the monolayer. The interactions with the water and oil layers are both approximated to be Helfrich-like. We can write the free energy of the system to be the sum of these two interactions. The interaction energy of two monolayers with oil in between them is written as V_o, and with water is written as V_w.

Using similar arguements as in Chapter 1, we will derive the expression for $\overline{B}$ for a monolayer system. We shall continue to use the notation of ϕ's as the volume fraction of the three components. The free energy of the system is a function of ϕ_o and ϕ_w only, and can be written as

$$F = \int d^3x f(\phi_o, \phi_w) \tag{4.25}$$

In this case, we can assume the free energy density to be the sum of two interaction energies.

$$f(\phi_o, \phi_w) = \frac{1}{d_p}[V_o(d_p\phi_o) + V_w(d_p\phi_w)] \tag{4.26}$$

Here $d_p\phi_o$ and $d_p\phi_w$ are the oil and water thickness respectively. $V_{o,(w)}$ is the interaction energy per unit area between two surfactant interfaces separated by the solvent layer of the thickness (x).

As was done in Chapter 1, we again, perform a Taylor expansion of f to second order of the concentration fluctuations $\delta\phi_o, \delta\phi_w$.

$$f = f_0 + \frac{1}{2}[\frac{\partial^2 f}{\partial\phi_o^2}\delta\phi_o^2 + \frac{2\partial^2 f}{\partial\phi_o\partial\phi_w}\delta\phi_o\delta\phi_w + \frac{\partial^2 f}{\partial\phi_w^2}\delta\phi_w^2] \tag{4.27}$$

The elastic constants of the two component smectic system were defined by the free energy density written as

$$f = f_o + \frac{B}{2}(\frac{\partial u}{\partial z})^2 + \frac{1}{2}K_1(\frac{\partial^2 u}{\partial x^2} + \frac{\partial^2 u}{\partial y^2})^2 + \frac{1}{2\chi}\delta c^2 + C_c \delta c \frac{\partial u}{\partial z} \tag{4.28}$$

Here we will only consider compression. Defining, $\delta c \equiv \delta\phi_o - \delta\phi_w$ as a concentration variable, and also using $\partial u/\partial z = \delta d_p/d_p = (\delta\phi_w + \delta\phi_o)/\phi_s$, and by comparing, 4.27 and 4.28 we get,

$$B = \frac{d_p}{4}[W_w(1 - \phi_o + \phi_w)^2 + W_o(1 - \phi_w + \phi_o)^2] \tag{4.29}$$

$$\chi^{-1} = \frac{d_p}{4}[W_w + W_o] \tag{4.30}$$

$$C_c = \frac{-d_p}{4}[W_w(1 - \phi_o + \phi_w) - W_o(1 - \phi_w + \phi_o)] \tag{4.31}$$

Where W_w, W_o are $\delta^2 V_w/\delta d_w^2$ and $\delta^2 V_o/\delta d_o^2$, respectively. Thus, using $\overline{B} = B - C_c^2\chi$ we get,

$$\overline{B} = d_p \frac{W_w \cdot W_o}{W_w + W_o} \tag{4.32}$$

Now, from our assumption that both V_o and V_w are Helfrich-like potentials, they can be written:

$$V_o = A\frac{kT^2}{\kappa d_o^2} \tag{4.33}$$

$$V_w = A\frac{kT^2}{\kappa d_w^2} \tag{4.34}$$

where $A = 3\pi^2/128$. Substituting into 4.32, and using, $d_o = d_p\phi_o$ $d_w = d_p\phi_w$ we get,

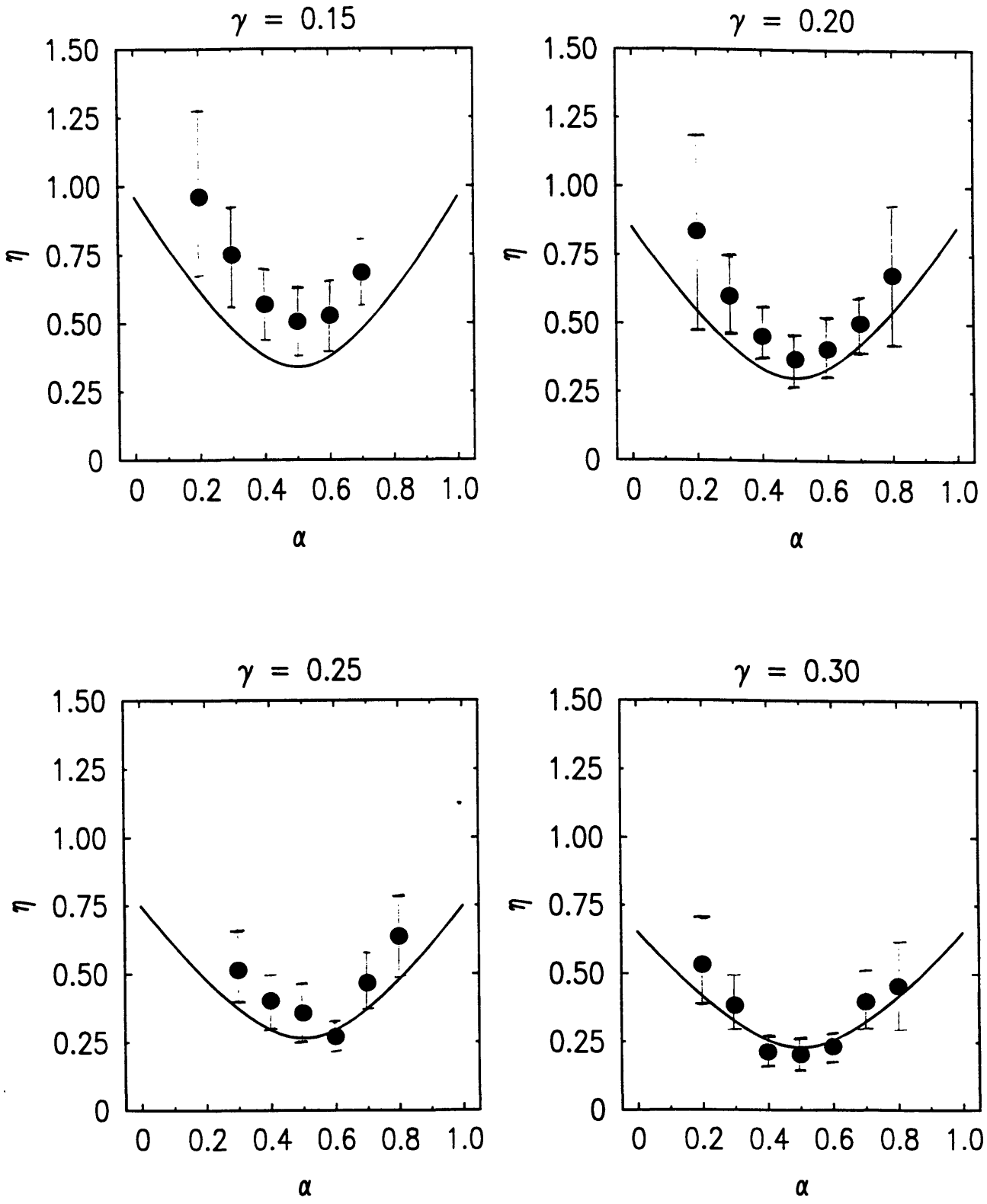

Figure 4-23: η from the fit(filled circle) is shown with the theoretically predicted model(solid line)

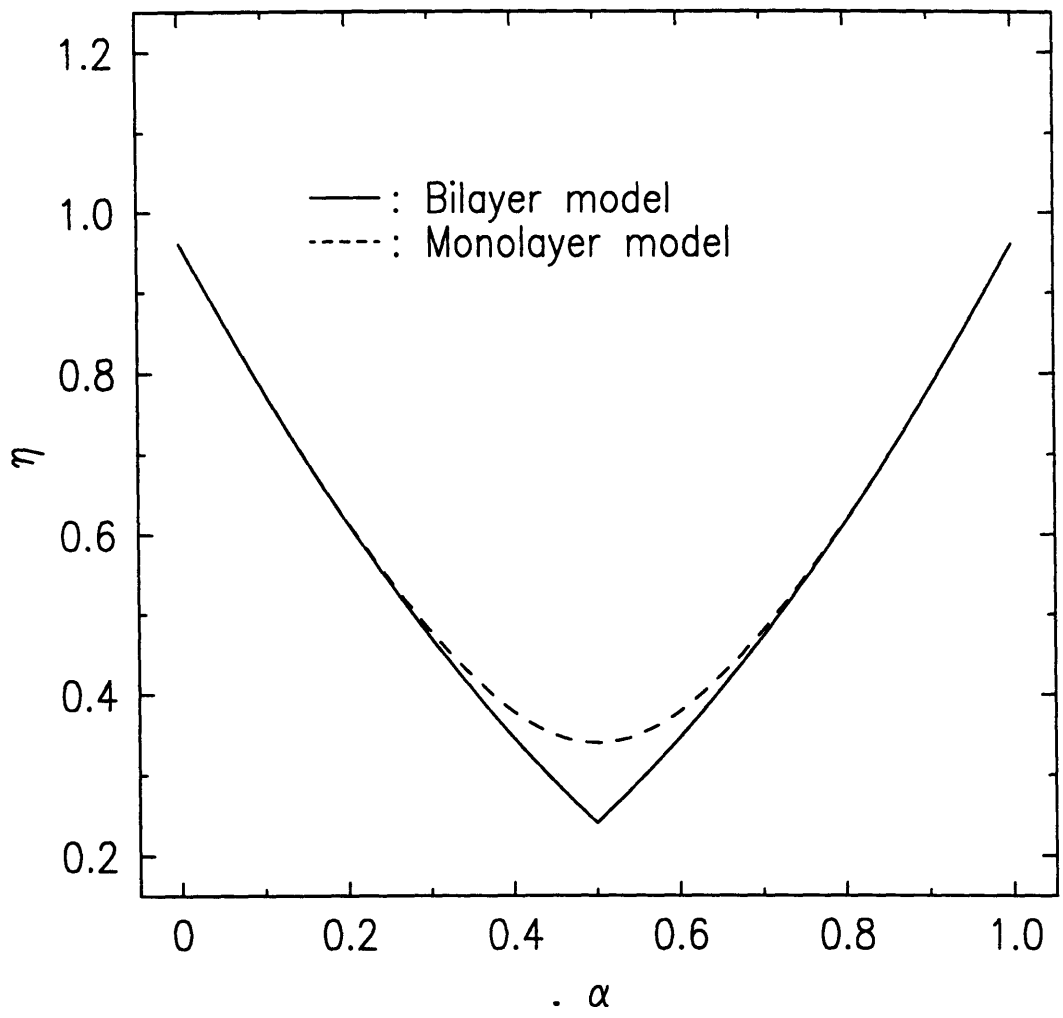

Figure 4-24: The two theoretical models are plotted for the same $\gamma = 0.15$. The solid line is the bilayer-mode approach, and the dashed line is the monolayer-model approach

$$\overline{B} = \frac{Ad(kT)^2}{\kappa} \frac{\frac{1}{(d\phi_o)^4} \cdot \frac{1}{(d\phi_w)^4}}{\frac{1}{(d\phi_o)^4} + \frac{1}{(d\phi_w)^4}} \tag{4.35}$$

$$\overline{B} = \frac{A(kT)^2}{\kappa d^3} \frac{1}{\phi_o^4 + \phi_w^4} \tag{4.36}$$

In the limit of $\phi_o \sim 0$ or $\phi_w \sim 0$, we get the value for the bilayer system which has been introduced previously i.e.:

$$\overline{B} = \frac{A(kT)^2}{\kappa d^3} \tag{4.37}$$

It should be noted that κ in this case is the bending rigidity of a single membrane. We can assume that $K \equiv \kappa/0.5d$ is on the average constant with α where d is the periodicity from a water/oil layer to the next water/oil layer: For $\alpha = 0.5, \kappa_{0.5} = \kappa_{mono}/0.5d$, for $\alpha = 0$ or 1, $\kappa_{0,1} = \kappa_{bilayer}/d = 2\kappa_{mono}/d = \kappa_{0.5}$.

Now, using again the definition of η, and also using $\phi_o = \alpha(1-\gamma)$, $\phi_w = (1-\alpha)(1-\gamma)$ we get:

$$\eta = q_0^2 \frac{kT}{8\pi\sqrt{\overline{B}K}}$$

$$\eta = \frac{4}{3}(1-\gamma)^2\sqrt{\alpha^4 + (1-\alpha)^4} \tag{4.38}$$

From Fig. 4-24 , we can see a good agreement of the η value, between the two models (the bilayer and the monolayer). For $\alpha \neq 0.5$ the bilayer model gives smaller value as $\alpha \rightarrow 0.5$.

We can also try to get the δ value for the monolayer. Using Eq. 1.36 and by substituting $d_p = d_{p,measured}/2$ we get,

$$\eta = 4/3(1 - \frac{\delta}{d_p/2})^2 \tag{4.39}$$

Here we get the value $\delta = 23.9 \pm 1.3$Å, which is larger than $\delta_{bilayer}/2 = 30/2 = 15$Å. In Fig. 4-25, γ vs η is plotted along with the theoretically predicted fit Eq. 4.39.

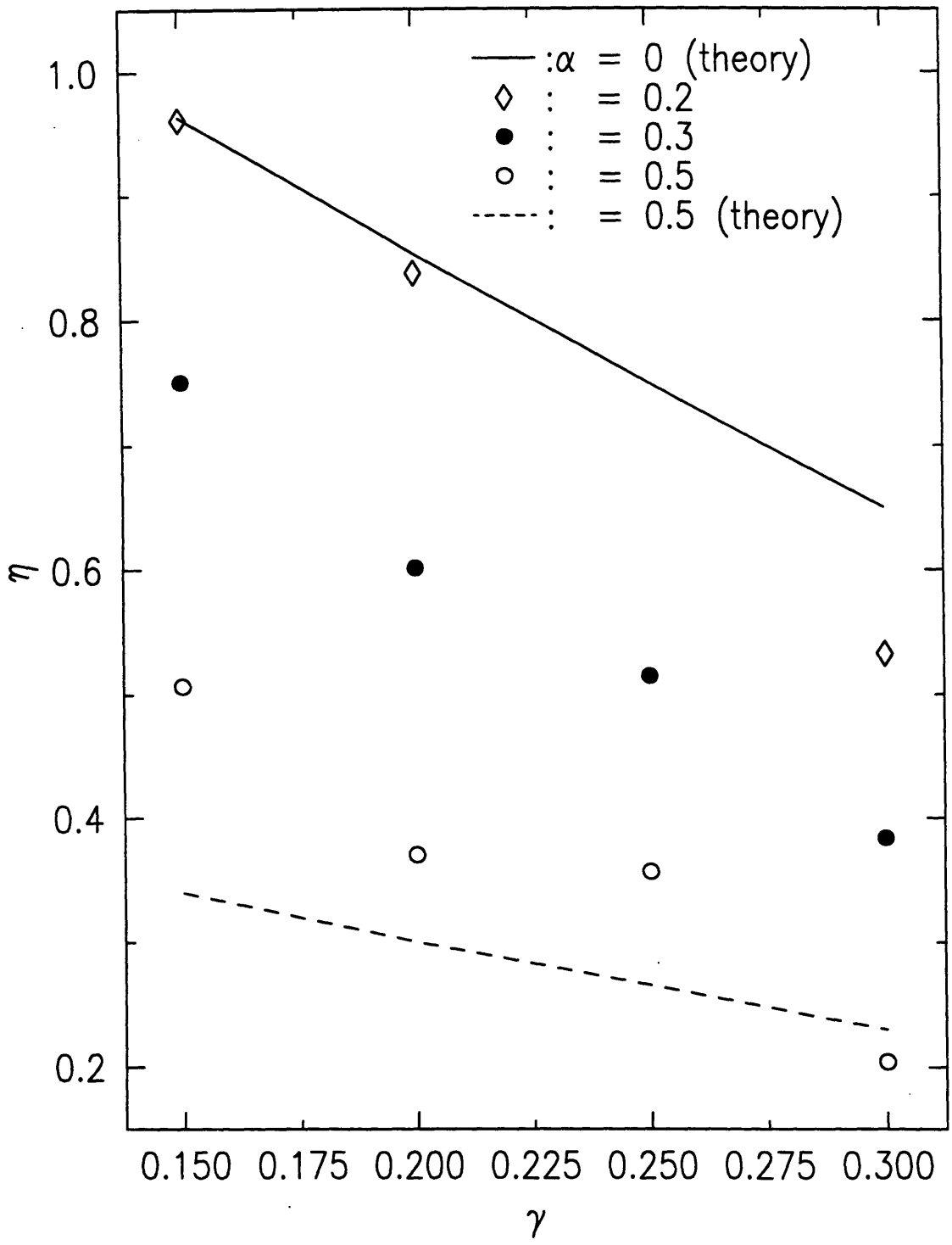

Figure 4-25: η vs γ for $\alpha = 0.2, 0.3$ and 0.5. The solid and dashed lines are the theoretical values for $\alpha = 0$, and 0.5.

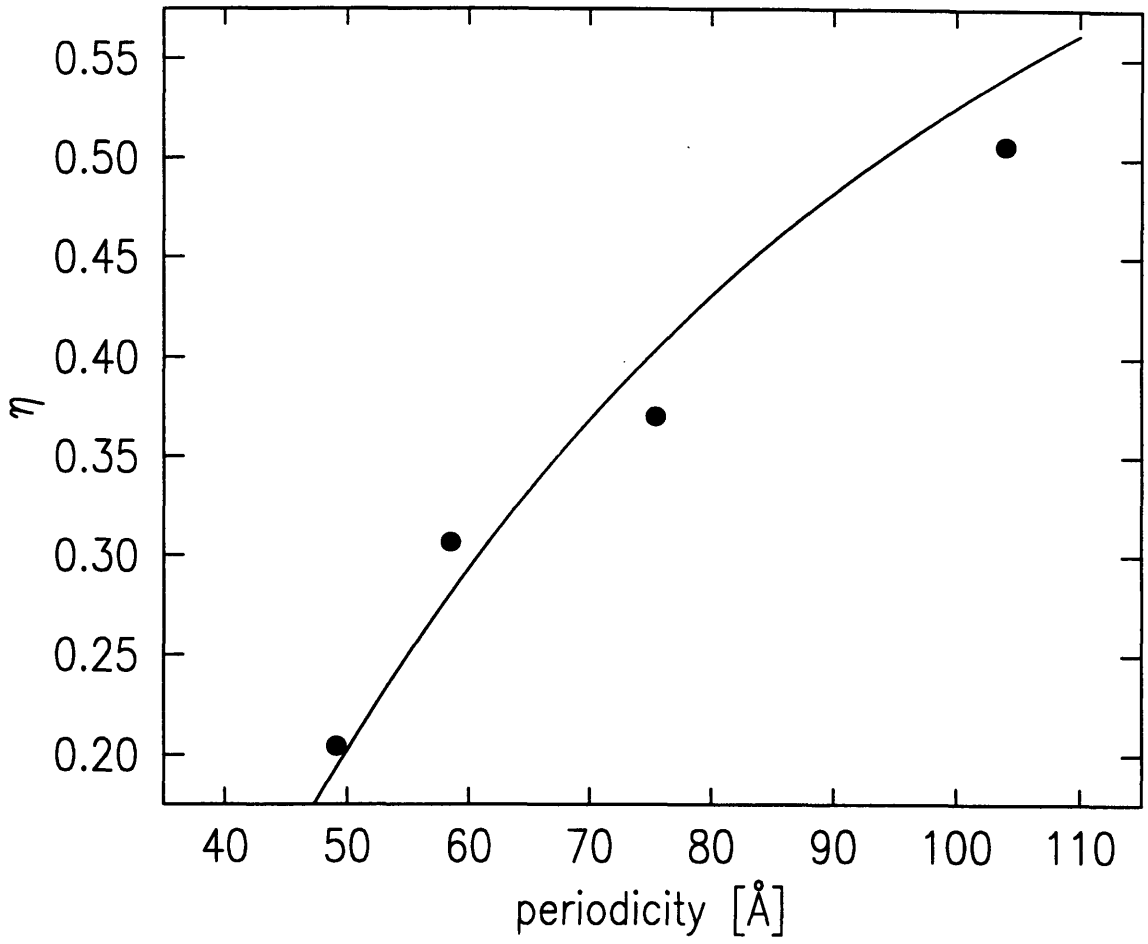

Figure 4-26: η as a function of the periodicity d_p. The solid line is the fit to Eq. (4.39)

Chapter 5

Data and Analysis: Aligned Sample

In this chapter, the data obtained from the aligned samples are presented. For these experiments, the samples chosen were

$$\frac{\text{surfactant}}{\text{surfactant} + \text{water} + \text{oil}} \equiv \gamma = \ 0.30.$$

$$\frac{\text{oil}}{\text{water} + \text{oil}} \equiv \alpha = \ 0.3,\ 0.4,\ 0.5,\ 0.6,\ 0.7.$$

5.1 Temperature dependence of the Lamellar Periodicity

For the oriented samples, it was found that even though a complete alignment can be achieved under the microscope, the mosaicity which affects the K-scans ($q_\perp$ direction scans) could not be effectively decreased in order to perform the satisfying line shape analysis. The typical mosaicity was $\sim 0.4°$ However, because the L-scans (q_z direction scans) were quite sharp, which allows to distinguish the difference in periodicity in the order of 0.1 Å. Therefore, we decided to concentrate on the investigation of the shift

of peak positions with temperature which was not possible with the low resolution powder-sample experiments.

Figs. 5-2 shows the evolution of the quasi-Bragg peak as the temperature was cooled down from the isotropic phase into the L_α phase.

As the temperature is lowered between $41°C \sim 39°C$, the peak position shifts towards larger values of the periodicity

When this is compared with the phase diagram in Chapter 3, we notice that this corresponds to the two-phase coexistence range between sponge and L_α phases. This means that the periodicities of the L_α in this region are smaller than the periodicity when the system is homogeneously in the L_α phase, and this leads to the argument that the surfactant density of L_α phase , in the biphasic region, is higher than the coexisting sponge phase, which is consistent with the observations made by optical investigations.

5.1.1 Logarithmic correction of the lamellar periodicity with thermal undulations.

Dilution Line

Another interesting feature is the temperature dependence of the peak position inside the L_α phase. The peak position shifts towards a larger values at higher temperatures. The shift is typically, $1\mathring{A}/10°C$. We have made sure that this is a reversible effect. This raised a question about the dilution line of the system: The solubility of surfactants in solvents is a function of temperature, therefore, when the observation of L_α is made with the change of temperature, we have to take into account this solubility effect as we change the temperature and measure the periodicity. Because, as the solubility increases, we *lose* more surfactant monomers from the membranes in the solvent, which will cause the swelling of the lamellae even though the total volumic fraction of the surfactant in the solution is fixed. In other words, the number of the surfactants in the membrane has to be fixed with the change of temperature, and when this solubility changes with temperature, we have to add or subtract in

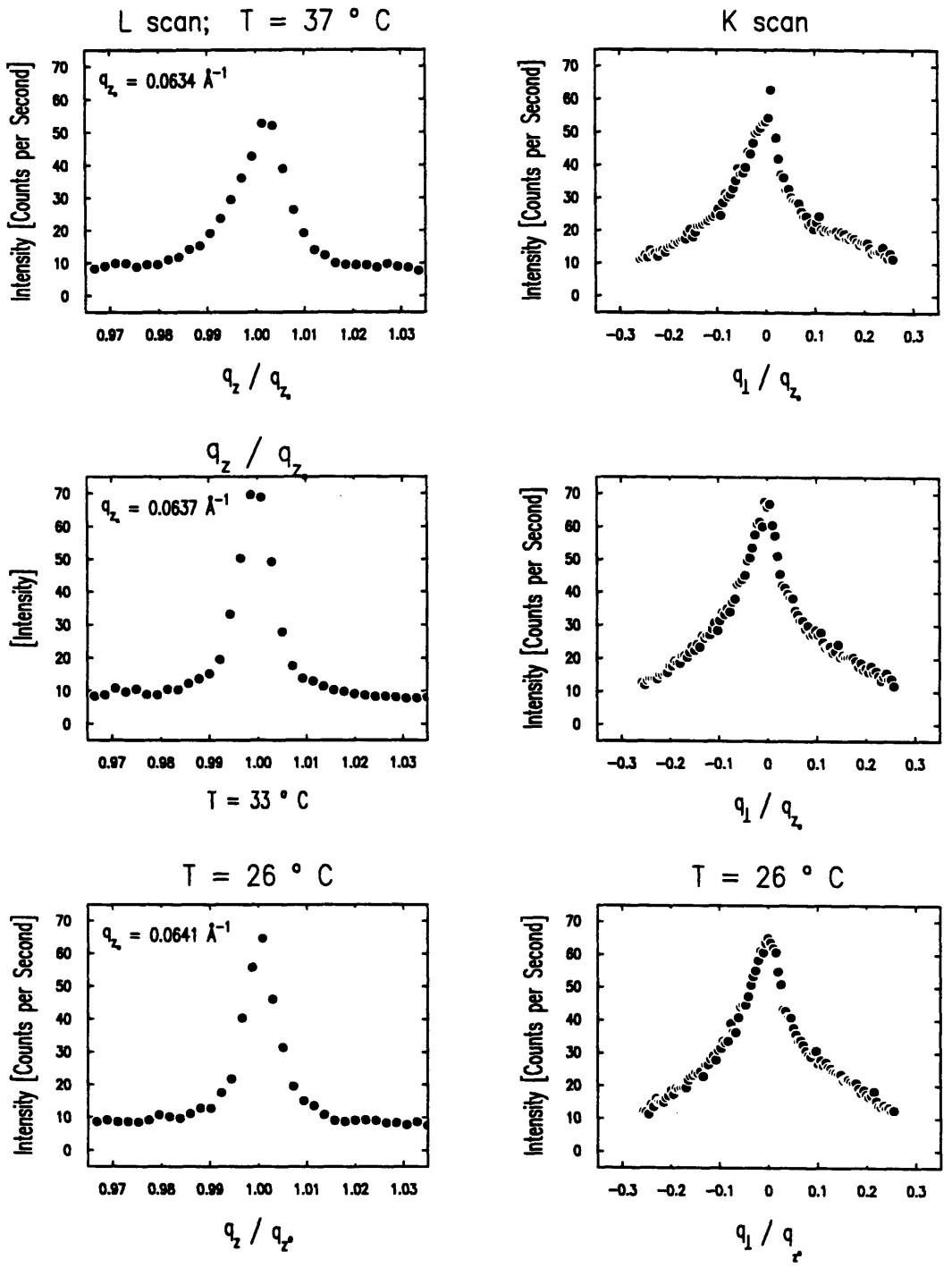

Figure 5-1: The Scattering Spectra from the oriented samples: $\gamma = 0.30$, $\alpha = 0.6$ with the temperature 37, 33 and 26 $°C$

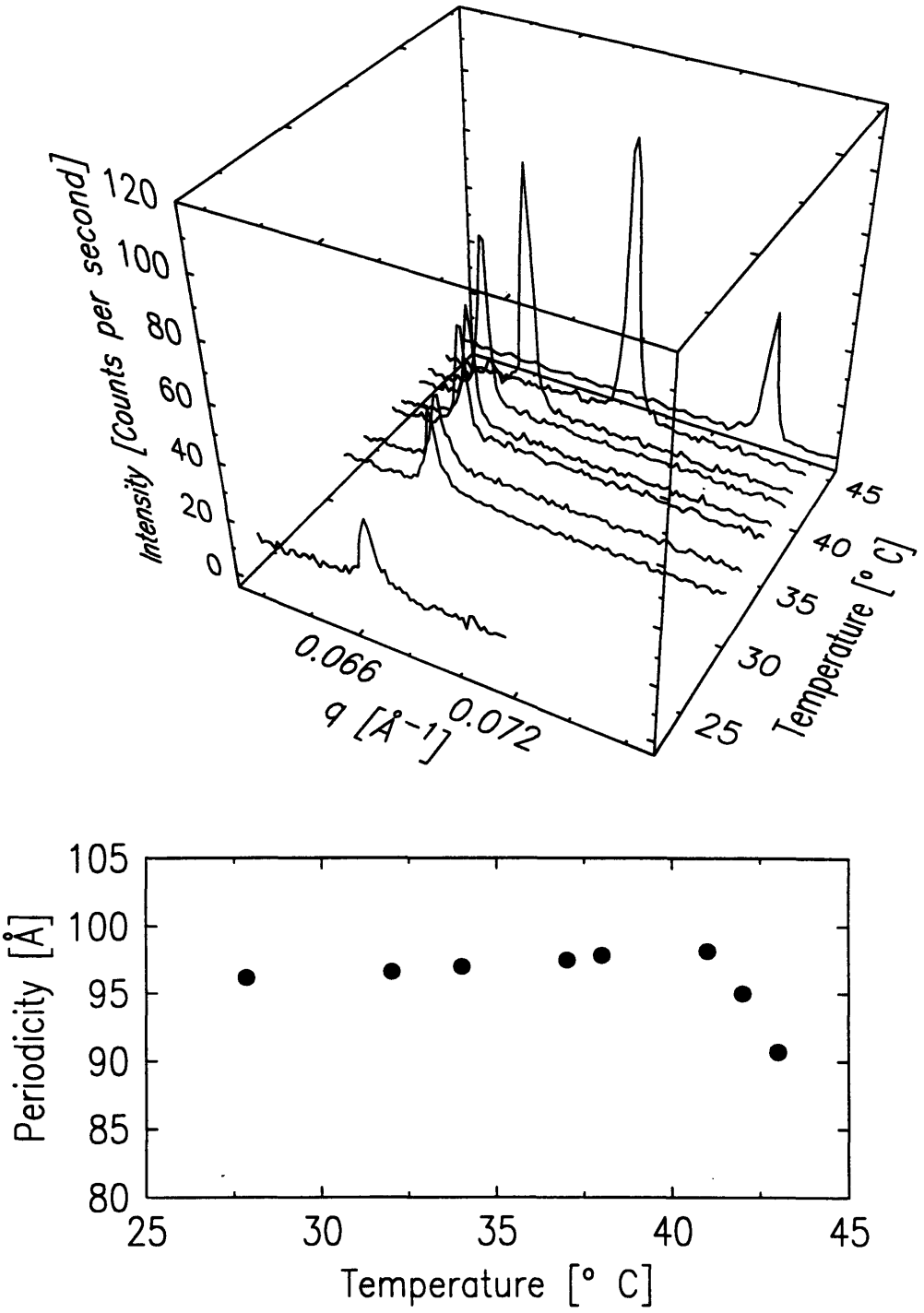

Figure 5-2: The Scattering Spectra and the temperature dependence of their peak positions: $\gamma = 0.30$, $\alpha = 0.6$ and the temperature is changed between 25 and 45 $°C$

order to maintain the same number of surfactant in the membrane. This line in the phase diagram is called dilution line.

We used the Critical Micellar Concentration(CMC) for estimating this effect. The Critial Micellar Concentration is the concentration beyond which, the surfactants are unstable to stay in the solvent as monomers and form micells. This may not be exactly the same concentration of the surfactants in the solvents in L_α phase, however, since both determine the saturation concentraion of monomer in the solvent, we estimated that the difference is not too large.

The solubility of $C_{12}E_5$ in water is known to be 0.002 wt% [42], moreover, the change is negative with the increase of the temperature, which should give a decrease in the periodicity with increasing temperature, since we could not measure such a small effect, thus, this will neglected within the range of the temperature of interest. No data for the solubility of $C_{12}E_5$ in octane could be found in the literature. However, finally we determined the effect not to be important from the following argument.

When the solubility of the surfactant monomers is an increasing function of temperature, and the temperature dependence of the solubility in water is neglected, the increase of the periodicity with the increase of temperature should be larger when the oil content in the sample is higher. So the increase of the periodicity should be higher for the larger α values. As it is shown in the table 5.1, the slope for the different oil to water ratio α does not increase with α. This allowed us to conclude that the temperature dependence of solubility of the monomer into the octane is not significant.

Logarithmic Correction

Thus, the reason for the change of the periodicity with temperature has to come from the thermodynamics of the system. We will again approach this problem using the theory of logarithmic correction to the periodicity of the of the lamellae caused by thermal fluctuations 1.45, which was introduced in Chapter 4

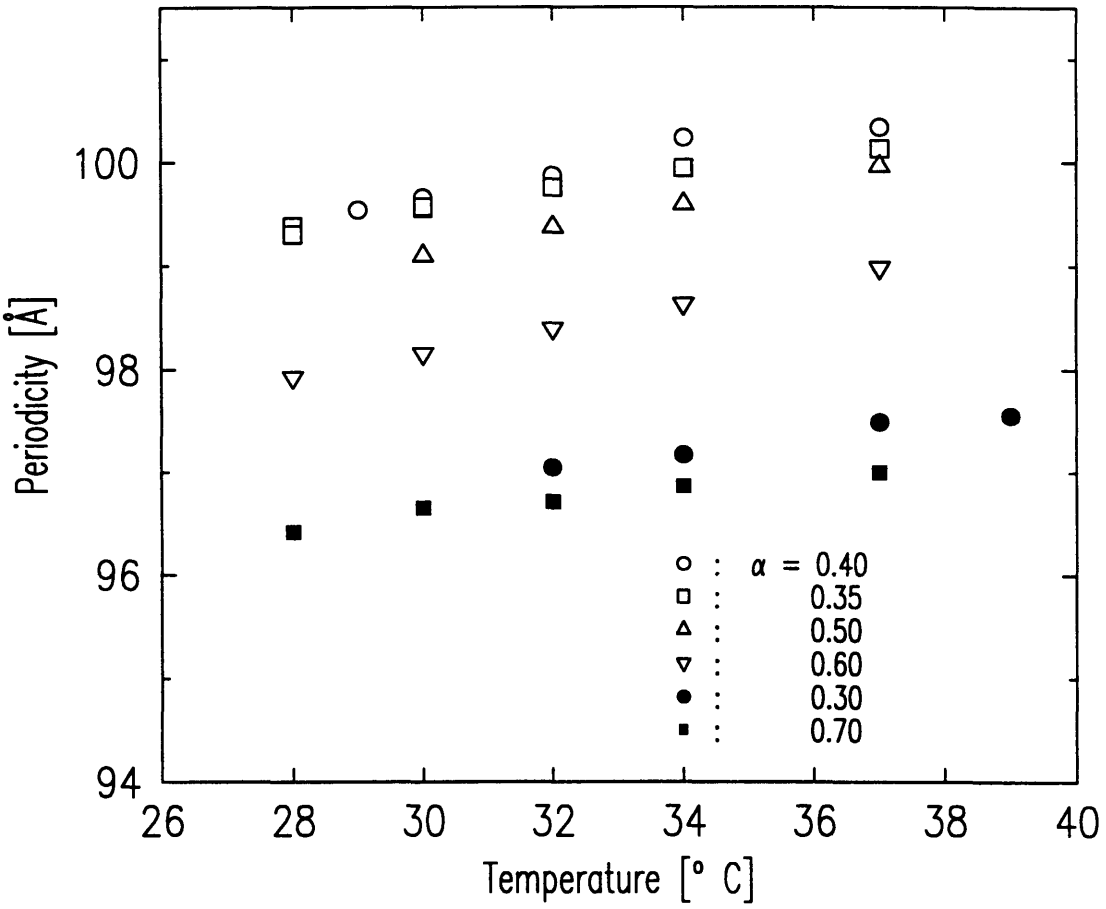

Figure 5-3: The temperature dependence of the lamellar periodicity for various oil/water ratios

$$d = \frac{\delta}{\phi}[1 + \frac{kT}{4\pi\kappa}\ln(\frac{c\delta}{a}\sqrt{\frac{\kappa}{kT}}\frac{1}{\phi})] \tag{5.1}$$

Here, a is the square root of the area per polar head for a surfactant molecule, c is a model dependent constant, and for the case of a dilute lyotropic smectic-A system, it has been proposed to be [18], $c = (32/3\pi)^{1/2} \approx 1.84$. δ is the thickness of the membrane.

In order to see the periodicity dependence on the temperature change, we may assume that the term inside the logarithm changes much slower than T. Therefore we get,

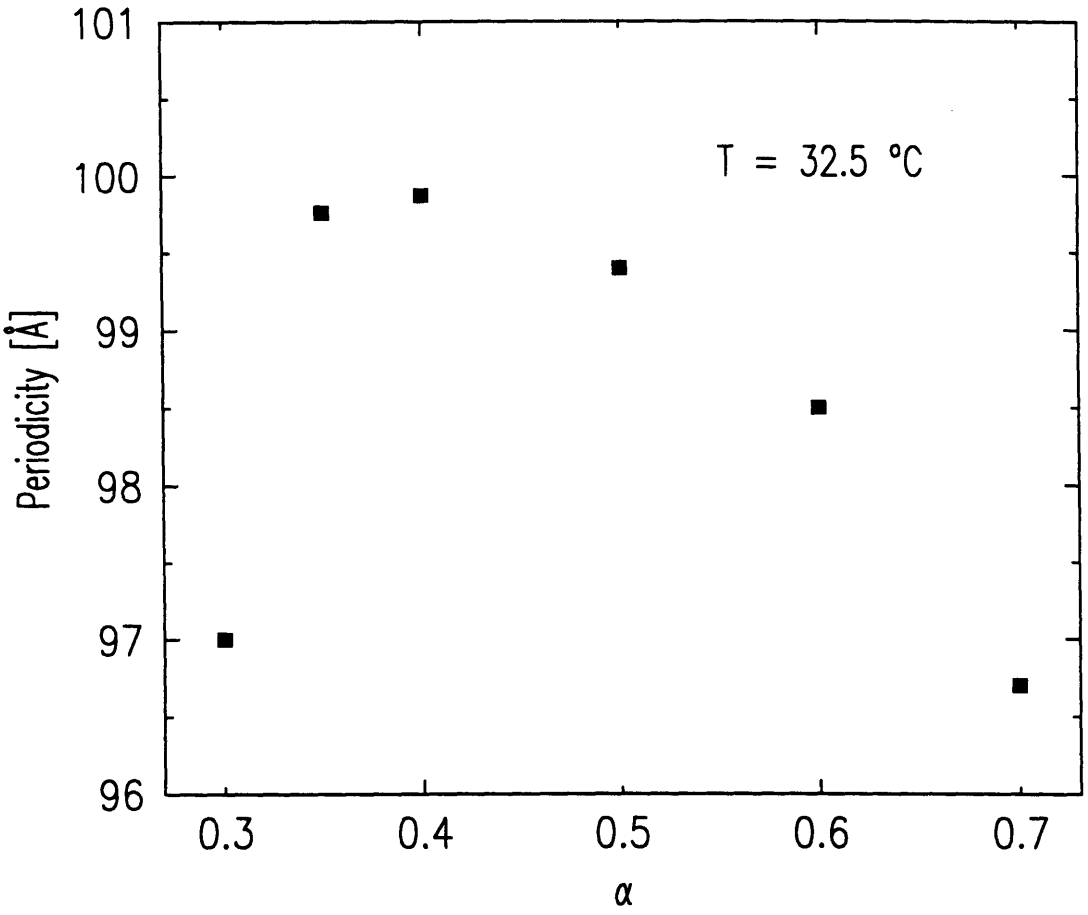

Figure 5-4: Lamellar periodicity vs α for T = 32.5 $°C$

$$\frac{\delta d_p}{\delta T} = \frac{\delta}{\phi}\frac{kT}{4\pi\kappa}\frac{1}{T}\log(\frac{c\delta}{a}\sqrt{\frac{\kappa}{kT}}\frac{1}{\phi}) \tag{5.2}$$

Now, if we make the approximation that $d_p \approx \delta/\phi = 100$ in first order and use the measured $d_p \approx 100$ Å, and $\phi = 0.3$, we get $\delta \approx 30$ Å, also substituting $a = 5$, $c = 1.84$, $\delta d_p/\delta T \approx 0.1$ we get $\kappa_{bilayer} \approx 0.95kT$. This is in close agreement with the value we got in Chapter 4 deduced from the swelling of monolayer 4.24 considering $\kappa_{bilayer} = 2\kappa_{mono}$.

5.1.2 Bilayer Monolayer transition

In Fig. 5-5, we show $\delta d/\delta T$ for the different samples with $\alpha = 0.30$, 0.35, 0.40, 0.50, 0.60, 0.70,

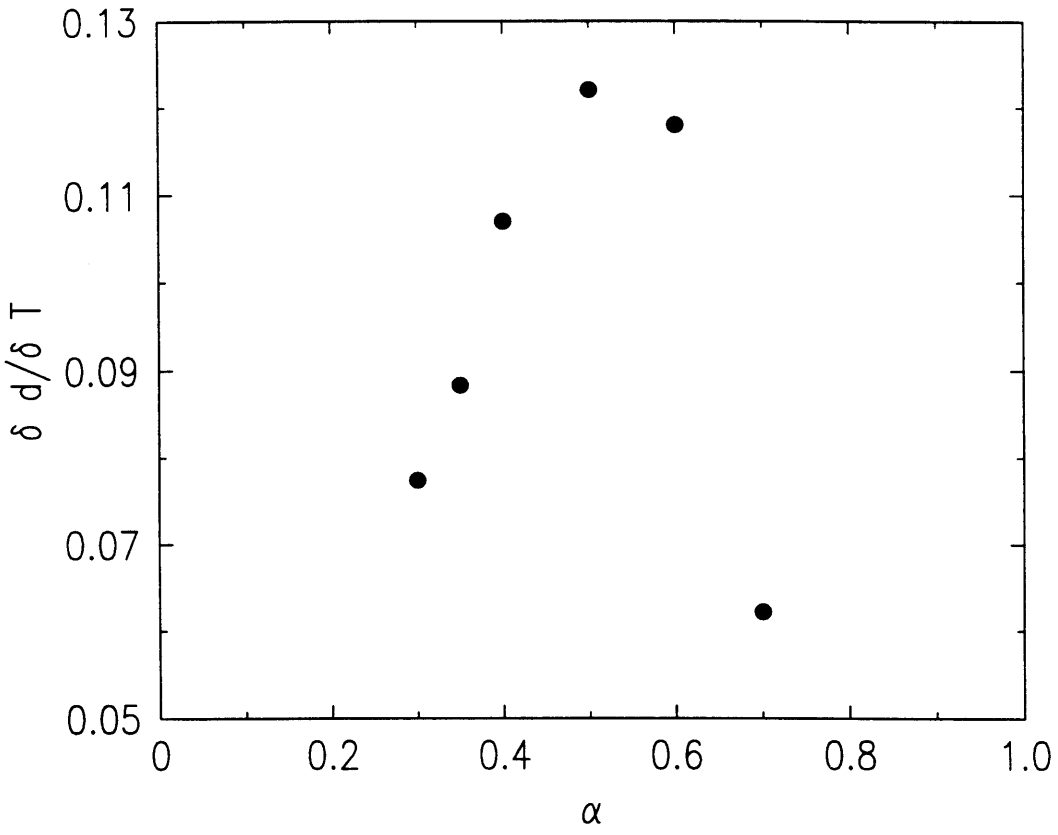

Figure 5-5: Variation of $\delta d/\delta T$ vs α

α	0.30	0.35	0.40
$\delta d/\delta T$	0.077 ± 0.010	0.088 ± 0.004	0.107 ± 0.014
α	0.50	0.60	0.70
$\delta d/\delta T$	0.122 ± 0.003	0.118 ± 0.001	0.062 ± 0.007

Table 5.1: $\delta d/\delta T$ for various α

From the Fig. 5-5, it is also shown that $\delta d/\delta T$ is largest for $\alpha = 0.50$ and decreases for the asymmetric cases of α. Now, as we have done in the Chapter 4, we will consider the case of $\alpha = 0.5$ to be the case where each monolayer is the oil/water interface. And each monolayer is separated by the distance $d' = d/2$, Also we shall neglect spontaneous curvature of the monolayer inside the lamellar phase, by assuming the interactions of interfaces with oil and interfaces with water are both steric (Helfrich)-

like interaction. From the Eq. 5.1, we can compare the two cases,

$$d_{bilayer} = \frac{\delta}{\phi}[1 + \frac{kT}{4\pi\kappa_{bilayer}} \ln(\frac{c\delta}{a}\sqrt{\frac{\kappa_{bilayer}}{kT}}\frac{1}{\phi})] \tag{5.3}$$

$$d_{mono} = \frac{\delta_{mono}}{\phi}[1 + \frac{kT}{4\pi\kappa_{mono}} \ln(\frac{c\delta_{mono}}{a}\sqrt{\frac{\kappa_{mono}}{kT}}\frac{1}{\phi})] \tag{5.4}$$

Where δ_{mono} is the thickness of the monolayer. Now, we approximate the thickness of bilayer and monolayer by $\delta_{mono} \approx \delta/2$. Also by realizing $d_{mono'}$ is not the distances between the interfaces but the periodicity, which determines the position of the Bragg peak. The real distance between the interfaces d_{mono} is:

$$d_{mono} = \frac{d_{mono'}}{2} \tag{5.5}$$

Thus, 5.4 becomes,

$$d_{mono'} = \frac{\delta}{\phi}[1 + \frac{kT}{4\pi\kappa_{mono}} \log(\frac{c\delta}{a}\sqrt{\frac{\kappa_{mono}}{kT}}\frac{1}{\phi})] \tag{5.6}$$

Using 5.2,

$$\frac{\delta d_{bilayer}}{\delta T} = \frac{\delta}{\phi}\frac{kT}{4\pi\kappa_{bilayer}}\frac{1}{T}\log(\frac{c\delta}{a}\sqrt{\frac{\kappa_{bilayer}}{kT}}\frac{1}{\phi}) \tag{5.7}$$

$$\frac{\delta d_{mono'}}{\delta T} = \frac{\delta}{\phi}\frac{kT}{4\pi\kappa_{mono}}\frac{1}{T}\log(\frac{c\delta}{a}\sqrt{\frac{\kappa_{mono}}{kT}}\frac{1}{\phi}) \tag{5.8}$$

Assuming the term inside the logarithm to be constant A, thus, the difference is simply,

$$\frac{\delta d_{bilayer}}{\delta T} = \frac{\delta}{\phi}\frac{kT}{4\pi\kappa_{bilayer}}\frac{A}{T} \tag{5.9}$$

$$\frac{\delta d_{mono}}{\delta T} = \frac{\delta}{\phi} \frac{kT}{4\pi\kappa_{mono}} \frac{A}{T} \tag{5.10}$$

This leads us to,

$$\frac{\delta d_{bilayer}}{\delta T} / \frac{\delta d_{mono}}{\delta T} = \kappa_{mono} / \kappa_{bilayer} \tag{5.11}$$

As we have seen from the previous chapter, the relation between the bending rigidity of monolayer and bilayer can be written as,

$$\kappa_{bilayer} = 2\kappa_{monolayer} \tag{5.12}$$

In our case we do not have the pure bilayer case, nevertheless, from the increase in $\delta d/\delta T$ as $\alpha \rightarrow 0.5$, we can confirm the relation between the thickness variation with temperature and the bending rigidity.

Also, if we compare Eqs. 5.1 and 5.6, they are in agreement with what is observed in Fig. 5-3 that the measured periodicity is larger for $\alpha = 0.50$ than $\alpha \neq 0.50$ Fig. 5-3 which also originates in the relation Eq. 5.12

From above, we could conclude that the temperature dependence of the change in periodicity originates in the thermal fluctuations which enhance the *actual* membrane area of a membrane with the increase of temperature from when it is in *flat* configuration, consequently, larger periodicity is observed. This fluctuation is higher for the more *flexible* membrane (smaller κ): in our case, the monolayer system.

This observation allows to extract the information of only κ while the study of the scattering intensity profile gives us η, which is a function of the product of the bending constant B and the elastic constant K.

Chapter 6

Conclusion

We have investigated the three-component lamellar phase with non-ionic surfactant, oil, and water. Samples with various oil-water ratios at fixed surfactant concentrations, where the systems consists of either water-rich bilayers, equal ratio of water and oil with monolayers, or oil rich bilayers were studied , as well as samples with different surfactant concentrations(dilution) at constant oil-water ratio. With optical investigations, we determined phase diagrams which show a temperature range where all the samples were in the lamellar phase.

The system was probed using x-ray scattering technique both with powder and aligned samples.

The first achievement was the success of the fitting of the powder sample peaks which are broadened by the undulation fluctuations. For the dilute lamellar phases which are sterically stabilized, the quasi-Bragg peaks of the powder samples are quite broad, and the usual approximation done for the structure factors which is to expand around the peak position and which is successful in explaining the intensity profiles only in the vicinity of the quasi Bragg peaks, failed in explaining the intensity profiles away from the peak positions. The contribution of the higher harmonic terms was also shown to be important. Our data show that , especially for the more concentrated samples, it is important to be able to fit the intensity profiles with the higher harmonics, which could not be reproduced with the usual structure factor as their approximation is constrained to be in the vicinity of the Bragg peak positions. The

structure factor proposed by Nallet et.al., provided the effective fit in all scattering vector range except the very small q where their approximation is not valid.

The validity of using the form factor was confirmed. As the membrane thickness becomes comparable to the periodicity itself, the form factor cannot be assumed to be constant. With a form factor based on the model to describe the electronic density distribution within and in the direction normal to the layers, we could successfully explain the variation of the membrane thickness. As we continuously changed the oil-water ratio at constant surfactant concentration, i.e. change the thickness of the membrane.

The excess scattering at $q \rightarrow 0$ was observed. The scattering which was caused by the concentration fluctuations, shows the increase in intensity as the system becomes more dilute. In the situations where the surfactant concentration was fixed and the water-oil ratio was varied, we found the decrease in intensity as the system was more symmetric, i.e. oil and water are equal in volume.

Another important effect observed was that we could establish the model for the monolayer system as the continuation of the bilayer lamellae. By employing the universal relation between the bilayer thickness, the periodicity and the critical exponent η which is the characteristic parameter for the density density correlation, thus the parameter which states the order of the system, we could rewrite this relation as a function only of the surfactant concentration and the oil to water ratio. The data could be described for the cases where the oil to water ratio was asymmetric. Close to the system where oil and water were equal in volume, this universal relation had to be reconsidered. We modeled the free energy as a sum of two compression energies of the two different solvents and by assuming the both energy to originate in Helfrich-like interactions, we could reproduce the relation between these three parameters through all the range of water to oil ratio. The data showed the agreement with the prediction which states that the approximation of taking both interactions to be Helfrich-like is indeed valid, This model states that η should be smaller for the more concentrated system, and also for the more symmetric system. Finally, this discussion leads to the conclusion that both the bending modulus and the compressibility of the system

are larger for the more concentrated systems. However the bending modulus is not affacted by the change of the symmetry of the system, (changing the oil-water ratio) while the compressibility is higher for the more symmetric cases, (water -oil ratio is equal), therefore the order parameter η is smaller for the symmetric case at the same surfactant concentrations.

By the deviation of the periodicity from the linear dilution law, we could see that the deviation was indeed logarithmic power of the surfactant concentration, even for the monolayer system, while the logarithmic correction theory assumes the bilayer system with the Helfrich interaction. From this we could get the bending rigidity of a monolayer.

Finally, the close agreement of the values for η and the membrane thickness from the fitting and the theoretically derived, confirmed the validity of the fitting function employed.

For the scattering done for oriented samples, because of the extreme sharpness of the peaks in q_z direction, and also because of the high stability with temperature acquired, we could get the stable and reproducible smectic periodicity as a function of temperature, and also it was possible to distinguish the very small differences in periodicities. It was found that even though the surfactant concentrations are constant, there is a small periodicity change with the change of the oil to water ratio, as well as with the change of temperature, This could be explained by taking into account the fluctuation of membranes: The fluctuation of the membranes increases as a function of temperature, thus the periodicity which is linearly related to temperature also increases. The dependence of this periodicity increase with temperature, which is the first derivative of the periodicity with temperature, depends on the bending rigidity of a single membrane, and by calculating the two extreme cases: monolayer and bilayer cases, the trend of the change in this derivative was explained which is also directly related to the difference in periodicity as a function of oil to water ratio at constant surfactant ratio.

Also from these calculations, we could deduce the bending rigidity of a membrane of the order $0.5kT$, which was in agreement with the value gotten from the powder

sample experiment.

.1 AppendixA : $\overline{B}$ and B,the comporessibility with the constant membrane thickness

At the equilibrium state, the chemical potential is defined as

$$\tilde{\mu} = \mu_{surfactant} - \mu_{solvent}$$

$$= \frac{1}{V}\frac{\partial F_{eq}}{\partial c}$$

where V is the sample volume.

for the perturbed state, the change in the chemical potential can be written as

$$\delta\tilde{\mu} = \frac{1}{V}\frac{\delta F}{\delta c}$$

$$= \frac{1}{V}\frac{\partial F_{eq}}{\partial \delta c}$$

Using the free energy defined 1.12,

$$\delta\tilde{\mu} = C_c\partial_z u + \chi^{-1}\delta c$$

so, when the chemical potential is constant, we get, $C_c\partial_z u = -\chi^{-1}\delta c$.

By substituting back to the '1.12, we get,

$$F = F_o + \frac{B - C_c^2\chi}{2}(\frac{\partial u}{\partial z})^2 + \frac{1}{2}K_1(\frac{\partial^2 u}{\partial x^2} + \frac{\partial^2 u}{\partial y^2})^2$$

$$F = F_o + \frac{\overline{B}}{2}(\frac{\partial u}{\partial z})^2 + \frac{1}{2}K_1(\frac{\partial^2 u}{\partial x^2} + \frac{\partial^2 u}{\partial y^2})^2$$

Now, the concentration c can be written as $c = \alpha/d$, where α is the layer thickness.

$$\frac{\delta\alpha}{\alpha} = \frac{\delta d}{d} + \frac{\delta c}{c}$$

$$= \frac{\partial u}{\partial z} + \frac{\delta c}{c}$$

When the chemical potential is constant,

$$= \delta c(\frac{1}{c} - \frac{1}{C_c \chi})$$

in the simple geometrical models, elastic constants C_c and χ are such that $C_c\chi = c$

Thus, when the chemical potential is constant, $\delta\alpha = 0$ which leads to the constant membrane thickness. And the $\overline{B}$ is the compressibility with the constant membrane thickness.

.2 AppendixB : The Density Density Correlation Function

The free energy is written as,

$$F = F_o + \frac{B}{2}(\frac{\partial u}{\partial z})^2 + \frac{1}{2}K_1(\frac{\partial^2 u}{\partial x^2} + \frac{\partial^2 u}{\partial y^2})^2 + \frac{1}{2\chi}\delta c^2 + C_c \delta c \delta_z u$$

We replace $\delta c(\mathbf{q})$ by $\tilde{\delta} c(\mathbf{q}) = \delta c(\mathbf{q}) + \chi C_c \partial u/\partial z$, then,

$$F = f_o + \frac{\overline{B}}{2}(\frac{\partial u}{\partial z})^2 + \frac{1}{2}K_1(\frac{\partial^2 u}{\partial x^2} + \frac{\partial^2 u}{\partial y^2})^2 + \frac{1}{2\chi}(\tilde{\delta} c^2)$$

Using the equipartition theorem,

$$< |u_{\mathbf{q}}|^2 >= \frac{kT}{\overline{B} q_z^2 + K q_\perp^4}$$

$$< |\delta \tilde{c}|^2 >= kT\chi$$

$$< \delta \tilde{c}(-\mathbf{q})\ u_{\mathbf{q}} >=< u_{-\mathbf{q}} \delta \tilde{c}(\mathbf{q}) >= 0$$

$$< |\delta c|^2 >=< (\tilde{\delta} c(\mathbf{q}) - \chi C_c u_q q_z)(\tilde{\delta} c(-\mathbf{q}) + \chi C_c u_{-q} q_z) >$$

$$< |\delta c|^2 >=< |\tilde{\delta c}|^2 > -2\chi C_c < \tilde{\delta c} u_q > q_z + \chi^2 C_2 < |u_q|^2 > q_z^2$$

$$= kT\chi + q_z^2\chi^2 C_2 \frac{kT}{\overline{B}q_z^2 + Kq_\perp^4}$$

$$= kT\chi \frac{Bq_z^2 + Kq_\perp^4}{\overline{B}q_z^2 + Kq_\perp^4}$$

$$< |\delta c(\mathbf{q}) u_{-q} >= i \frac{kT\chi C q_z}{\overline{B}q_z^2 + Kq_\perp^4} \tag{.1}$$

.3 AppendixC : The Displacement Correlation Function, Caillé's Calculation

The displacement correlation function proposed by Caillé is written as,

$$< |u(\mathbf{r}) - u(\mathbf{0})|^2 >= \frac{2kT}{(2\pi)^3} \int \frac{(1 - e^{-i\mathbf{q}\cdot\mathbf{r}})}{\overline{B}q_z^2 + Kq_\perp^4} 2\pi q_\perp dq_\perp dq_z \tag{.2}$$

This integral was performed first over q_z using

$$\int_{-\infty}^{\infty} \frac{1 - cos[a(b-x)]}{x^2 + c^2} dx = \frac{\pi}{c}[1 - e^{-ac} cos(ab)]$$

Thus .2 becomes,

$$\int_0^{\infty} \frac{1 - cos[q_z z + \mathbf{q}_\perp \cdot \rho]}{q_z^2 + \lambda^2 q_\perp^4} dq_z = \frac{\pi}{2\lambda q_\perp^2}[1 - e^{-\lambda q_\perp^2 z} cos(\mathbf{q}_\perp \cdot \mathbf{r}_\perp)] \tag{.3}$$

With θ as the angle between $\mathbf{q}_\perp$ and $\mathbf{r}_\perp$

$$\int_0^{2\pi} [1 - e^{-\lambda q_\perp^2 z} cos(\mathbf{q}_\perp \cdot \mathbf{r}_\perp)] d\theta$$

$$= 2\pi - exp(-\lambda q_\perp^2 z) \int_0^{2\pi} cos(q_\perp \rho cos\theta) d\theta$$

This integral can be compared to the bessel function ,

$$J_0(x) = \frac{1}{\pi} \int_0^{\pi} cos(x cos\theta) d\theta$$

The integral in the equation .2 can be writen as,

$$= \frac{kT}{4\pi} \int_{q_{min}}^{q_{max}} \frac{1 - exp(-\lambda q_\perp^2 z) J_0(q_\perp \rho)}{\lambda q_\perp^2} q_\perp dq_\perp$$

q_{max} can be estimated as $2\pi/a$ where a is the distance between the two surfactant molecules, and $q_{min} = 0$, so, if we substitute the series expantion for $J_0(x)$,

$$J_0(x) = \sum_{n=0} \frac{x^{2n}(-1)^n}{2^{2n} n! n!}$$

Then comparing with the exponential integral function $E_1(x)$,

$$E_1(x) = -\gamma - \log x - \sum_{n=1}^{\infty} \frac{(-1)^n x^n}{n(n!)}$$

γ is the Euler's constant, we find

$$< |u(\mathbf{r}) - u(\mathbf{0})|^2 >= \frac{kT}{q_z^2(\pi)\sqrt{K\bar{B}}} (2\gamma q + ln(\frac{r_\perp^2}{a^2}) + E_1(\frac{r_\perp^2}{4\lambda |z|})) \qquad (.4)$$

.4 AppendixD: Gaussian Variable

For a Gaussian Variable x,

$$P(x) = \frac{e^{-(x^2/2\sigma^2)}}{\sqrt{2\sigma^2}}$$

$$< cos(x) >= \frac{1}{\sqrt{2\sigma^2}} \int_{-\infty}^{\infty} cos(x) e^{-\frac{x^2}{2\sigma^2}} dx$$

$$= \frac{1}{2\sqrt{2\sigma^2}} \int_{-\infty}^{\infty} (e^{ix} + e^{-ix}) e^{-\frac{x^2}{2\sigma^2}} dx$$

$$= \frac{1}{2\sqrt{2\sigma^2}} \int_{-\infty}^{\infty} e^{-\frac{1}{2\sigma}(x+i\sigma)^2 + \frac{\sigma^2}{2}} + e^{-\frac{1}{2\sigma}(x-i\sigma)^2 + \frac{\sigma^2}{2}} dx$$

$$= e^{\frac{\sigma^2}{2}}$$

Now,

$$< x^2 >= \frac{1}{\sqrt{2\sigma^2}} \int_{-\infty}^{\infty} x^2 e^{-\frac{x^2}{2\sigma^2}} dx$$

$$= \frac{1}{\sqrt{2\sigma^2}} \int_{-\infty}^{\infty} (-\frac{d}{d\beta} e^{-\beta x^2}) dx$$

$$= \frac{1}{\sqrt{2\sigma^2}} - \frac{d}{d\beta} \frac{1}{\sqrt{\beta}}$$

$$= \sigma^2$$

Thus, we can derive the following relation,

$$< cos(x) >= e^{-\frac{<x^2>}{2}}$$

References

[1] F.Brochard and P.G.DeGennes, Pramana **1**, 1 (1975).

[2] C.R.Safinya *et al.*, Phys.Rev.Lett **57**, 2718 (1986).

[3] F.C.Larche *et al.*, Phys.Rev.Lett. **56**, 1700 (1986).

[4] M.E.Cates, D.Roux, D.Andelman, and S.Milner, Europhys.Lett. **5**, 733 (1988).

[5] G.Porte, J.Marignan, P.Bassereau, and R. May, Europhys.Lett. **7**, 713 (1988).

[6] L.Landau and E.Lifshitz, *Statistical Physics* (Oxford:Pergamon, 1958), Vol. 5.

[7] W.Helfrich, Z.Naturforsh **28**, 693 (1973).

[8] W.Helfrich, J.Phys.France **46**, 1263 (1985).

[9] S. L.Peliti, Phys, Rev. Lett. **54**, 1690 (1986).

[10] F.David, *Statistical Mechanics of Membranes and Surfaces* (World Scientific, Sinfapore, 1989).

[11] P. Gennes and C. Taupin, J.de Phys.Chem. **86**, 2294 (1982).

[12] G.Porte, J.Appell, P.Bassereau, and J.Marignan, J.Phys. France **50**, 1335 (1989).

[13] P. Gennes, J.Phys. France **30**, C4 (1969).

[14] R.E.Peierls, Helv.Phys.Acta Suppl. **7**, 81 (1934).

[15] L.D.Landau, Phys.Z.Sowjetunion **2**, 26 (1937).

[16] J.Als-Nielsen, J.D.Litster, R.J.Birgenau, and A.-A. S. M.Kaplan, C.Safinya, Phys.Rev.B **22**, 312 (1980).

[17] F.Nallet, D.Roux, and J. Prost, J. Phys. France **50**, 3147 (1989).

[18] L.Golubovic and T.C.Lubensky, Phys. Rev. A **41**, 4343 (1990).

[19] W.Helfrich, Z.Naturforsh **33**, .

[20] D.Roux and C.Safinya, J.Phys.France **49**, 307 (1988).

[21] S.Liebler and R.Lipowsky, Phys.Rev.B **35**, 7004 (1987).

[22] J.Israelachvili, *Intermolecular and Surfaces Forces* (Academic Press:Orlando, 1985), p. 265.

[23] A.Parsegian, N.Fuller, and R.P.Rand, Proc. Nat.Acad.Sci.USA **76**, 2750 (1979).

[24] B.W.Ninham and V.Parsegian, J.of Phys.Chem. **53**, 3398 (1970).

[25] J.Marra and V.Parsegian, Coll.Int.Sci. **109**, 11 (1986).

[26] W.Helfrich, J.Phys. France **46**, 1263 (1985).

[27] D.Roux and F.Nallet, Europhys.Lett. **17**, .

[28] J. Brock, Ph.D. thesis, Massachusetts Institute of Technology, 1987.

[29] A.Caillé, C.R.Acad.Sc.Paris B **274**, 891 (1972).

[30] L.Gunter, Y. Imry, and J.Lajzerowicz, Phys.Rev.A **22**, 1733 (1980).

[31] F.nallet, D.Roux, and J.Prost, J.Phys.France **50**, 3147 (1989).

[32] F.Nallet, D.Roux, and S.Milner, J.Phys.France **51**, 2333 (1990).

[33] P.Dutta and S.K.Sinha, Phys.Rev.Lett **47**, 50 (1981).

[34] F.Nallet, R.Laversanne, and D.Roux, J. Phys. France(2) **3**, 487 (1993).

[35] R.Strey and M.Kahlweit, J.of Col.Int.Sci. **118**, 436 (1987).

[36] J.F.Bodet *et al.*, J. of Phys.Chem. **92**, 1898 (1988).

[37] W.Benton and C.A.Miller, J. of Phys.Chem. **87**, 4981 (1983).

[38] P. Bassereau, Ph.D. thesis, Université Montpellier, 1990.

[39] P.Boltenhagen, O.Laventovich, and M.Kleman, J. of Phys. (France) **1**, 1233 (1991).

[40] A.Noel and R.B.Meyer, Amer.Ins.Phys. **22**, 493 (1973).

[41] V.M.Kaganer, B.I.Ostrovskii, and W. Jeu, Phys.Rev.A **44**, 8158 (1991).

[42] M.Kahlweit, R.Strey, and G.Bosse, J. of Phys.Chem. **94**, 3881 (1990).